University of Szeged

Faculty of Pharmacy

Institute of Pharmaceutical Technology and Regulatory Affairs

Head: Prof. Dr. habil. Ildikó Csóka, PhD

THE UTILIZATION OF TITANATE NANOTUBES AS DRUG DELIVERY SYSTEMS

PhD Thesis

By

Yasmin Ranjous

Pharm.D., M.Sc.

Supervisors:

Dr. habil. Géza Regdon jr., PhD

and

Dr. habil. Tamás Sovány, PhD

Szeged

2021

LIST OF ORIGINAL PUBLICATIONS

1. **Ranjous, Y.**, Regdon jr., G., Pintye-Hódi, K., & Sovány, T. (2019). Standpoint on the priority of TNTs and CNTs as targeted drug delivery systems, Drug Discovery Today. 24(9), 1704-1709 (2019).

   IF: 6.880

2. **Ranjous, Y**., Regdon jr., G., Pintye-Hódi, K., Varga, T., Szenti, I., Kónya, Z., & Sovány, T. Optimization of the production process and product quality of titanate nanotube–drug composites, Nanomaterials 9(10), 1406 (2019).

   IF: 4.324

3. **Ranjous, Y**., Kósa, D., Ujhelyi, Z., Regdon jr., G., Szenti, I., Nagy, KA., Kónya, Z., Bácskay, I., & Sovány, T. Toxicity and permeability investigation of functionalized titanate nanotubes on Caco-2 cell line, Acta Pharmaceutica Hungarica 91, 31-39 (2021).

PRESENTATIONS RELATED TO THE THESIS

Verbal presentations:

1. **Yasmin Ranjous**, Géza Regdon jr., Tamás Sovány: Formulating different TNT-API composites as (targeted) drug delivery systems. I. Symposium of Young Researchers on Pharmaceutical Technology, Biotechnology and Regulatory Science. January 31, 2019. Szeged, Hungary.
2. **Yasmin Ranjous**, Géza Regdon jr., Tamás Sovány: Investigation the effect of solvent selection on the production process and product quality of titanate nanotube-drug composites. II Fiatal Technológusok Fóruma. April 10, 2019. Budapest, Hungary.
3. **Yasmin Ranjous**, Géza Regdon jr., Tamás Sovány: The role of solvents in enhancing the production process of titanate nanotube-drug composites. Towards a Knowledge Economy for Postwar Syria, The Role of Syrian Researchers at Home and Expatriate. August 7-8, 2019. Damascus, Syria.
4. Sovány Tamás, **Yasmin Ranjous**, Sipos Barbara, Hódi Klára, Kónya Zoltán, ifj. Regdon Géza: Titanát nanocső-hatóanyag kompozitok előállításának optimalizálása. Gyógyszertechnológiai és Ipari Gyógyszerészeti Konferencia. September 26-28, 2019. Siófok, Hungary.
5. **Yasmin Ranjous**, Géza Regdon jr., Tamás Sovány: The prominence of titanate nanotubes' functionalization on their physicochemical properties and biological applications as drug delivery system. II. Symposium of Young Researchers on Pharmaceutical Technology, Biotechnology and Regulatory Science. January 23-24, 2020. Szeged, Hungary.
6. **Yasmin Ranjous**, Géza Regdon jr., Zoltán Kónya, Tamás Sovány: Investigation of physical properties, toxicity and permeability of functionalized titanate nanotubes as novel vectors for drug delivery. EUGLOH Annual Student Research Conference. September 28-30, 2020. Online conference.
7. **Yasmin Ranjous,** Dóra Kósa, Zoltán Ujhelyi, Krisztina Anita Nagy, Zoltán Kónya, Ildikó Bácskay, Géza Regdon jr., Tamás Sovány: The use of functionalized titanate

nanotubes as drug delivery systems. III Fiatal Technológusok Fóruma. December 14, 2020. Online conference.

8. **Yasmin Ranjous**, Dóra Kósa, Zoltán Ujhelyi, Géza Regdon jr., Krisztina Anita Nagy, Zoltán Kónya, Ildikó Bácskay, Tamás Sovány: Optimization of the functionalization method of titanate nanotubes in order to use them as drug delivery systems. III Symposium of Young Researchers on Pharmaceutical Technology, Biotechnology and Regulatory Science. January 20-22, 2021. Online conference.

Poster presentations:

9. **Yasmin Ranjous**, Géza Regdon jr., Zoltán Kónya, Tamás Sovány: Optimization of the production process and product quality of titanate nanotube–drug composites. 12th Central European Symposium on Pharmaceutical Technology and Regulatory Affairs. September 20-22, 2018. Szeged, Hungary.

PRESENTATIONS NOT RELATED TO THE THESIS

1. **Yasmin Ranjous**, Géza Regdon jr., Tamás Sovány, Jamelah Hasian: Improvement of Gabapentin's Stability by Using Different Excipients and Varying the Ambient Conditions. EUFEPS Annual Meeting. May 24-26, 2018. Athens, Greece.

TABLE OF CONTENTS

LIST OF ORIGINAL PUBLICATIONS ii
PRESENTATIONS RELATED TO THE THESIS iii
PRESENTATIONS NOT RELATED TO THE THESIS iv
TABLE OF CONTENTS 1
ABBREVIATIONS 3
1. INTRODUCTION 5
2. AIMS 7
3. LITERATURE BACKGROUND 8
3.1. Preparation methods of TNTs 8
3.2. Applications of TNTs 8
3.3. Physicochemical properties of TNTs 9
3.4. Functionalization 9
3.5. Solid state dispersion 11
3.6. Toxicity of nanotubes 13
3.6.1. Toxicity of CNTs 13
3.6.2. Toxicity of titanium dioxide nanoparticles 13
3.6.3. Toxicity of TNTs 15
4. MATERIALS 17
4.1. Hydrothermally synthetized titanate nanotubes and their composites 17
4.2. Functionalization 17
5. METHODS 17
5.1. Preparation of TNTs and their composites 17
5.1.1. Hydrothermal synthesis of TNTs 17
5.1.1.1. Pristine sodium trititanate ($Na_2Ti_3O_7$) nanotubes (TNTs) 17
5.1.1.2. Hydrogen trititanate ($H_2Ti_3O_7$) nanotubes (H-TNTs) 18
5.1.1.3. Magnesium trititanate ($MgTi_3O_7$) nanotubes (Mg-TNTs) 18
5.1.2. Preparation of TNT-drug composites 18
5.1.2.1. TiATN- Methanol 18
5.1.2.2. TiATN-HCl/ TiHCT-DMF/ TiHCT-DMSO 19
5.1.2.3. TiHCT-NaOH 19
5.2. Functionalization of TNTs 20

5.2.1. TCOS-TNTs 20
5.2.2. MgSt- TNTs 20
5.3. Morphology and size investigation 20
5.4. FT-IR spectrophotometer 21
5.5. Surface free energy measurement 21
5.6. Thermoanalytical analysis 22
5.7. Drug release 22
5.8. CHNS elemental analysis 22
5.9. Cytotoxicity and permeability detection 23
5.9.1. Cytotoxicity test 23
5.9.2. Permeability test 24
6. RESULTS AND DISSCUSSION 25
6.1. Optimization of the composite formation process and product quality 25
6.1.1. Properties of the TNT and TNT-HCl 25
6.1.2. Effect of various solvents on composite formation with ATN 27
6.1.3. Effect of various solvents on composite formation with HCT 32
6.2. The functionalization of TNTs 38
6.2.1. Physical properties of functionalized TNTs 38
6.2.2. Toxicity and permeability of functionalized TNTs 41
6.2.3. Permeability results 42
7. CONCLUSIONS AND PRACTICAL USEFULNESS 44
8. REFERENCES 45
ACKNOWLEDGEMENTS v

ABBREVIATIONS

APIs	Active pharmaceutical ingredients
ATN	Atenolol
APTES	3-aminopropyltriethoxysilane
BCS	Biopharmaceutical Classification System
BMP_2	Bone morphogenetic protein 2
CDI	N, N carbonyl diimidazole
CNTs	Carbon nanotubes
DMF	Dimethylformamide
DMSO	Dimethyl sulfoxide
DSC	Differential scanning calorimetry
DTA	Differential thermal analysis
DWNTs	Double-walled carbon nanotubes
EFSA	European Food Safety Authority
FT-IR	Fourier transform infrared
GIT	Gastrointestinal tract
HCl	Hydrochloric acid
HCT	Hydrochlorothiazide
hMSCs	Human mesenchymal stem cells
H_xTiO_{y+z}	Hydrogen titanate
IARC	International Agency for Research on Cancer
MgSt-TNT	Magnesium stearate- titanate nanotubes
NaOH	Sodium Hydroxide
Na St	Sodium Stearate
Na_xTiO_{y+z}	Sodium titanate
NPs	Nano particles
OCA	Optical contact angle
PEG	Polyethylene Glycol
PEI	Polyethylene imine
PK	Pharmacokinetics

PhoA	11-hydroxy-undecylphosphonic acid
PVP	Polyvinylpyrrolidone
SEM	Scanning electron microscope
TEER	Transepithelial electrical resistance
TCOS-TNT	Trichloro octyl silane- titanate nanotube
TEM	Transmission electron microscope
TGA	Thermogravimetric analysis
THF	Tetrahydrofuran
Ti-ATN	Titanate nanotube-ATN composite
TNT-HCl	Titanate nanotube treated with hydrochloric acid
Ti-HCT	Titanate nanotubes-HCT composite
TiO_2	Titania
TiO_2 NPs	Titanium dioxide nanoparticles
TNTs	Titanate nanotubes
XRPD	X-ray Diffractometry

1. INTRODUCTION

Conventional drug delivery systems may have limitations such as poor solubility, fluctuation in plasma concentration, patient incompliance, concentration decrease at the site of action, and poor pharmacokinetics (PK) (1). In contrast, nanotechnology-based drug delivery systems can help in delivering sparingly water-soluble drugs to their target location, achieving higher oral bioavailability, prolonging the drug blood circulation period, thus causing fewer plasma fluctuations with reduced adverse effects, easing the cell uptake of drugs (2). Furthermore, nanosized drugs may show better stability and, therefore, enhance the shelf life and acceptability of drugs by increasing either their uptake efficacy or patient compliance.

The cell internalization of nanosized delivery structures is more efficient compared to micro-sized particles (3). Metallic, organic, inorganic and polymeric nanostructures are often used as targeted drug delivery systems, particularly for poorly soluble and poorly permeable APIs. The biophysical and chemical characteristics such as shape and size have a significant influence on nanostructure efficacy (4). Nanotubes have a surface area five times higher than that of other NPs and an ideal inner diameter of 5–6 nm, which is suitable for loading even with large biological molecules. Furthermore, tubular NPs can be cell internalized in a higher percentage compared to their spherical counterparts (5).

The first nanotubes to be synthesized were carbon nanotubes (CNTs) in 1991 by Lijima, whereas titanate nanotubes (TNTs) were synthesized in 1996 by Hoyer (6). CNTs and TNTs display considerable similarities regarding their impressive mechanical, electrical, and optical properties. CNTs have promising results as drug delivery systems, but due to their high hydrophobicity, they accumulate in the human body, which leads to a risk of toxicity and carcinogenicity. Thus, CNTs are insoluble in aqueous solutions and cannot be used immediately in biomedical applications, whereas TNTs display strong hydrophilicity due to the capillary effect and their partially hydroxylated surface that can combine with hydrogen bonds, causing outstanding wettability. Moreover, TNTs display excellent biocompatibility due to their good wettability and therefore improve cell adhesion (3). Furthermore, the surface charge of CNTs is a function of the pH of the solution, but TNTs have negative ζ-potential due to their partially hydroxylated surface. Based on the

previously mentioned distinctive and promising characteristics of TNTs, we have selected them for further investigations.

2. AIMS

Tablets are the most common solid dosage form amongst marketed medicines and they enhance patient compliance thanks to their wide-ranging advantages. However, it has been detected that 60–70% of the drug molecules are poorly water-soluble and/or poorly permeable, which leads to difficulties in their absorption from the GIT following oral administration (7). Many approaches were taken to overcome this challenge, such as crystalline solid formulations, including salt formation and micronization of the crystalline compound (8), amorphous formulations, including solid solutions and other formulation strategies (9), and lipid formation, including solid dispersion (10). Nevertheless, these methods still face many obstacles, such as the unachievable salt formation of neutral compounds, the undesired particle size reduction of poorly wettable drugs, the uncertain physical stability of the product, potential drug or polymer crystallization, or low surfactant tolerance in chronic use (7). Therefore, poorly water-soluble and poorly permeable drugs still pose a major challenge to be manufactured as tablets.

TNTs have captivating characteristics, such as biocompatibility, hydrophilicity, surface chemistry, tunable geometries, and the ability to modify drug release kinetics (11). Furthermore, TNTs can load a higher amount of drug compared to CNTs (12) and TNTs are superior to CNTs from the aspect of processability, biocompatibility and wettability.
For this purpose, our study was performed to demonstrate the importance of not only the optimized TNT-drug composites as an oral drug delivery system, but also their functionalization effect on enhancing drug absorption from the GIT.

<u>The main hypotheses of my research work were as follows:</u>

I. The optimization of the product quality of TNT-drug composites may be achieved by choosing a solvent with proper characteristics, e.g., dissolving ability, protic-aprotic nature and evaporation properties.
II. The functionalization of TNTs enables their hydrophobicity to be tailored, thereby improving their permeability.
III. Functionalization will not affect the toxicity profile of TNTs negatively.

3. LITERATURE BACKGROUND

3.1. Preparation methods of TNTs

Titania (TiO_2) is distinctive among the different types of ceramics due to its special optical, chemical, and electrical properties. TiO_2 exists as rutile, anatase or brookite, which have different structural features. Furthermore, nanosized titania displays unique chemistry, in which its particle size, amount of structural defects and methods of synthesis hugely affect its stability, interphase transition and interfacial contact (13).

TNTs are classified according to the synthesis parameters used to prepare TNTs, such as template-assisted synthesis, hydrothermal treatments, or electrochemical treatments (5), which cause variations in their physical features (e.g., length, and inner diameter and outer diameter distributions).

Each preparation method has pros and cons. The electrochemical treatment results in self-organized TNT layers with large (~100 nm) diameter, suitable for the surface modification of Ti implants. However, the length varies (2–101 μm) and they are not suitable for many biomedical applications due to their size and potential clearance by the reticuloendothelial system (14). Template-assisted synthesis provides variable (50–400 nm) diameters based on the template pore size (15). Hydrothermal treatment produces small (5–10 nm) diameter and (100–1000) nm length with variable dimensions, porosity and specific surface depending on temperature, NaOH concentration, sonication and acidic post-treatment. However, nanosheets result as byproducts (~10% of batch) and the produced TNTs are strongly agglomerated, which need to be dispersed before bioapplication (14).

3.2. Applications of TNTs

Nanotubes have distinctive characteristics such as their biocompatibility, mechanical properties, hollow monolithic structure, considerable molecule-binding capacity and versatile binding mechanisms, which make them ideal carriers in pharmaceutical applications. Nanotubes can bind drugs by wrapping or filling; functional groups are used to attach the biological molecules to the surface in the former, whereas biological molecules are loaded inside nanotubes in the latter (16).

CNTs have been widely used in the medical field with promising results, such as using them in the diagnosis of diseases as biosensors (17), bone tissue-engineering as bioactive scaffolds (18), implanted catheters (19).

TNTs have so far been applied mainly in dentistry, orthopedics, and cardiovascular surgery (20). However, based on their unique properties, such as surface characteristics, chemical resistivity, biocompatibility, and promising toxicological profiles, they are also a promising technique as oral drug delivery systems.

3.3. Physicochemical properties of TNTs

CNTs display highly hydrophobic surfaces characteristics since they preserve the apolar characteristics of native graphene/graphite nanosheets, which leads to the blockage of body organ pathways and toxicity (21). Functionalization can improve their solubility and reduce their toxicity (19). However, there is still a need to find other alternatives with similar characteristics and better processability, wettability and biocompatibility.

By contrast, TNTs show strong hydrophilic characteristics due to their partially hydroxylated surface, and their combination with hydrogen bonds causes superior wettability (22) but often leads to the agglomeration of the particles, especially in dry forms (14). In addition, the hydrophilicity of TNTs is also supported by the capillary effect, resulting in the quick penetration of water droplets into the tube pores, and by their crystallinity, given that the amorphous, mixed crystalline phase shows high polarity because of the O–Ti–O bonds and the extensive presence of hydroxyl groups on the TNT surface. TNTs have good wettability due to their high surface energy and polarity, which improve cell adhesion and hence their biocompatibility; bone cell adhesion and differentiation were improved by the use of TNT-covered implants. Moreover, TNTs were nontoxic when internalized by cells (23). Therefore, TNTs are expected to have good applicability for therapeutic use in the clinic (24).

3.4. Functionalization

Functionalization is the attaching of appropriate molecules to the nanostructure surface to improve aqueous solubility, reduce toxicity, increase biocompatibility (25), achieve

targeted drug delivery, obtain selective binding to the desired epitope, achieve controlled drug release, facilitate cellular internalization, enhance bio-distribution, and improve biofluid circulation. Many types of functionalization molecules have been used, such as polyethylene glycol (PEG), polyvinylpyrrolidone (PVP), cellulose, polypeptides, dextran, and silica (26).

CNTs can be functionalized covalently or non-covalently on the tips and side walls, although CNT tips have a higher functionalization affinity compared with the side walls (25). Noncovalent functionalization, including Van der Waals interactions, π-π interactions and hydrophobic interactions, causes minimal damage to the CNT surface and maintains the aromatic structure and, consequently, the electronic characteristics of CNTs. However, the disadvantage is that this kind of functionalization is not appropriate for targeted drug delivery applications because of the weak forces formed (27). By contrast, covalent functionalization of CNTs can be achieved via oxidizing them by strong acids, such as nitric and sulfuric acids (28). Hence, the forming of carboxylic acid groups because of the high negative charge increases the hydrophilicity, water solubility, and biocompatibility of CNTs (29). By contrast, the disadvantage is that covalent functionalization damages CNT side walls and, thus, CNTs cannot be used in some applications, such as imaging (30).

Similarly, the surface characteristics, such as the negative charge at physiological pH caused by the presence of hydroxyl groups on their surface above their isoelectric point (pH 3.7), enable TNTs to react with a variety of functional molecules (31). The functionalization of TNTs improves their stability for vectorization applications and enables them to carry therapeutic molecules (32). Table 1 details the methods for the functionalization of TNTs.

Table 1: Functionalization possibilities of TNTs

Reagent(s)	Aim of functionalization/ grafting	Res
Dopamine; Tris buffer; with bone morphogenetic protein 2 (BMP_2)	Enhance bone osseointegration	(33)
3-isocyanatopropyltriethoxy Silane; PEG; PEI	Enhance the dispersion of TNTs in water and their surface reactivity	(34)
Allyltriethoxysilane; propyltriethoxysilane	Form stable suspensions in THF	(35)
Antimicrobial peptides (HHC-36)	Prevent formation of biofilms (based on bactericide and bacteriostatic effects)	(36)
APTES; RGD peptide	Promote initial attachment and proliferation of hMSCs	(37)
KRSR	Increase osteogenic differentiation and preosteoblast adhesion and spreading on the TNT surface	(38)
CDI; PhoA; EGF and BMP_2 growth factors	Increase number and activity of MSCs	(39)
Gelatin-stabilized gold NPs	Improve MC3T3-E1 osteoblast cell adhesion and propagation (achieved)	(40)
Chitosan	Achieve sustained release of loaded drug (selenium or quercetin) from TNTs	(41, 42)

3.5. Solid state dispersion

Conventional drugs face many obstacles, such as limited solubility, poor pharmacodynamics, low selectivity and side effects. Most of the current drugs on the market are hydrophobic and poorly soluble or insoluble in water, which restricts their systemic delivery (43). Drugs in the oral administration route ought to be released and dissolve before absorption. Therefore, many approaches have been used to improve their bioavailability, such as particle size reduction, solid-state alternation, complexation, solid dispersions, soft gel technology, forming emulsions, microemulsions, micelles, polymeric micelles, liposomes, pharmaceutical salts, and pro-drugs (44).

Particle size reduction causes an increment in the specific surface area and thus in dissolution rate and absorption (45) although the stabilization of particle size can be a critical issue. On the other hand, solid state dispersion can not only improve the solubility, dissolution rate, and bioavailability of poorly water-soluble drugs, but also sort out the stability problems of micronized/nanonized drugs due to their dispersion in an inert solid carrier or matrix as fine particles or molecularly (46). This approach has other advantages,

such as increasing the glass transition temperature of the solid dispersion matrix (47), boosting stability due to the potential interactions between the drug and carrier functional groups (48), or the displacement of crystalline structure by an amorphous form (49), which leads to local solubility and wettability improvement of poorly soluble drugs (50) and higher solubility and dissolution rate for the metastable drug polymorphs connected to the carrier due to the suppression of drug precipitation from the supersaturated solution (51). Solid dispersions can be classified into many categories, including solid solutions, drug–carrier complexes, glassy solutions or suspensions, simple eutectic mixtures, and amorphous drug precipitates in a crystalline carrier. The preparation method of solid state dispersions can vary, including the fusion process, the solvent method, the fusion-solvent method, spray drying, lyophilization, hot-melt extrusion, the electrospinning method, supercritical fluid technology, and spraying on beads using a fluidized-bed coating system (44).

In the solvent method, both the drug and the carrier dissolve in a suitable solvent. After that, the solvent evaporates at an elevated temperature or under vacuum. The components are supersaturated and simultaneously precipitated, leading to a solid residue. The advantages of this method are the ability to control drug particle size by monitoring the temperature and the solvent evaporation rate (45), the capability of evaporating solvents at a lower temperature, and reduced pressure for thermolabile drugs or for frozen systems. The drawbacks of this method are the difficulty of choosing the appropriate solvent for both the drug and the carrier, since most of the carriers are hydrophilic, while the drugs are hydrophobic (52), the necessity of complete solvent removal, especially if the solvents can plasticize the carrier (53), and the large volume of solvent required to dissolve both the drug and the carrier, which is not economical in some cases (44). It is important to totally remove the organic and/or toxic solvents from the system under vacuum. For this purpose, many sensitive techniques can be used to detect the trace amounts of solvents, such as differential scanning calorimetry (DSC), thermogravimetric (TG) analysis, or differential thermal analysis (DTA) (44).

In the present work, we tried to improve the bioavailability of poorly water-soluble and poorly permeable drugs by dispersing them in TNTs as a solid carrier using the solvent method.

3.6. Toxicity of nanotubes

3.6.1. Toxicity of CNTs

CNTs have highly hydrophobic surfaces, which leads to the accumulation of highly apolar molecules in the tissues, resulting in the blockage of body organ pathways and toxicity. Nonetheless, many factors affect the toxicity of CNTs, such as size, shape, purity, surface chemistry, and the existence of transition metal catalysts (54). Furthermore, the toxicity of CNTs is related to their administration route, in which mild symptoms were observed after intravenous, oral and dermal administration, while severe inflammation with toxicity in the respiratory system was reported after inhalation (3). However, no significant lung inflammation or tissue damage was noticed after direct inhalation of CNTs according to another study (3).

3.6.2. Toxicity of titanium dioxide nanoparticles

Titanium dioxide nanoparticles (TiO_2 NPs) are widely used in various fields, such as food, agriculture, environmental protection or medicine, building engineering and cosmetic industry (55). TiO_2 NPs exist in three different crystal structures: as anatase, rutile, and brookite (56), which differ in the Ti-O bond length range, which is 1.931-2.004 Å for rutile, 1.914-2.005 Å for anatase and 1.850-2.099 Å for brookite (Fig 1).

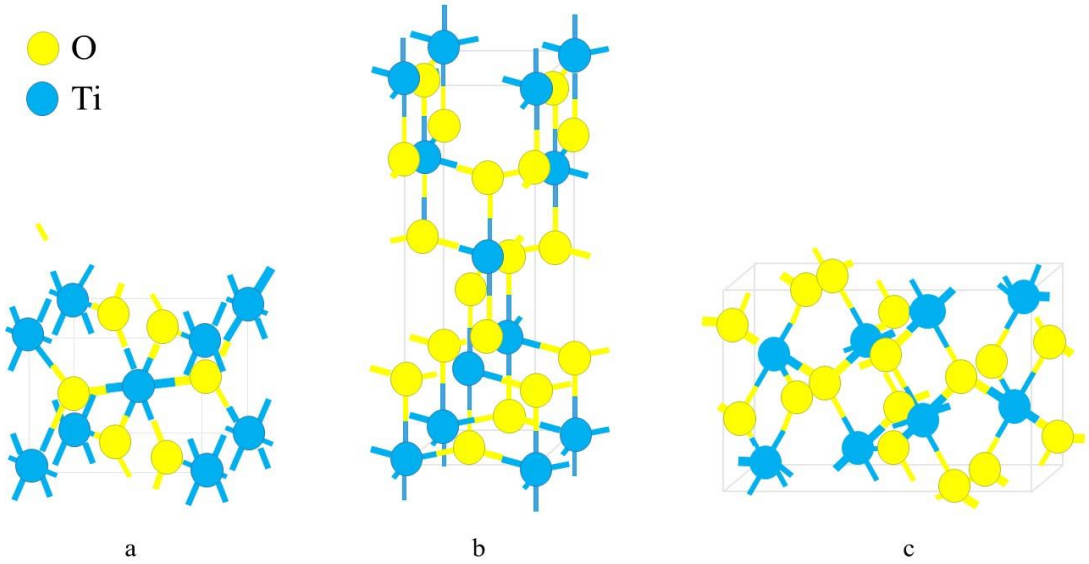

Figure 1. The primitive unit cell of (a) rutile, (b) anatase and (c) brookite TiO_2.

Anatase has more industrial applications because of its photocatalytic activity, though it is the most toxic form in comparison to rutile and brookite (56). Furthermore, the global market released 117 various products in the food and beverage field based on nanotechnology (57). Using TiO_2 NPs in foodstuff is permissible in the USA and Europe where its percentage does not exceed 1% of the total product weight in the former and the quantum satis concept is applied in the latter (58). In Great Britain, children up to 10 years old can take 2–3 mg TiO_2 NPs/1 kg of body weight (bw) per day, whereas adults can take about 1 mg TiO_2/kg bw/day (56). Nonetheless, there has been much debate on the safety of TiO_2 NPs due to their various applications in food industry, regarding toxicity considerations. The International Agency for Research on Cancer (IARC) classified TiO_2 NP pigment as a prospective carcinogenic factor from group 2B (59). On the other hand, the European Food Safety Authority (EFSA) was not concerned about E171 (titanium dioxide) safety in 2016 (58). However, there is still no sufficient research data on the acceptable daily intake of TiO_2 NPs and the safety margin was determined as 2.25 mg TiO_2 NPs/kg bw/day based on tests involving animals (58).

The toxicity of TiO_2 NPs in the human body is mostly linked to apoptosis (60) and might lead to DNA damage (61) and disturb glucose and lipid homeostasis in mice and rats according to some studies. Moreover, TiO_2 NPs might accumulate after inhalation or oral exposure in the heart, cardiac muscle, lungs, alimentary tract, liver, kidneys and spleen

(62). The toxicity and accumulation of TiO_2 NPs in body organs are affected by the size of the nanoparticle, since after one single dose of oral administration to mice particles with 80 nm diameter accumulated in the liver, while particles with the size of 25 nm assembled in the spleen and slightly in the lungs and kidneys (63).

PEG alters TiO_2 NPs properties by reducing the cytotoxicity and the stress-related stimulation of genes (64). The presence of PEG, combining catalytic chain transfer and thiolene polymer layers around TiO_2 NPs, reduces protein adsorption onto their surface and adjusts particle surface chemistry, which lead to an increment of cellular uptake and reduction of the cytotoxicity of human lung epithelial cell lines A549 and NCI-H1299 (65).

The transfer of TiO_2 NPs from the gastro-intestinal tract (GIT) into blood circulation is influenced by many factors, such as species, type of nanoparticles, size, dispersability or particle charging (66). According to recent studies, TiO_2 NPs were scarcely absorbed from the GIT in humans and rats. In addition, their particle size did not affect absorption after administering various particle sizes (15 nm/100 nm/ < 5000 nm) as a single dose of TiO_2 NPs (5 mg/kg bw/day), which may correlate with their hydrophilicity (67).

3.6.3. Toxicity of TNTs

TNTs are remarkable compared to other TiO_2 derived nanomaterials in application fields due to their nanotubular structure (68). TNTs are superior to CNTs from the aspect of toxicity; TNTs displayed no cytotoxicity on A549 lung epithelial cell lines compared to CNTs in a 7-day incubation study (69). In addition, another study showed that TNTs exhibited no cytotoxicity on Caco-2 cells up to 5 mg/mL concentration in short-term treatment. However, non-tubular high-density granules were identified as TiO_2 NPs on the surface of the endoplasmic reticulum in the treated cells because they could pass into the Caco-2 monolayer. Thus, hydrothermal TNTs are auspicious carries for intestinal drug delivery (24). Nonetheless, it should be considered that the surface characteristics such as its charge highly influence the cytotoxicity of TNTs. Sodium titanate Na_xTiO_{y+z} displays low toxicity (68-69) in comparison to hydrogen titanate H_xTiO_{y+z}, which poses a considerable cytotoxic risk on H596 human lung tumor cell line (69, 70) and on HEp-2 cells (71). Likewise, manganese and potassium titanate nanotubes and nanofibers promoted reactive oxygen species in some mammalian cell lines (72, 73).

TiO_2 nanostructures have been reported to increase the risk of neurological events risk after passing the blood–brain barrier (74, 75). Other studies reported the accumulation of unmetabolized TiO_2 nanostructures in some organs such as the liver and spleen, and with a less degree in the brain, kidneys, lungs, GIT and heart (76, 77). Many factors play a role in the tissue distribution of TiO_2 nanostructures such as their morphology (78), size and surface charge (79, 80). Different tissue distribution and toxicity profiles were demonstrated after a single and successive intravenous administration of TiO_2 nanotubes, rods, and ribbons in rats, in which nanotubes displayed the most toxic effect and the largest accumulation, following that nanorods and ribbons (80).

The biodistribution and excretion of TNTs also are highly affected by their physicochemical properties like their hydrophilicity, surface charge, and hydrodynamic diameter (dH), in which small NPs with dH < 6 nm could be cleared through the kidneys, while larger NPs with dH > 6 nm could be eliminated through the liver and reticuloendothelial system (RES). The clearance of NPs from the body could be increased partially by polymer coatings or fastly by surface charge due to the adsorption of plasma proteins (14).

Ren et al, investigated the toxicity, uptake pathways and excretion of TNTs in three strains of free-living ciliates of the genus Tetrahymena which are a wild type strain (SB210) and two mutant strains (SB255, NP1). The results revealed that TNTs caused cytotoxicity in high concentrations. Using 10 mg/l of TNTs for 120 min resulted in their accumulation in NP1 and SB255 in a higher or comparable percentage comparing to SB210, whereas using 10 mg/l of TNTs for 24 h caused a larger decline in cell density of NP1 (38.2 %) and SB255 (36.8 %) in comparison to SB210 (26.5 %) (81).

4. MATERIALS

4.1. Hydrothermally synthetized titanate nanotubes and their composites

TiO_2 and NaOH were used to prepare the hydrothermal TNTs. HCl 0.01 M was used to prepare TiHCl. Atenolol (ATN) (TEVA Pharmaceuticals PLC, Debrecen, Hungary), methanol (0.0168% water content) (Molar Chemicals Kft, Hungary) and 0.01 M aqueous solution of HCl (HCl 0.01 M) (Molar Chemicals Kft, Hungary) were applied to prepare TNT-ATN composites (TiATN). Hydrochlorothiazide (HCT) (TEVA Pharmaceuticals PLC, Debrecen, Hungary), 1 M aqueous solution of sodium hydroxide (NaOH 1M) (Molar Chemicals Kft, Hungary), DMF (0.012% water content) (Molar Chemicals Kft, Hungary), and DMSO (0.027% water content) (Molar Chemicals Kft, Hungary) were used for the synthesis of TNT-HCT (TiHCT).

4.2. Functionalization

Trichloro-octyl-silane (TCOS) (Sigma-Aldrich, St. Louis, Missouri, United States) and Sodium stearate (NaSt) (VWR International, Radnor, Pennsylvania, United States) and $MgCl_2$ (Molar Chemicals Kft, Hungary) were used to functionalize TNTs.

5. METHODS

5.1. Preparation of TNTs and their composites

5.1.1. Hydrothermal synthesis of TNTs

5.1.1.1. Pristine sodium trititanate ($Na_2Ti_3O_7$) nanotubes (TNTs)

120 g of NaOH was added to 300 mL of distilled water on a magnetic stirrer for a few minutes and then 75 g of TiO_2 (anatase) for 15 min was added. The mixture was put in the autoclave inside an oven at 185 °C for 24 h and then cooled at room temperature for 2 h, followed by cooling with cold water. After that, TNTs were washed with distilled water under vacuum and by using filter No#4.

5.1.1.2. Hydrogen trititanate ($H_2Ti_3O_7$) nanotubes (H-TNTs)

A homogenous suspension was prepared by adding 50 g of TNTs in 300 mL of HCl 0.01 M in an ultrasonic bath. After that, 200 mL of HCl 0.01 M was added to the previous suspension on a magnetic stirrer and the mixture was dried in a drying oven for 24 h to remove the solvent.

5.1.1.3. Magnesium trititanate ($MgTi_3O_7$) nanotubes (Mg-TNTs)

100 g of Na-TNT was added to 1L of 0.1 M $MgCl_2$ solution on a magnetic stirrer for 1 day. Then, the mixture was filtered by using glass filter No#4 under vacuum to obtain Mg-TNTs. This procedure was repeated three times to make sure that no Na-TNTs existed anymore. Finally, Mg-TNTs were washed with distilled water 8 times under vacuum and by using glass filter No#4.

5.1.2. Preparation of TNT-drug composites

5.1.2.1. TiATN- Methanol

Figure 2. represents the general flow chart of the preparation of TNT-drug composites on the example of TiATN-methanol composites.

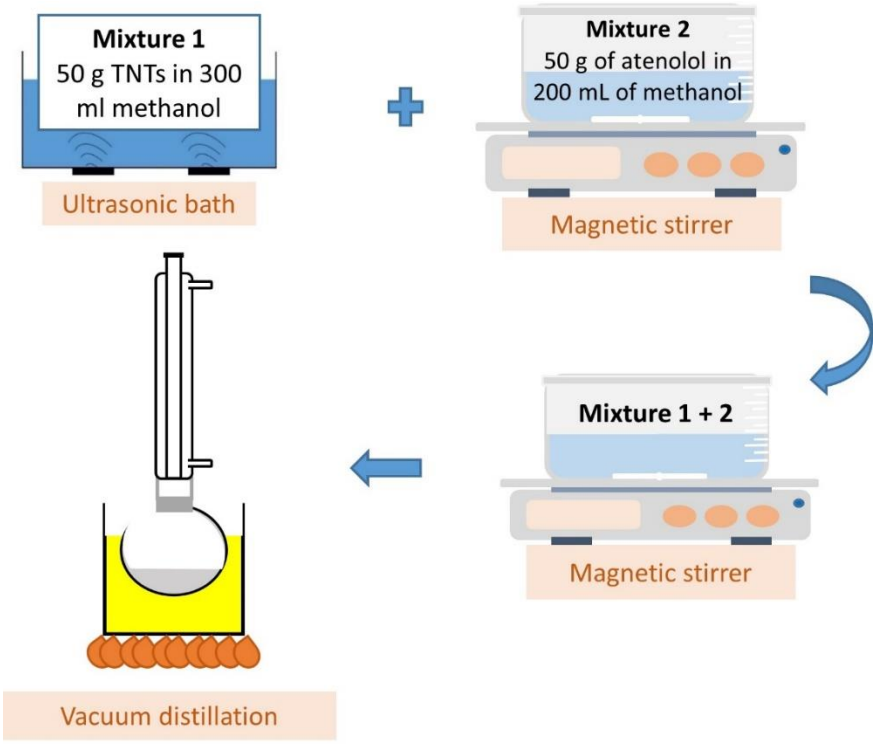

Figure 2. Preparation scheme of (1:1) TiATN composites using methanol as solvent.

5.1.2.2. TiATN-HCl/ TiHCT-DMF/ TiHCT-DMSO

1:1 ratio of TiATN-HCl, TiHCT–DMF and TiHCT–DMSO composites were prepared by adding 50 g of TNTs in 1000 mL of the respective solvent in an ultrasonic bath, and 50 g of ATN or HCT with 1000 mL of the solvent on a magnetic stirrer. Then, the two prepared mixtures were added to each other on a magnetic stirrer until a homogenous mixture was obtained, which was put in a vacuum distillation device to remove the solvent.

5.1.2.3. TiHCT-NaOH

1:1 ratio of TiHCT–NaOH composite was prepared by adding 50 g of TNTs to 1000 mL of NaOH 1 M in an ultrasonic bath to get a homogenous suspension, and 50 g of HCT in 500 mL of NaOH 1 M on a magnetic stirrer until complete dissolution. Then the two prepared mixtures were added to each other on a magnetic stirrer until reaching homogeneity. After that, 130 mL of HCl 37% was added to neutralize the final mixture,

which was washed with distilled water in a vacuum dryer until pH = 9 to eliminate the solvent. Finally, the obtained powder was dried in a drying oven (Sanyo Electric Co., Ltd, Osaka, Japan) for 24 h to get the required composite.

5.2. Functionalization of TNTs

5.2.1. TCOS-TNTs

For functionalization with TCOS, hydrogen trititanate ($H_2Ti_3O_7$) nanotubes (H-TNTs) were prepared by ion exchange via the washing of TNTs with HCl. TOCS-TNTs were prepared by adding 0.5 g of H-TNTs to 15 mL of toluene in ultrasonic bath for 1 h until a homogenous suspension was obtained. After that, the suspension was heated to 80 °C in a condenser, which was connected to nitrogen gas for 30 min. Then, TCOS reagent was added to the previous system in different concentrations, e.g. 1- 2- 10- 50- 100- 500- 1000 µl, covering the 0.001:1 - 2:1 molar ratios, respectively and mixed for one day. Finally, the functionalized TNTs were washed by hexane 8 times and dried in a drying oven at 80 °C.

5.2.2. MgSt- TNTs

10 g of Mg-TNTs was added to 200 mL of distilled water in ultrasonic bath for 30 min. Following that, the mixture was heated to 80 °C in a magnetic stirrer (Thermo Fisher Scientific, Waltham, MA, USA) and Na stearate was added in different (e.g. 0.001:1-0.1:1) molar ratios to this system for 1 night. Finally, St-TNTs were filtered by using filter No#4 under vacuum and dried in a drying oven.

5.3. Morphology and size investigation

Scanning electron microscope (SEM) (Hitachi 4700, Hitachi Ltd., Tokyo, Japan) and transmission electron microscope (TEM) (FEI Tecnai G2 20 X-TWIN, Hillsboro, OR, USA) were used to study the morphology and size of TNTs. The APIs, TNTs, and the composites were coated with a thin conductive gold layer by a sputter coating unit (Polaron E5100, VG Microtech, London, UK) for the SEM measurements. The images were taken at an accelerating voltage of 10.0 kV, the used air pressure was 1.3–13 mPa during the

analyses. TEM images were taken at 100 kV of electron energy, and those images served to analyze the particle size of TNTs by using Image J 1.47 t (National Institute of Health, Bethesda, MD, USA) software.

5.4. FT-IR spectrophotometer

The interactions between the APIs and the TNTs were determined by using a Thermo Nicolet Avatar 330 FT-IR spectrometer (Thermo Fisher Scientific Ltd., Waltham, MA, USA). Measurements were conducted with a Transmission E.S.P. accessory by using 256 scans at a resolution of 4 nm and applying H_2O and CO_2 corrections. Spectragryph 1.2.8 software (Friedrich Menges, Obersdorf, Germany) was used to evaluate the results. For better comparability of the original spectra of raw materials with their composites, the signal of TNTs was subtracted from the composite spectra and the spectra were normalized to the highest peak which belongs to C=O stretching.

5.5. Surface free energy measurement

The surface free energy was determined with a DataPhysics OCA20 (DataPhysics Instruments GmbH, Filderstadt, Germany) optical contact angle tester by using the sessile drop method. Water and diiodomethane were applied as the polar and apolar test liquids by dropping them onto the surface of 13-mm-diameter tablets prepared with a Specac hydraulic press (Specac Ltd., Orpington, UK) at a pressure of 3 tons. Wu Equations (1) and (2) were used to calculate the disperse (γ_s^D) and polar (γ_s^P) components of the total surface free energy (γ_s) of the solid.

$$(1-\cos\Theta_1)\gamma_1=4(((\gamma_1^D\gamma_s^D)/(\gamma_1^D+\gamma_s^D))+((\gamma_1^P\gamma_s^P)/(\gamma_1^P+\gamma_s^P))) \quad (1)$$

$$(1-\cos\Theta_2)\gamma_2=4(((\gamma_2^D\gamma_s^D)/(\gamma_2^D+\gamma_s^D))+((\gamma_2^P\gamma_s^P)/(\gamma_2^P+\gamma_s^P))) \quad (2)$$

Where γ_1 and γ_2 are the surface tension of the first and second liquids, respectively. Polarity was calculated according to Equation (3):

$$\text{Polarity} = \gamma_s^P / \gamma_s * 100 \quad (3)$$

5.6. Thermoanalytical analysis

Thermogravimetric analysis (TGA) and differential scanning calorimetry (DSC) were utilized to investigate the thermal behavior of TNTs, APIs, and composites. A TGA/DSC1 simultaneous analyzer (Mettler-Toledo Ltd., Budapest, Hungary) was used to carry out TGA and DSC tests, in which the samples were heated steadily from 25 to 500 °C with a heating rate of 10 K/min, using nitrogen as purge gas. The mass of the samples was 10 ± 1 mg in a closed aluminum pan (100 µL). STARe Software (Mettler-Toledo Ltd, Budapest Hungary) was used to assess the obtained curves, where the curves of APIs, TNTs, and the composite were compared by normalizing the results to sample weight and to the temperature of the reference pan.

5.7. Drug release

A DT700 (Erweka GmbH, Heusenstamm, Germany) dissolution tester was used to study drug release using the USP II method and a dissolution media of pH 1.2 enzyme-free artificial gastric juice at 37 °C. Samples of 5 mL were taken after 5 min, 10 min, 15 min, 30 min, 60 min, 90 min, and 120 min. A GENESYS 10S UV–VIS spectrophotometer (Thermo Fisher Scientific Ltd., Waltham, MA, USA) was used to measure the concentrations of the released drug, which were assessed with Sigmaplot v12 (Systat Sofware Inc., San Jose, CA, USA) software.

5.8. CHNS elemental analysis

The content of carbon, hydrogen, nitrogen, and sulphur in organic materials was investigated rapidly by conducting CHNS elemental analysis. A Vario EL cube elemental analyzer (Elementar, Langenselbold, Germany) was used to analyze H, C, N, and S contents in the samples. 50 to 100 mg of samples (no flux added) were ignited in an

oxygen–He gas atmosphere furnace at around 1150 °C and filled in Sn-foils. A set of chromatographic columns with a thermal conductivity detector was used to detect the resulting gases containing N, C, H, and S. The sample measurement time was 9 mins and was repeated 3 times, and the values were calibrated against the reference materials BAM-U110, JP-1, and CRPG BE-N.

5.9. Cytotoxicity and permeability detection

Unfunctionalized nanotubes (Na-, H- and Mg-TNTs), and samples with the possible highest, and moderate hydrophobicity were selected form TCOS- and St-TNT series were selected for toxicity and permeability tests. Permeability and cytotoxicity experiments were tested on a Caco-2 human adenocarcinoma cell line. Cells were maintained at 37 °C in a 5% CO_2 atmosphere by regular passage in Dulbecco's modified Eagle's medium (Sigma–Aldrich), supplemented with 2 mM L-glutamine, 100 mg/L gentamycin and 10% heat inactivated foetal bovine serum (Sigma-Aldrich). The passage number of the cells was between 25 and 42. Dulbecco's modified Eagle's medium (Sigma–Aldrich) was used to keep the cells' regular passage of 25 to 42 on average. Both experiments were performed 7 days after cell passaging when the monolayer was formed. The reagents were purchased from Sigma-Aldrich (Budapest, Hungary) and the Caco-2 cell line was obtained from the European Collection of Cell Cultures (UK). The cells had been monitored before and after the treatment via Olympos CKX41 Inverted Microscope by eye estimation. The monolayer did not show any alteration during the procedure.

5.9.1. Cytotoxicity test

Cytotoxicity was tested by the 3-(4,5-dimethylthiazol-2-yl)-2,5-diphenyltetrazolium bromide (Sigma catalog no. M2128) (MTT) assay in which Caco-2 cells were implanted in 96-well plates at a final density of 10^4 cells/well (VWR International, Radnor, Pennsylvania, United States) and exposed to increased concentrations of TNT in Hank's balanced salt solution (HBSS) at 37 °C for 120 min.

The 5 mg/ml solution of MTT in PBS was filtered to sterilize and remove the remaining insoluble residue of MTT. The MTT solution (10 µl/100 µl medium) was added to all wells

which were incubated at 37°C for 4 h followed by the addition of HCl-isopropanol which was mixed rigorously to dissolve the dark blue crystals. Within one hour, the plates were read on a Dynatech MR580 Microelisa reader using a test wavelength of 570 nm, a reference wavelength of 690 nm and a calibration setting of 1.99 (or 1.00 if the samples were strongly colored). Extreme high concentrations were applied to evaluate MTT test sensitivity in these measurements. To exclude any interferences between the absorbance of living cells performed formazan crystals and the test solutions, a phosphate buffer (PBS) washing method had been deployed after the TNTs sample incubation. Cell viability was represented as a percentage of the untreated control.

5.9.2. Permeability test

To test permeability, Caco-2 cells were seeded on ThinCert™ (Greiner Bio-One, Hungary) inserts at a final density of $8x10^4$ cells/insert, and monolayers were incubated apically with 2 ml of 1 mg/ml TNT for 120 min after removing cell culture medium. The donor and acceptor phases were then completely removed. The concentration of Ti in the two phases were measured with an energy dispersive X-ray fluorescent analyzer (Philips MiniPal PW 4025, Philips Analytical, the Netherlands), using standard sample holder, with a 3.6 μm thick polyesterpetp X-ray film. The internal diameter of the sample holders was narrowed to 8 mm to ensure approx. 1 cm layer thickness, with 500 μL sample volume. 30 s measurement time was applied with 100 μA current and 8 kV acceleration voltage, using Kapton filter. For calibration, a series of standards were prepared by dissolving TiO_2 in phosphate buffered saline, with a Ti content of 10, 50, 100, 200, 500 and 1000 ppm, respectively, where 10 ppm equals with the approximate limit of detection. The accuracy of the method is 1 ppm. The R^2 of the calibration curve was 0.9987. Six parallel measurements were performed with each sample.

6. RESULTS AND DISSCUSSION

6.1. Optimization of the composite formation process and product quality

Based on the results of a previous study (82), the quality of TNT-drug composites is also related to the parameters of the chosen solvent. Thus, in our first hypothesis the protic-aprotic nature, the volatility and the solubility of drugs were identified as key factors of optimal solvent selection, in which a strong interaction between the drug and the carrier could be achieved. The characteristics of the produced TNT-drug composites were investigated by using SEM, TEM, OCA, TG/DSC and FT-IR measurements. Additionally, a UV-VIS dissolution tester was utilized to test the drug release profile.

6.1.1. Properties of the TNT and TNT-HCl

TNTs prepared by hydrothermal synthesis have an asymmetric, open-ended, and particular spiral cross-sectioned tubular structure (82). The first step of our study was to test the reproducibility and robustness of the previously described synthesis method of TNTs (82) to ensure constant quality since the synthesis conditions strongly affect the dimensions and surface characteristics of TNTs.

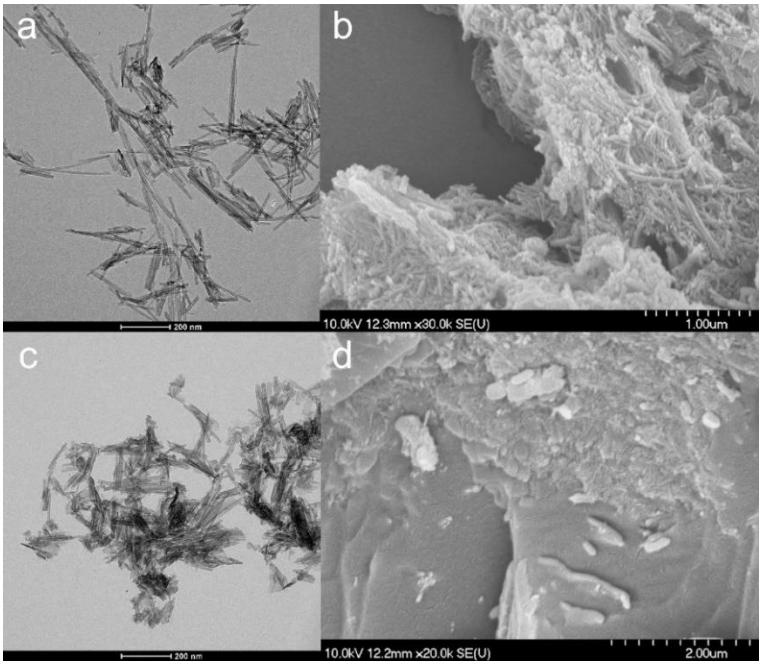

Figure 3. TEM (**a**,**c**) and SEM (**b**,**d**) micrographs of TNTs (**a**,**b**) and TNT–HCl 0.01 M (**c**,**d**) samples

The TEM images (Figure 3a) showed that the preparation method was successful in which TNTs were produced without nanowire formation, where the average length of TNTs was 116.22 nm (SD ± 49.49 nm) and the average diameter was 10.99 nm (SD ± 10.15 nm), which considerably approaches the previously described results of Sipos et al. (82).

The SEM images (Figure 3b) displayed the characteristic aggregates of almost distinct and randomly oriented TNTs. Furthermore, there was no considerable difference in the surface characteristics of the new and the previous batch of TNTs according to the contact angle measurements (Table 2).

Table 2: Surface free energy and polarity of TNTs, atenolol (ATN), hydrochlorothiazide (HCT), and their composites.

Material	γ_S (mJ/m²)	SD	γ_S^{Disp} (mJ/m²)	SD	γ_S^{Pol} (mJ/m²)	SD	Polarity%
TNTs (previous)	80.72	±0.64	43.78	±0.54	36.94	±0.35	45.76
TNTs (current)	80.85	±1.18	44.55	±0.53	36.31	±1.04	44.90
TNT-HCl	78.63	±2.07	43.10	±0.27	35.53	±2.05	45.19
ATN	59.48	±3.99	36.70	±2.96	22.77	±2.68	38.20
TiATN-ethanol	60.14	±4.25	40.45	±1.48	19.68	±3.87	32.72
TiATN-methanol	58.04	±2.01	37.12	±1.19	20.92	±1.47	36.04
TiATN-HCl	68.37	±2.26	34.83	±0.05	33.54	±2.26	49.06
HCT	69.51	±2.71	43.33	±0.79	26.18	±2.59	37.60
TiHCT-ethanol	78.25	±0.86	44.65	±0.57	33.60	±0.64	42.93
TiHCT-NaOH 1M	77.54	±1.89	44.52	±0.80	33.02	±1.71	42.59
TiHCT-DMF	71.47	±2.63	42.53	±0.29	28.94	±2.63	40.49
TiHCT-DMS	73.92	±1.42	45.29	±0.08	28.63	±1.42	38.72

The effect of diluted 0.01 M HCl on the properties of TNTs was tested by preparing TNT–HCl samples as a reference, since the nanotubular structure may be decomposed in the strong acidic media (Figure 3c,d). The TEM images showed a slight decrease in the dimensions of TNT-HCl compared to native TNTs, with an average length of 83.92 nm (SD ± 42.48 nm) and an average diameter of 8.78 nm (SD ± 1.76 nm). Nevertheless, neither the surface characteristics (Table 2) nor the FT-IR spectrum (Fig. 4) displayed a considerable difference from the results of native TNTs. Therefore, no noteworthy difference was expected in the behavior of TNT and TNT–HCl from the aspect of composite formation ability.

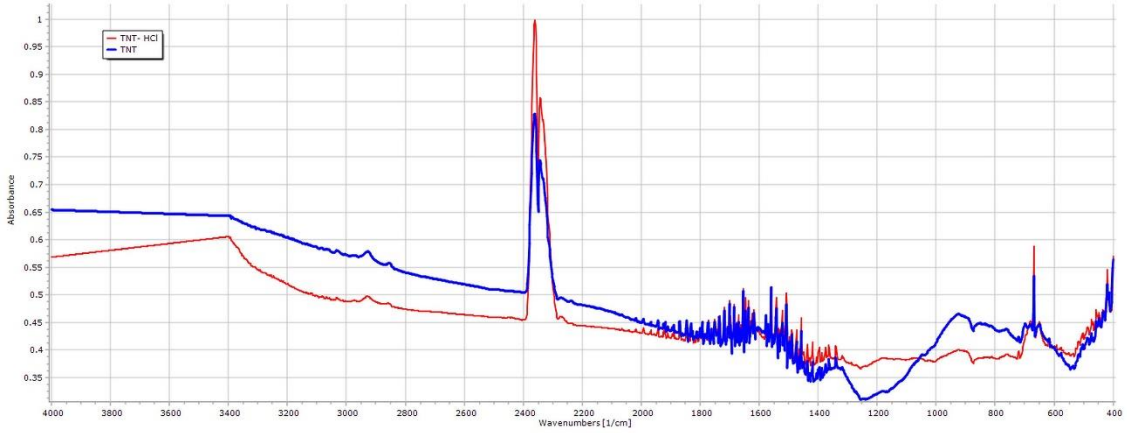

Figure 4. FT-IR spectra of TNTs and TNT–HCl 0.01 M.

6.1.2. Effect of various solvents on composite formation with ATN

In the previous study of Sipos et al. (82) it was confirmed that composite formation was insufficient for TiATN-ethanol (Fig. 5b) since both the aggregates of TNTs and the smooth surfaced particles of crystalline ATN (Fig. 5a) were clearly visible in the SEM images. A stronger interaction but still insufficient composite formation was observed in the TiATN-methanol sample (Fig. 5c), in which a strong surface coverage of ATN particles with TNTs could be noticed. Interestingly, a more adequate composite formation and the accumulation of ATN nanocrystals on the surface of the composite without the existence of individual ATN crystals was achieved in TiATN-HCl (Fig. 5d), where a rough surface and highly ordered aggregations were detected.

The OCA measurement (Table 2) showed that the γs for TiATN-ethanol, TiATN-methanol and ATN were almost identical to each other, which may indicate not pure TNTs but TNT-ATN composites aggregated to the surface of bigger ATN particles. In contrast, distinctly different values of γs and polarity for TiATN-HCl were detected, which may reflect not only a kind of interaction between NH_3^+ from ATN and the hydrophilic sites in TNTs enriching the hydrophobic regions in TNTs, but also a different particle forming mechanism than in the case of other solvents, which leads to a different expected behavior during processing and use.

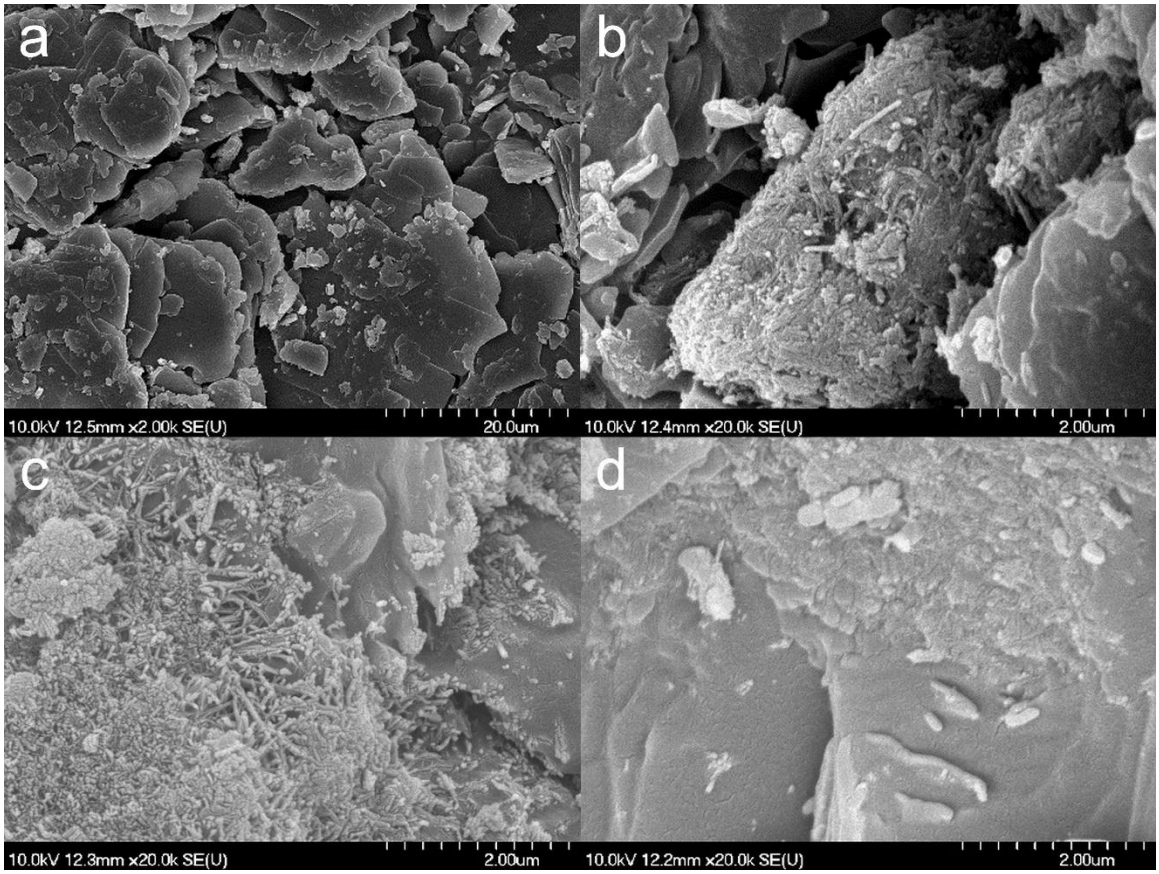

Figure 5. SEM micrographs of atenolol (a), TiATN-ethanol (b), TiATN-methanol (c), and TiATN-HCl 0.01 M (d).

However, the results obtained from the morphological investigations were only partially supported by the DSC/TG and FT-IR measurements. Fig. 6 displays that the DSC curve of ATN contains an endothermic and a broad exothermic peak. The sharp endothermic peak at 155.21 °C represents the fusion of the compound and the exothermic peak describes its decomposition, which is supported by the TG curve of ATN. Likewise, TiATN-ethanol and TiATN-methanol composites have an endothermic peak at 161 °C and 159.84 °C, respectively. The enthalpy of fusion declined from -154.795 Jg^{-1} in ATN to -74.97 Jg^{-1} and -50.71 Jg^{-1} in TiATN-ethanol and TiATN-methanol, respectively, which may indicate the poor composite formation when using ethanol or methanol as solvents. Only a minor size reduction may be achieved in the case of TiATN-methanol. On the other hand, a higher shift in fusion temperature and a significant decrease in fusion enthalpy to -40.55 Jg^{-1} were detected in the TiATN-HCl composite, which may be due to the stronger interactions and the considerable particle size reduction of ATN (83).

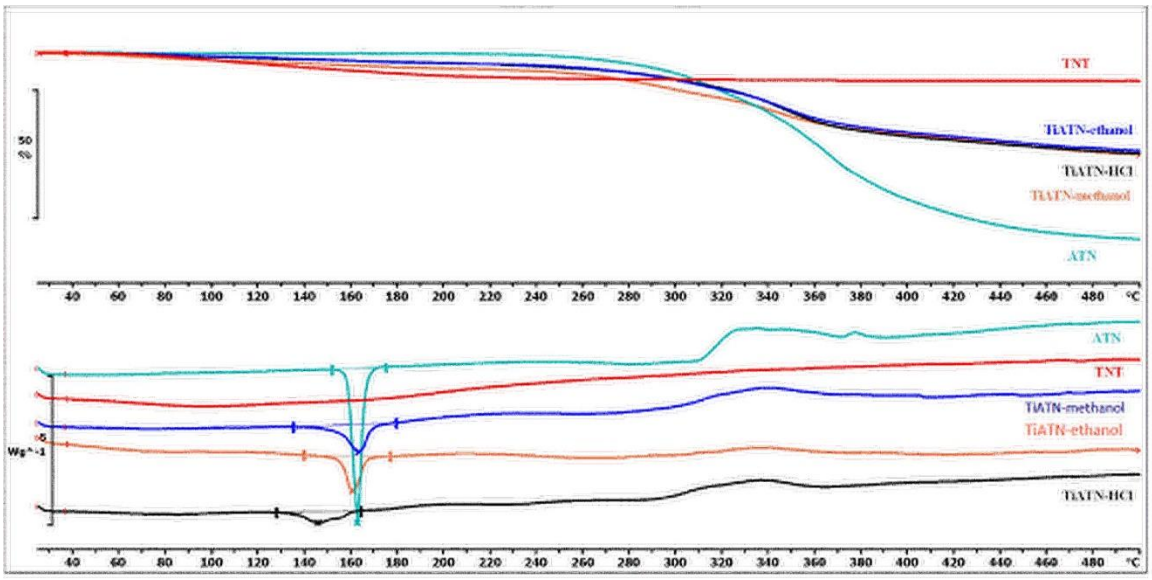

Figure 6. DSC and TG curves of TNT, ATN, TiATN-methanol, TiATN-ethanol and TiATN-HCl

These results were in accordance with the SEM images, where less crystallization was observed and they were also supported by the FT-IR spectra, which displayed no substantial differences between the spectra of ATN, TiATN-ethanol and TiATN-methanol (Fig. 7). On the other hand, changes in the TiATN-HCl spectrum were observed, namely the appearance of a new peak at 1560 cm^{-1}, indicating the protonation of the carbonamide group and wide low intensity peaks between 1900-2100 cm^{-1} and 2300-2500 cm^{-1}, indicating the protonation of the secondary amino group.

For better comparability, the spectra of ATN and its composites were normalized to the C=O stretching peak at 1637 cm^{-1} (Fig. 7). The non-considerable differences in the characteristic peaks of pure ATN at 2964 cm^{-1} (C-H stretching in CH_3), 2922 cm^{-1} (C-H stretching in CH_2), 2865.8 cm^{-1} (C-H stretching), 1614 cm^{-1} (conjugated C=C in the aromatic ring), and 885.9 cm^{-1} ($C=CH_2$ vibrations) suggest that the C-C skeleton of the molecule is not affected by the composite formation process. Nevertheless, the minor left-shift of the peak at 2800 cm^{-1} indicates the involvement of the secondary amino group in the drug-carrier interactions in TiATN-HCl samples.

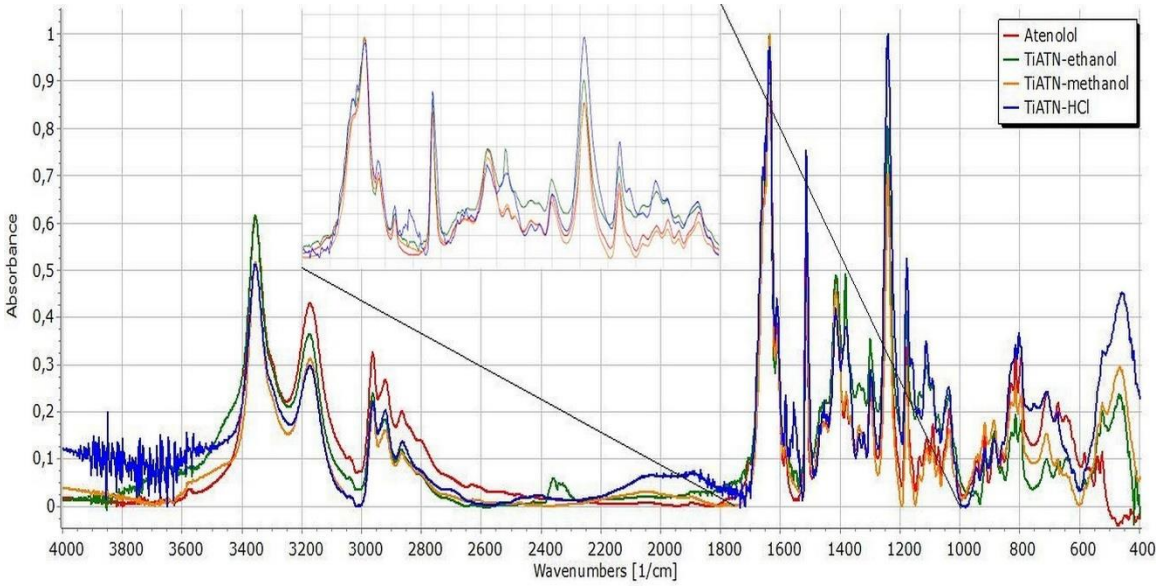

Figure 7. FT-IR spectra of ATN, TiATN-ethanol, TiATN-methanol and TiATN-HCl0.01M.

TiATN-methanol and TiATN-HCl showed a considerable decrease in the relative intensity at 3356 cm^{-1} compared to ATN and TiATN-ethanol, which indicates the participation of the secondary -OH as a hydrogen donor in TNT-ATN conjugation. In addition, TiATN-methanol and TiATN-HCl displayed a similar decrease in the relative intensity of the peak at 3173 cm^{-1}, which suggests the participation of the carbonamide group in hydrogen bonding formation. The shift of the peak from 1637 cm^{-1} to 1650 cm^{-1} and 1659 cm^{-1} in TiATN-HCl and TiATN-ethanol samples, respectively, and the appearance of a peak at 1558 cm^{-1} in TIATN-HCl also supports the participation of amide N as H donor and C=O as H acceptor in the conjugation process.

Moreover, the formation of ATN chloride salt was indicated by the appearance of a new broad peak at around 2000 cm^{-1}. The participation of secondary alcohol in the conjugation was observed by the shift of the peak in TiATN-ethanol from 1382 cm^{-1} to 1385 cm^{-1} belonging to the associated β-OH vibration. Furthermore, a stronger association between TNTs and ATN in TiATN-HCl was investigated by the stronger shifts of the peaks belonging to β-OH deformation vibration.

All these data suggest that the considerable differences in the formation process of TiATN composites depend on the chosen solvent. The SEM and OCA results of TiATN-ethanol samples indicate that ATN nanocrystals covered Ti nanotubes besides the existence of bigger ATN crystals in the system. This may be explained by the phenomenon that the highest solubility of ATN can be observed in the 70 w/w% ethanol solution (84). The fast supersaturation of the solution was induced by the fast evaporation of the ethanol content during solvent removal, which resulted in an intensive nanocrystal formation on the surface of TNTs as nuclei, whereas the rest of the ATN may undergo a slower crystallization process due to the slower evaporation rate of and strong H-bond based interactions with water. Similarly, the fast nanocrystal formation on the surface of TNTs was characterized by the fast evaporation of water-free methanol, which led to stronger composites. However, the strongest reaction between TNTs and ATN was achieved by using HCl 0.01 M as a solvent in spite of the slow evaporation rate, which can be explained by the protonation of the carboxyl amide and secondary amino groups of ATN, resulting in repulsion between ATN molecules and in a possible increase in their H-bonding strength in the presence of polyfunctional carriers as TNTs (85). These effects also cause characteristic ATN-TNT interactions, which result in an increased dissolution rate from the composites due the formation of stable nanocrystals on the surface of the carrier (Fig. 8).

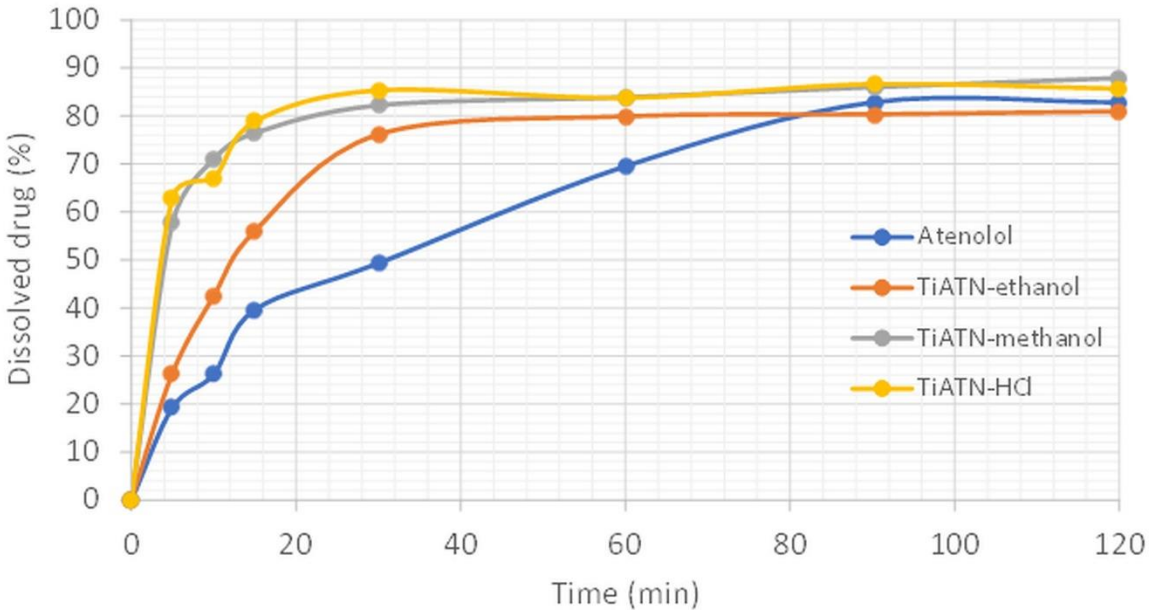

Figure 8. Dissolution study of TiATN composites in gastric juice (non-sink conditions)

In conclusion, ATN shows good solubility in 70 w/w% ethanol solution, methanol and HCl 0.01M. The Janus-faced properties of the TiATN-ethanol sample can be explained by the fast supersaturation of the solution resulting from the fast evaporation of the ethanol content followed by the slower speed of water removal, which induced the concentration of ATN molecules and promoted the formation of ATN-ATN bonds instead of ATN-TNT ones. This latter effect was not observed during the fast removal of water-free methanol, whereas the repulsive effect between protonated ATN molecules prohibited the formation of ATN-ATN interactions despite the slower solvent removal speed in 0.01 M HCl solution.

6.1.3. Effect of various solvents on composite formation with HCT

The SEM micrographs display the strong recrystallization of HCT (Fig. 9a) from ethanol and NaOH (Fig. 9b,c) with the appearance of HCT crystals covered by the composites. On the other hand, no considerable recrystallization was observed in TiHCT-DMF and TiHCT-DMSO (Fig. 9d,e), and only strong compacts of TNTs with increased thickness are visible, which suggests an appropriate loading of the nanotubes with the API, which was also supported by the results of the OCA measurements (Table 2) and DSC analysis.

The OCA results showed that γs and polarity values for TiHCT-ethanol and TiHCT-NaOH were higher compared to HCT due to the accumulation of TNTs on the surface of HCT crystals. In contrast, TiHCT-DMF and TiHCT-DMSO revealed γs values similar to HCT due to the surface coverage of TNTs with HCT molecules.

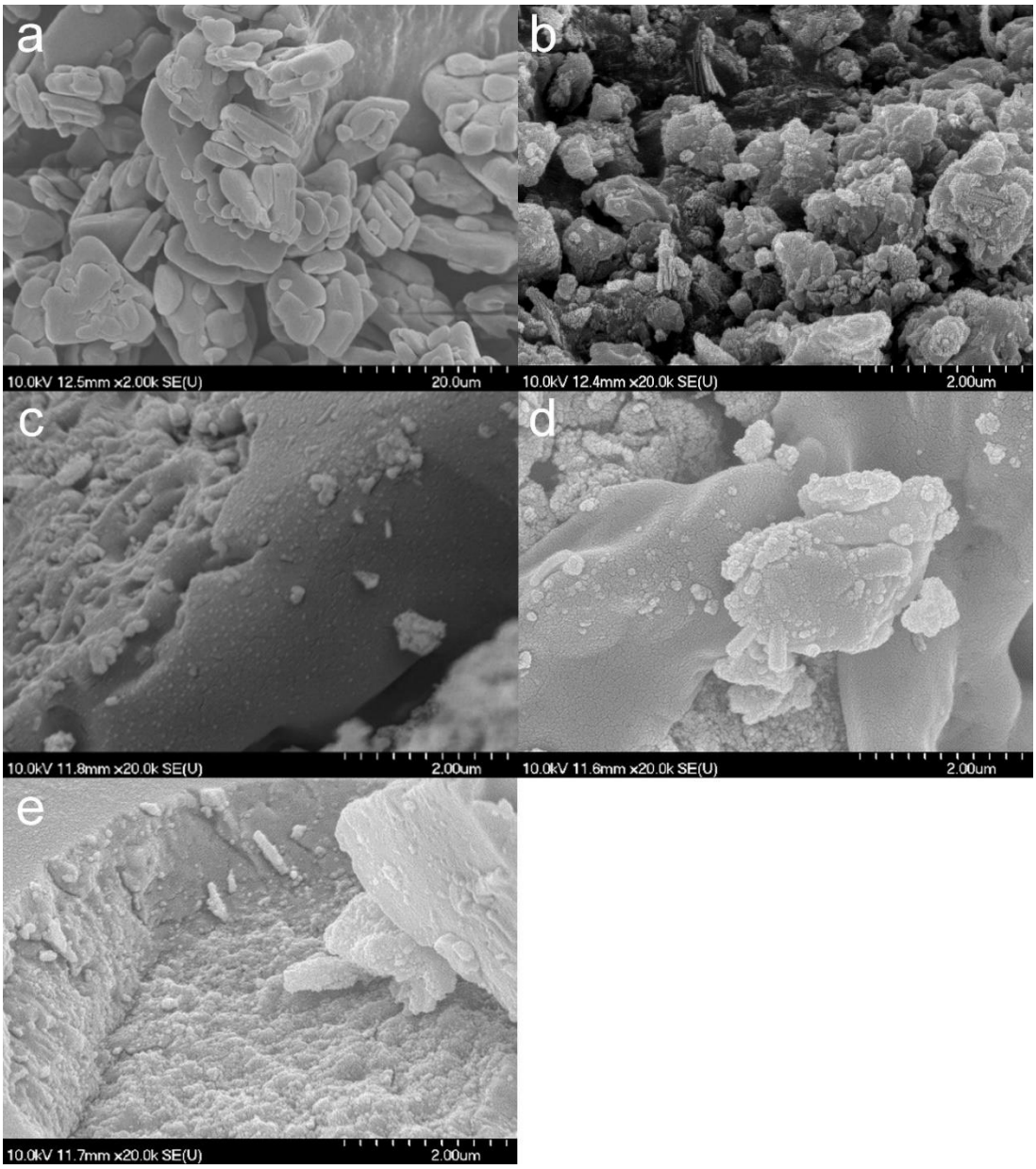

Figure 9. SEM micrographs of HCT (a), TiHCT-ethanol (b), TiHCT-NaOH (c), TiHCT-DMF (d), TiHCT-DMSO (e).

The DSC curve (Fig. 10) of HCT shows that the fusion of the API could be recognized near 270.67 °C, which was followed by a characteristic exothermic event near 320 °C, ascribed to the decomposition of the material. The TiHCT-NaOH composite exhibited a slight shift in the melting peak to 269.74 °C, which indicates poor composite formation from this solvent, and this can be explained by the long evaporation time of the aqueous medium, which resulted in the domination of crystal growth and not core formation. This

effect is also strengthened by the deprotonation of the sulfonamide group, which decreases the H-bond forming ability of HCT. TiHCT-ethanol and TiHCT-DMF revealed a higher shift in the melting peak at 257.2 °C and 234.17 °C, respectively, which indicates a stronger interaction when using ethanol and DMF. The explanation for what happened in TiHCT-ethanol samples is the same as for ATN, that the fast evaporation of ethanol indicates nuclei formation, while the slow evaporation of water shows the growth of HCT crystals. Nevertheless, improved composite formation was expected in the water-free DMF and DMSO samples in spite of the slower evaporation rate due to their aprotic nature, which induced the recrystallisation of HCT on the surface of TNTs as nuclei. The expectation was right for DMF, but interestingly, no fusion peak can be seen in the case of TiHCT-DMSO composites, which can be explained by the formation of amorphous HCT particles instead of nanocrystals.

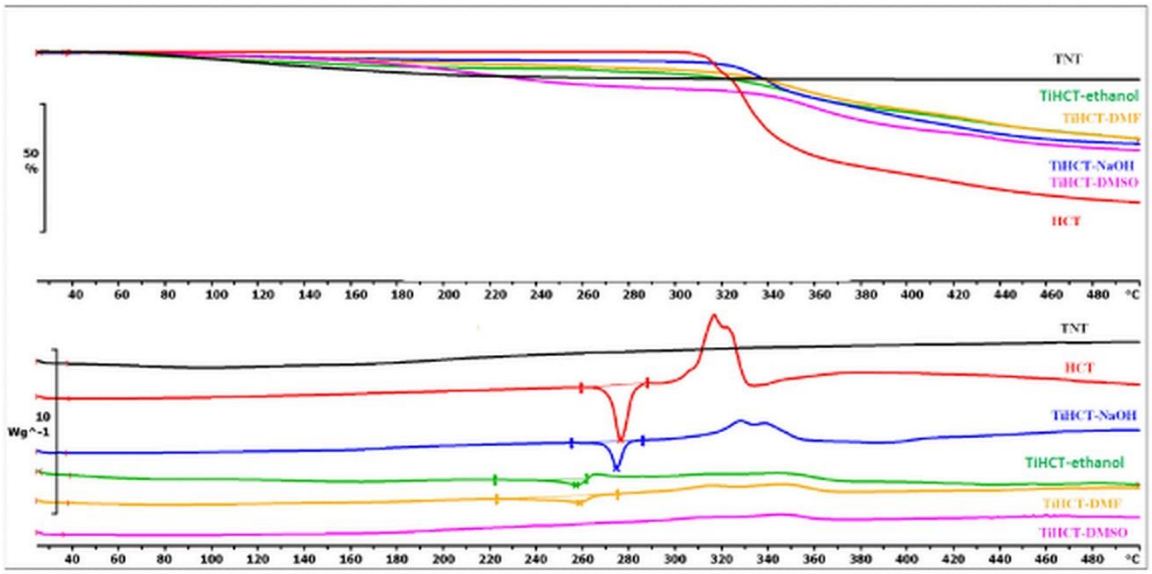

Figure 10. DSC and TG curves of TNT, HCT, TiHCT-ethanol, TiHCT-NaOH, TiHCT-DMF and TiHCT-DMSO.

All those findings were in accordance with the results of the XRPD results (Fig. 11).

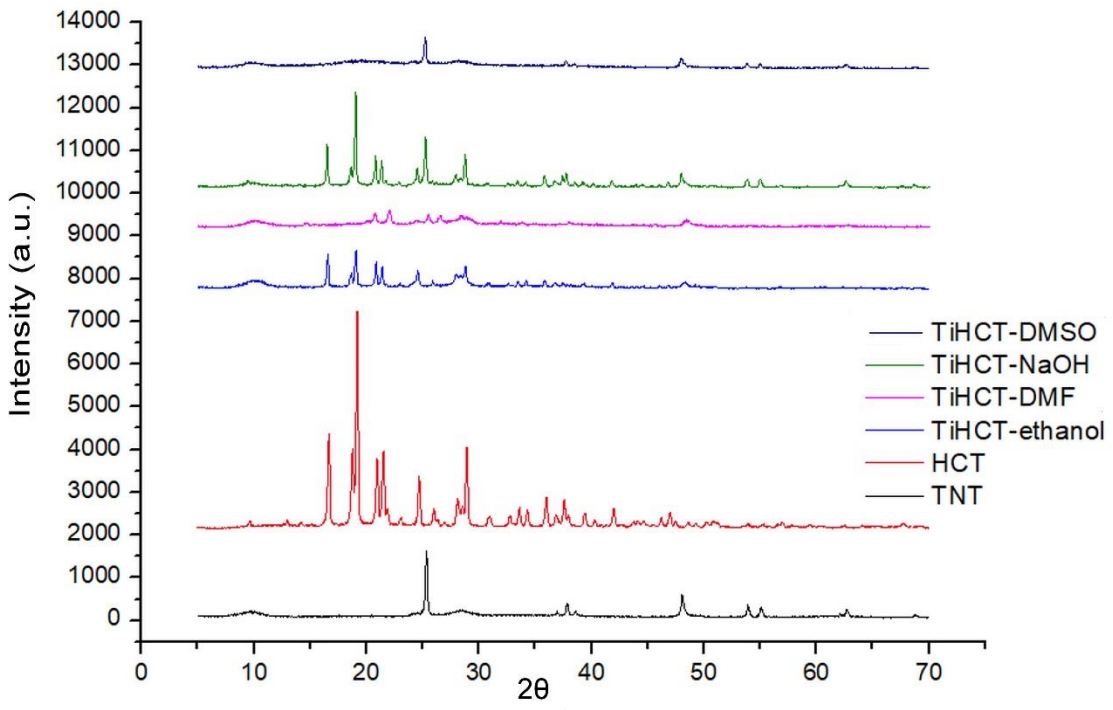

Figure 11. XRPD spectra of HCT and its composites

The X-ray diffractogram of TiHCT-DMSO shows only the characteristic peaks of the crystalline TNTs, which clearly shows HCT bonding with TNTs in an amorphous form, which is highly expected to ensure an improved dissolution rate, whereas the other composites contained HCT in a (nano)crystalline form. However, a new polymorphic form of HCT was recrystallized from DMF (the metastable Form II or DMF solvate instead of the starting stable Form I) (86, 87).

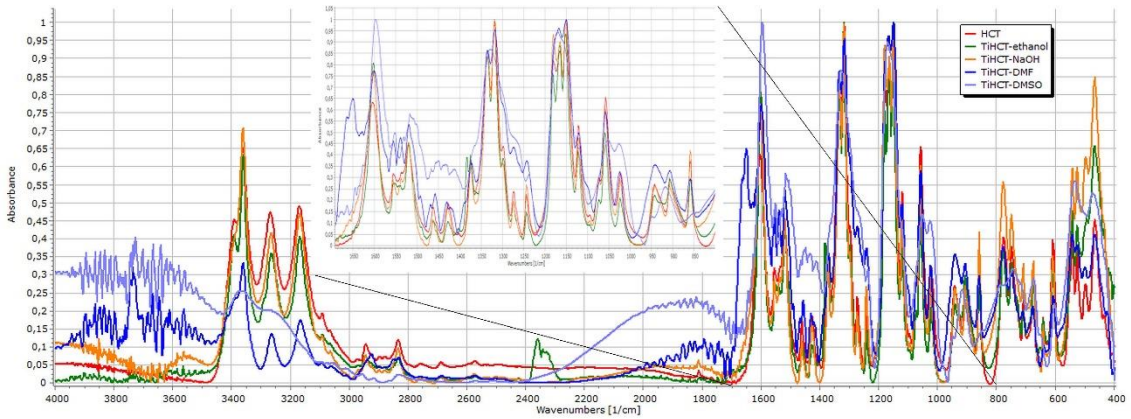

Figure 12. FT-IR spectra of HCT and its composites

The FT-IR spectra were normalized to the peak at 1319 cm^{-1} (Fig. 12). The peaks at 3391 cm^{-1} show non-associated NH stretching, and the right shift of this peak at 3269 cm^{-1} indicates the increasing strength of interactions between TNT and HCT in the order of TiHCT-ethanol, TiHCT-NaOH, TiHCT-DMF and TiHCT-DMSO. The merging of these peaks in DMSO suggests a very strong association, which may also be due to the amorphous state of the drug in the composite. The slight right shift of the N-H bend signal at 1605 cm^{-1} and the change in the intensity ratio of the peaks at 1555 cm^{-1} and 1538 cm^{-1} also relate to the participation of sulfonamide and secondary amino groups in the composite formation.

The minor modification of the C=N stretch signals between 1319-1375 cm^{-1}, or the varying intensities in the 420-910 cm^{-1} region due to C-Cl stretching alteration and benzothiazidine ring skeletal vibration also indicate these interactions. Meanwhile, the left shift and the merging of the peak triplet at 1182 cm^{-1}, 1058 cm^{-1} and 1151 cm^{-1} indicate the involvement of S=O groups as hydrogen acceptors in the interactions.

The strength of interactions fundamentally determines the dissolution rate of the drug from the composites (Fig. 13). There was no considerable difference in the dissolution rates of pure HCT and TiHCT-ethanol composite, in which the weakest interaction was observed. The increasing strength of the interactions resulted in a controlled dissolution rate, which was similar to that of diclofenac-TNT composites (82) and led to the switch of release kinetics from first order to power law model described by Korsmeyer and Peppas.

TiHCT-DMSO exhibited the most considerable elongation of drug release despite the amorphous state of the drug, which may suggest an increased release rate, due to the lack of crystal lattice. It is well visible that the decrease in the release rate of TiHCT-NaOH was higher than expected, which may be due to the large size of the HCT particles due to the slow recrystallization of the drug from the solvent.

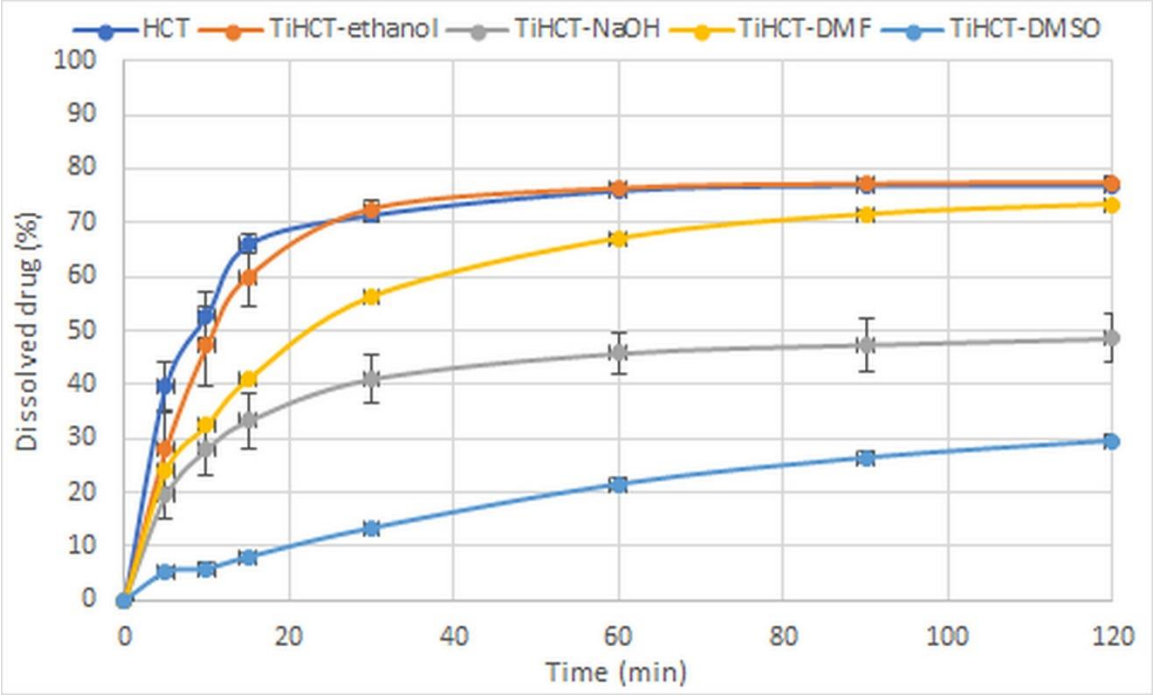

Figure 13. Dissolution study of TiHCT composites in gastric juice (non-sink conditions).

In conclusion, the results of HCT composites were not so obvious. HCT was dissolved in 70 w/w% ethanol solution and NaOH 1 M as an analog of the experiments with ATN. Nevertheless, the quality of the TiHCT-NaOH composites did not meet expectations, which can be explained by the strong drug-solvent interaction resulting in the deprotonation of the drug molecule and a decrease in the intensity of drug-carrier interactions within the composites. Therefore, DMF and DMSO were applied to eliminate this effect and detect the impact of their use on the efficacy of composite formation. DMF and DMSO were successful in forming the TiHCT composites since H-bonding was formed between HCT and TNTs due to the lack of drug-solvent interactions. Nevertheless,

despite the stabilized nanocrystalline form or HCT "recrystallizing" from DMSO in an amorphous form, an extended release of HCT from the composites was noted due to the very strong drug-carrier interactions.

Overall, the assumptions of the first hypothesis were confirmed as protic-aprotic nature, solvent volatility and drug solubility play key roles in the composite formation process. The formation of strong TNT-API composites may be achieved optimally by choosing a highly volatile aprotic solvent. Nevertheless, taking into consideration the privileged use of protic solvents if the drug is protonable. However, the high strength of drug-carrier interactions may influence drug detachment and thus the final product characteristics, including release rate and behaviour in biological environment. The strength of interactions may be optimized by tailoring the surface characteristics of TNTs by functional modifications.

6.2. The functionalization of TNTs

Besides the optimization of the strength of drug-carrier interactions, the functionalization of TNTs is essential to achieve proper bioavailability since the hydrophilicity of TNT-drug composites negatively affects their permeability through the GIT. Therefore, in the present study, TCOS and MgSt were selected to functionalize TNTs, to prove that the functionalization of hydrophilic TNTs with hydrophobic materials is a good technique to enhance their absorption into the systemic circulation. The success of functionalization was detected using OCA and CHNS elemental analysis. The Caco-2 cell line was utilized to test cytotoxicity and permeability by using MTT assay and energy dispersive X-ray fluorescent analyzer, respectively.

6.2.1. Physical properties of functionalized TNTs

Pristine Na-TNTs (Fig 14a) have a considerably elongated structure with an outer diameter of 8-12 nm, and highly variable length (100-1000 nm). H-TNTs (Fig 14b) show identical physical dimensions but have an increased aggregation tendency due to the decreasing electrostatic repulsion resulting from the removal of Na^+ ions. Mg-TNTs (Fig. 14c) have the same diameter of 8-12 nm but the mechanical agitation during the ion-exchange procedure resulted in considerable fragmentation, so the length of the nanotubes

varies mostly in the 100-300 nm range. Similar fragmentation of the longer nanotubes was observed in the case of the functionalized samples (Fig. 14d-g) along with a slight increment of the outer diameter, which depends on the amount and orientation of the functionalizing agent on the surface of TNTs. Nevertheless, all samples have a strongly elongated tubular structure with an aspect ratio >10.

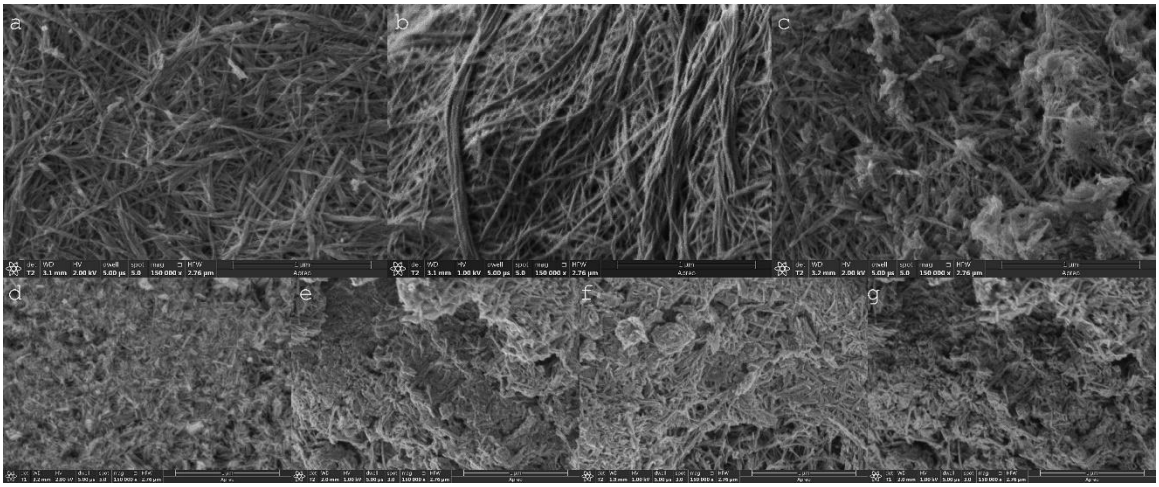

Figure 14. Scanning electron micrographs of Na-TNT (a), H-TNT (b), Mg-TNT (c), TCOS-TNT 10 (d), TCOS-TNT 50 (e), St-TNT (0.05:1) (f) and St-TNT (0.1:1) (g) samples with 150000x magnification

The OCA measurement showed a gradual increment in the aqueous contact angle with the increasing concentration of TCOS up to a concentration of 100 μL. These results were supported by the CHNS elemental analysis, which displayed continuous augmentation in carbon percentage with the increasing amount of functionalizing TCOS (Fig.15).

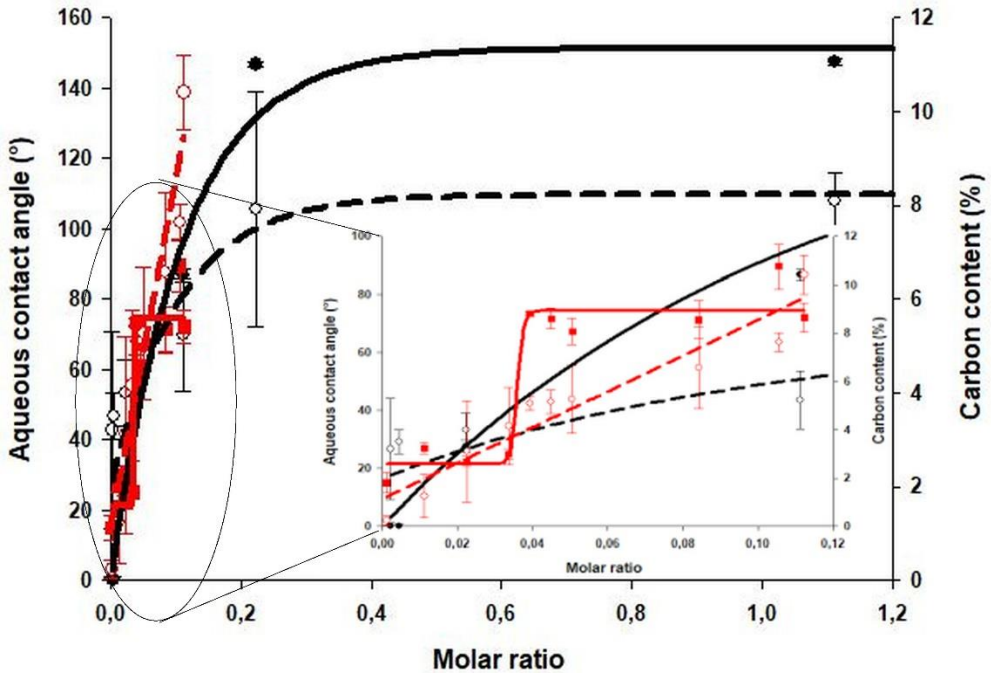

Figure 15. The aqueous contact angles (CA) and carbon percentage (C%) of TCOS-TNTs and St-TNTs at different reagent concentrations (CA of TCOS-TNT (black line); C% of TCOS-TNT (black dashed line), CA of St-TNT (red line), C% of St-TNT (red dashed line)

In contrast, the OCA measurement revealed that low concentrations of St could just slightly increase the aqueous contact angle of Mg-TNTs, but after exceeding a certain threshold around 0.035:1 ratio and despite the linear increment of the carbon content, the surface turned from hydrophilic to hydrophobic (Fig. 15). A possible explanation that above this threshold the St molecules are oriented differently on the surface of TNTs, prohibiting the access of water to the sample. After that only a slight increment could be detected until it stabilizes between 80-90°, but it should be noted, that the maximum aqueous contact angle is considerably smaller as in the case of TOCS-TNTs.

According to OCA and CHNS measurements for TCOS-TNTs, it is well visible that the increasing amount of the reagent highly increased the surface hydrophobicity and complete surface coverage was achieved by the application of 100 µL reagent volume (e.g. 0.2:1 molar ratio). However, the results were different in case of MgSt-TNTs where less St coverage resulted in getting a hydrophobic surface that may bear an advantage of keeping

more binding sites for the drugs which may lead to a higher possible drug load in this system.

6.2.2. Toxicity and permeability of functionalized TNTs

In a previous study (24), no detectable cytotoxicity of Na-TNTs was observed up to a concentration of 5 mg/mL, but in the current study a considerable decrease in cell viability was observed if Mg-TNTs were applied in this concentration (Fig. 16).

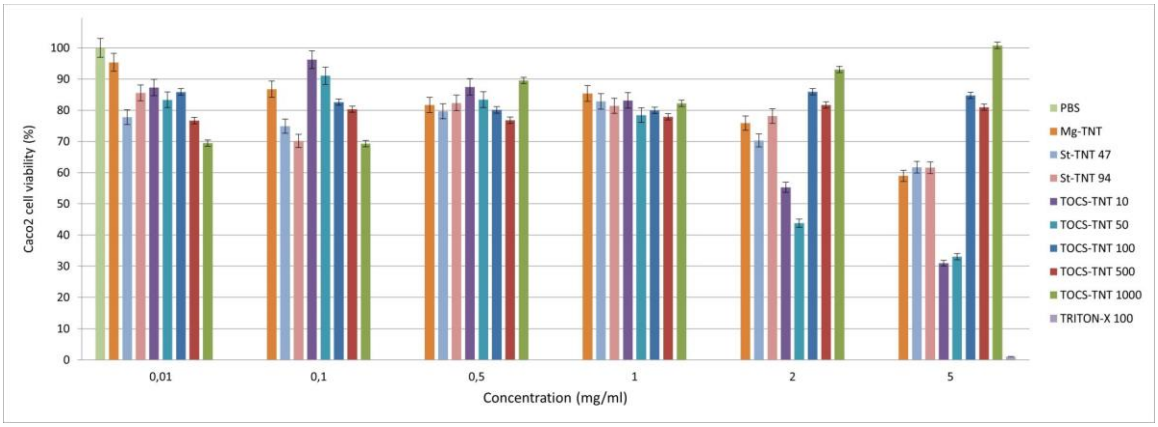

Figure 16. The viability assays of Caco-2 cells after being exposed to functionalized TNTs

This may indicate that the replacement of Na^+ to Mg^{2+} ions on the surface of TNTs also has negative influence on cell interactions, but based on the MTT cytotoxicity test, it is still considered as non-cytotoxic in the concentration range of 0.01-2 mg/mL. In addition, considerable differences were observed in the toxicity of various functionalized TNTs, especially at higher concentrations. The toxicity results displayed a considerable decrease in cell viability for TCOS-TNT 10 and 50 µl samples, possibly due the use of H-TNT as a starting material, which would be in accordance with the previously discussed findings (69, 70). However, no similar effect was shown by the 100, 500, and 1000 µL samples. A possible explanation is that these samples were too hydrophobic for appropriate dispersion/dissolution in the aqueous media and were therefore not taken up by the cells. In the case of St functionalized samples, a decrease in cell viability was only observed at 5 mg/mL, which showed no difference from the values observed for Mg-TNTs, which

indicates that the effect may be connected to the presence of Mg^{2+} ions and not to St molecules.

6.2.3. Permeability results

During the permeability test, the highest safe concentration (1 mg/mL) was applied to achieve a higher maximum drug-dose during further utilization. The transepithelial electrical resistance (TEER) of the cells before TNT exposure was 602±116 Ω/cm^2. For Caco-2 cells, this value may vary in a very large range (200-2400 Ω/cm^2) (88), the obtained results indicate an intact cell layer. Nevertheless, a considerable decrease (22.1±16.7%, 12.4±11.1%, 37.1±8.4% and 23.6±17.4% for TCOS-TNT 10, TCOS-TNT 50, St-TNT (0.05:1), and St-TNT (0.1:1) samples, respectively) in the TEER values was observed after exposure to TNTs, which indicates the perturbation of the integrity of the cell membrane or tight-junctions. However, microscopic investigation showed no change in the cell morphology or layer-integrity, before and after the test, which may indicate a periodic distortion of the membrane integrity by the penetrating nanotubes. Nevertheless, the relative change of various samples showed partial correlation with the results of the permeability tests (Table 3), which revealed that the aqueous contact angle (CA) values should be between 60-90° to achieve appropriate absorption, while the cell integrity was exhibited the smallest distortion for samples between 80-90°CA. Below 40° the surface is too hydrophilic to achieve passive transportation through the cell membrane, while in the 40-60° range the samples may be absorbed considerably slower than the ones with 60-90° CA, and causes higher distortions in cell integrity, possibly due to the higher hydrophilicity. In a previous study Fenyvesi et al. (24) have found no detectable number of pristine Na-TNTs on the basolateral side of the cell monolayer, indicating that the intestinal cell layer is impermeable to this material, possibly due to its high hydrophilicity. In contrast, present study revealed that functionalized samples exhibited considerable permeability through the cell monolayer (Table 3). According to the results, the penetration of samples with small (30°) CA is hindered as more than 40% of the originally inserted value was still detected on the apical side. The best permeability rate was observed for samples with 70-90° CA, where the amount permeated to the basolateral side was increased

with the increasing CA. In case of sample TCOS-TNT 100 where the CA was around 140° no detectable amount was measured both in apical and basal compartment. A possible explanation that due to the inappropriate wetting and dispersion, the TNTs were sedimented and adhered to the cell layer without visible absorption through the membranes or were completely accumulated in the cells, which would bear a potential risk of toxicity. Nevertheless, in both cases the sample is inappropriate for the planned application.

Table 3: Results of the permeability tests

Material	Aqueous CA (°)	Apical amount (%)	Basal amount (%)
TCOS-TNT 10	27.70±2.10	40.94±10.49	8.47±0.30
TCOS-TNT 50	86.66±1.90	27.94±14.83	8.39±0.24
TCOS-TNT 100	146.65±0.60	n.m	n.m
St-TNT 47	71.75±3.58	26.98± 6.66	8.75±0.78
St-TNT 94	89.55±7.66	27.16±11.13	11.49±0.67

This part of the experimental work emphasized the importance of functionalizing TNTs to improve their absorption after oral administration. We confirmed the second hypothesis, according to which increasing the hydrophobicity of TNTs may increase cell permeability. Nevertheless, the validity of the third hypothesis, namely that increased hydrophobicity may not affect toxicity, should be partially reconsidered since the functionalized samples exhibited slightly increased toxicity, but it was connected to the altered surface charge due to ion exchange during the functionalization procedure.

7. CONCLUSIONS AND PRACTICAL USEFULNESS

In this study, TNT composites with ATN and HCT were prepared to improve the drug dissolution profile from the composites in which ATN and HCT were chosen as model drugs from the third and fourth classes of BCS.

I. Choosing the appropriate solvent is essential from the aspect of composite formation efficacy. Solvent volatility is important, but its protic/aprotic nature depends on the drug properties, with protic solvents being preferable for protonable drugs, otherwise aprotic solvents are more advantageous.

II. The extent of the strength of interaction between TNTs and drugs directly affects drug detachment inside the human body, thus it should be estimated based on the administered oral dosage form, in which weak interaction is enough in immediate release drugs and strong interaction is favored for extended-release purposes.

TNTs were functionalized to obtain increased hydrophobicity and enhance their absorption from the GIT, with two different methods compared to each other. For this purpose, TCOS and St were used in different concentrations with a view to optimizing the functionalization method and determining the optimal functionalization percentage.

I. The functionalization of TNTs is crucial to enhance their hydrophobicity and therefore their permeability and may strengthen the interaction between TNTs and drugs.

II. The toxicity of functionalized TNTs has to be checked due to the changed surface charge.

The practical relevance and new approaches of this research work are the following

I. Our hypothesis of choosing the optimal solvent proved to be a promising approach for enhancing the solubility of poorly water-soluble drugs.

II. Functionalized TNTs are potential drug carriers for the oral administration route since they display good permeability and toxicity profiles.

8. REFERENCES

1. Suri SS, Fenniri H, Singh B. Nanotechnology-based drug delivery systems, J. Occup. Med. 2, 16 (2007).
2. De Villiers MM, Aramwit P, Kwon GS, editors. Nanotechnology in drug delivery, Springer Science & Business Media. (2008).
3. Ranjous Y, Regdon jr G, Pintye-Hódi K, Sovány T. Standpoint on the priority of TNTs and CNTs as targeted drug delivery systems, Drug Discov. Today. 24, 1704-1709 (2019).
4. Mirza AZ, Siddiqui FA. Nanomedicine and drug delivery: a mini review, Int. Nano Lett. 4, 94 (2014).
5. Kulkarni HP. Synthesis and applications of titania nanotubes, Drug delivery and ionomer composites: The University of North Carolina at Chapel Hill. (2008).
6. Mahajan D. Carbon Nanotubes: A Review on Synthesis, Electrical and Mechanical Properties and Applications, Asian J. Appl. Sci. Technol. 1, 15-20 (2017).
7. Gupta S, Kesarla R, Omri A. Formulation strategies to improve the bioavailability of poorly absorbed drugs with special emphasis on self-emulsifying systems, Int. Schol. Res. Notices. 848043 (2013).
8. Merisko-Liversidge E, Liversidge GG, Cooper ER. Nanosizing: a formulation approach for poorly-water-soluble compounds, Eur. J. Pharm. Sci.18, 113-120 (2003).
9. Patel BD, Modi RV, Thakkar NA, Patel AA, Thakkar PH. Development and characterization of solid lipid nanoparticles for enhancement of oral bioavailability of Raloxifene, J. Pharm. Bioallied Sci. 4(Suppl 1), S14 (2012).
10. Pouton CW. Formulation of poorly water-soluble drugs for oral administration: physicochemical and physiological issues and the lipid formulation classification system, Eur. J. Pharm. Sci. 29, 278-287 (2006).
11. Wang Q, Huang JY, Li HQ, Zhao AZ, Wang Y, Zhang KQ, Sun HT, Lai YK. Recent advances on smart TiO2 nanotube platforms for sustainable drug delivery applications, Int. J. Nanomedicine. 12, 151 (2017).
12. Lai S, Zhang W, Liu F, Wu C, Zeng D, Sun Y, Xu Y, Fang Y, Zhou W. TiO2 nanotubes as animal drug delivery system and in vitro controlled release, J. Nanosci. Nanotechnol. 13, 91-97 (2013).
13.Godbole V, Kim Y-S, Kim G-S, Dar M, Shin H-SJEA. Synthesis of titanate nanotubes and its processing by different methods, Electrochim. Acta. 52, 1781-1787 (2006).
14. Boudon J, Papa A, Paris J, Millot N. Titanate nanotubes as a versatile platform for nanomedicine, Nanomedicine. 403, 403 (2014).
15. Rørvik PM, Tadanaga K, Tatsumisago M, Grande T, Einarsrud MA. Template-assisted synthesis of PbTiO3 nanotubes, J. Eur. Ceram. Soc. 29, 2575-2579 (2009).
16. Sahoo NG, Bao H, Pan Y, Pal M, Kakran M, Cheng HKF, et al. Functionalized carbon nanomaterials as nanocarriers for loading and delivery of a poorly water-soluble anticancer drug: a comparative study, ChemComm. 47, 5235-5237 (2011).
17. Liu Z, Tabakman S, Welsher K, Dai H. Carbon nanotubes in biology and medicine: in vitro and in vivo detection, imaging and drug delivery, Nano Res. 2, 85-120 (2009).
18. Harrison BS, Atala A. Carbon nanotube applications for tissue engineering. Biomaterials. 28,344-353 (2007).

19. Kumar SP, Prathibha D, Shankar NG, Parthibarajan R, Mastyagiri L, Shankar M. Pharmaceutical application of carbon nanotube-mediated drug delivery system, Int. J. Pharm. Sci. Nanotech. 5, 1685-1696 (2015).
20. Rahman ZU, Haider W, Pompa L, Deen K. Electrochemical & osteoblast adhesion study of engineered TiO 2 nanotubular surfaces on titanium alloys, Mater. Sci. Eng.: C. 58, 160-168 (2016).
21. Liu Z, Tabakman S, Welsher K, Dai H. Carbon nanotubes in biology and medicine: in vitro and in vivo detection, imaging and drug delivery, Nano Res. 2, 85-120 (2009).
22. Wang F, Shi L, He WX, Han D, Yan Y, Niu ZY, Shi SG. Bioinspired micro/nano fabrication on dental implant–bone interface, Appl. Surf. Sci. 265, 480-488 (2013).
23. Fenyvesi F, Kónya Z, Rázga Z, Vecsernyés M, Kása P, Pintye-Hódi K, Bácskay I. Investigation of the cytotoxic effects of titanate nanotubes on Caco-2 cells, AAPS PharmSciTech. 15, 858-861 (2014).
24. Wang Q, Huang JY, Li HQ, Chen Z, Zhao AZ, Wang Y, Zhang KQ, Sun HT, Al-Deyab SS, Lai YK. TiO2 nanotube platforms for smart drug delivery: a review, Int. J. Nanomedicine. 11, 4819 (2016).
25. Prato M, Kostarelos K, Bianco A. Functionalized carbon nanotubes in drug design and discovery, Acc. Chem. Res. 41, 60-68 (2008).
26. Raliya R, Singh Chadha T, Haddad K, Biswas P. Perspective on nanoparticle technology for biomedical use, Curr. Pharm. Des. 22, 2481-2490 (2016).
27. Liu Z, Sun X, Nakayama-Ratchford N, Dai H. Supramolecular chemistry on water-soluble carbon nanotubes for drug loading and delivery, ACS nano. 1, 50-56 (2007).
28. Klumpp C, Kostarelos K, Prato M, Bianco A. Functionalized carbon nanotubes as emerging nanovectors for the delivery of therapeutics, Biochim. Biophys. Acta Biomembr. 1758, 404-412 (2006).
29. Nagasawa S, Yudasaka M, Hirahara K, Ichihashi T, Iijima S. Effect of oxidation on single-wall carbon nanotubes, Chem. Phys. Lett. 328, 374-380 (2000).
30. Liu Z, Tabakman SM, Chen Z, Dai H. Preparation of carbon nanotube bioconjugates for biomedical applications, Nat. Protoc. 4, 1372-1381 (2009).
31. Wang Y, Iqbal Z, Mitra S. Microwave-induced rapid chemical functionalization of single-walled carbon nanotubes, Carbon. 43, 1015-1020 (2005).
32. Papa AL, Maurizi L, Vandroux D, Walker P, Millot N. Synthesis of titanate nanotubes directly coated with USPIO in hydrothermal conditions: a new detectable nanocarrier, J. Phys. Chem. C. 115, 19012-19017 (2011).
33. Papa AL, Boudon J, Bellat V, Loiseau A, Bisht H, Sallem F, Chassagnon R, Bérard V, Millot N. Dispersion of titanate nanotubes for nanomedicine: comparison of PEI and PEG nanohybrids, Dalton Trans. 44, 739-746 (2015).
34. Lai M, Cai K, Zhao L, Chen X, Hou Y, Yang Z. Surface functionalization of TiO2 nanotubes with bone morphogenetic protein 2 and its synergistic effect on the differentiation of mesenchymal stem cells, Biomacromolecules. 12, 1097-1105 (2011).
35. Byrne MT, McCarthy JE, Bent M, Blake R, Gun'ko YK, Horvath E, Konya Z, Kukovecz A, Kiricsi I, Coleman JN. Chemical functionalisation of titania nanotubes and

their utilisation for the fabrication of reinforced polystyrene composites, J. Mater. Chem. 17, 2351-2358 (2007).
36. Kazemzadeh-Narbat M, Lai BF, Ding C, Kizhakkedathu JN, Hancock RE, Wang R. Multilayered coating on titanium for controlled release of antimicrobial peptides for the prevention of implant-associated infections, Biomaterials. 34, 5969-5977 (2013).
37. Oh S, Moon KS, Lee SH. Effect of RGD peptide-coated TiO2 nanotubes on the attachment, proliferation, and functionality of bone-related cells, J. Nanomater. (2013).
38. Oliveira WF, Arruda IR, Silva GM, Machado G, Coelho LC, Correia MT. Functionalization of titanium dioxide nanotubes with biomolecules for biomedical applications, Mater. Sci. Eng.: C. 81, 597-606 (2017).
39. Bauer S, Park J, Pittrof A, Song YY, von der Mark K, Schmuki P. Covalent functionalization of TiO2 nanotube arrays with EGF and BMP-2 for modified behavior towards mesenchymal stem cells, Integr. Biol. 3, 927-936 (2011).
40. Neupane MP, Park IS, Bae TS, Yi HK, Uo M, Watari F, Lee MH. Titania nanotubes supported gelatin stabilized gold nanoparticles for medical implants, J. Mater. Chem. 21, 12078-12082 (2011).
41. Chen X, Cai K, Fang J, Lai M, Hou Y, Li J, Luo Z, Hu Y, Tang L. Fabrication of selenium-deposited and chitosan-coated titania nanotubes with anticancer and antibacterial properties, Colloids Surf. B: Biointerfaces 103, 149-157 (2013).
42. Mohan L, Anandan C, Rajendran N. Drug release characteristics of quercetin-loaded TiO2 nanotubes coated with chitosan, Int. J. Biol. Macromol. 93, 1633-1638 (2016).
43. Wolinsky JB, Colson YL, Grinstaff MW. Local drug delivery strategies for cancer treatment: gels, nanoparticles, polymeric films, rods, and wafers, J. Control. Release. 159, 14-26 (2012).
44. Kumar P, Singh C. A study on solubility enhancement methods for poorly water soluble drugs, Am. J. Pharmacol. Sci. 1, 67-73 (2013).
45. Habib MJ. Pharmaceutical solid dispersion technology, CRC Press. (2000)
46. Joshi HN, Tejwani RW, Davidovich M, Sahasrabudhe VP, Jemal M, Bathala MS, Varia SA, Serajuddin AT. Bioavailability enhancement of a poorly water-soluble drug by solid dispersion in polyethylene glycol–polysorbate 80 mixture, Int. J. Pharm. 269, 251-258 (2004).
47. Van den Mooter G, Wuyts M, Blaton N, Busson R, Grobet P, Augustijns P, Kinget R. Physical stabilisation of amorphous ketoconazole in solid dispersions with polyvinylpyrrolidone K25, Eur. J. Pharm. Sci. 12, 261-269 (2001).
48. Konno H, Taylor LS. Influence of different polymers on the crystallization tendency of molecularly dispersed amorphous felodipine, Eur. J. Pharm. Sci. 95, 2692-2705 (2006).
49. Yu L. Amorphous pharmaceutical solids: preparation, characterization and stabilization, Adv. Drug Deliv. Rev. 48, 27-42 (2001).
50. Verheyen S, Blaton N, Kinget R, Van den Mooter G. Mechanism of increased dissolution of diazepam and temazepam from polyethylene glycol 6000 solid dispersions, Int. J. Pharm. 249, 45-58 (2002).

51. Martınez-Oharriz MC, Martın C, Goni MM, Rodrıguez-Espinosa C, Tros-Ilarduya MC, Zornoza A. Influence of polyethylene glycol 4000 on the polymorphic forms of diflunisal, Eur. J. Pharm. Sci. 8, 127-132 (1999).
52. Nelson E, Knoechel EL, Hamlin WE, Wagner JG. Influence of the absorption rate of tolbutamide on the rate of decline of blood sugar levels in normal humans, Int. J. Pharm. 51, 509-514 (1962).
53. Lin SL, Lachman L, Swartz CJ, Huebner CF. Preformulation investigation I: relation of salt forms and biological activity of an experimental antihypertensive, J. Pharm. Sci. 61, 1418-1422 (1972).
54. Smart S, Cassady A, Lu G, Martin D. The biocompatibility of carbon nanotubes, Carbon. 44, 1034-1047 (2006).
55. Hong F, Yu X, Wu N, Zhang YQ. Progress of in vivo studies on the systemic toxicities induced by titanium dioxide nanoparticles, Toxicol. Res. 6, 115-133 (2017).
56. Samat MH, Ali AM, Taib MF, Hassan OH, Yahya MZ. Hubbard U calculations on optical properties of 3d transition metal oxide TiO2, Results Phys. 6, 891-896 (2016).
57. Vance ME, Kuiken T, Vejerano EP, McGinnis SP, Hochella Jr MF, Rejeski D, Hull MS. Nanotechnology in the real world: Redeveloping the nanomaterial consumer products inventory, Beilstein J. Nanotechnol. 6, 1769-1780 (2015).
58. Chen Z, Wang Y, Zhuo L, Chen S, Zhao L, Luan X, Wang H, Jia G. Effect of titanium dioxide nanoparticles on the cardiovascular system after oral administration, Toxicol. Lett. 239, 123-130 (2015).
59. IARC Working Group on the Evaluation of Carcinogenic Risks to Humans. Carbon black, titanium dioxide, and talc, IARC Monogr. Eval. Carcinog. Risks Hum. 93, 1 (2010).
60. Acar MS, Bulut ZB, Ateş A, Nami B, Koçak N, Yıldız B. Titanium dioxide nanoparticles induce cytotoxicity and reduce mitotic index in human amniotic fluid-derived cells, Hum. Exp. Toxicol. 34, 74-82 (2015).
61. Jugan ML, Barillet S, Simon-Deckers A, Herlin-Boime N, Sauvaigo S, Douki T, Carriere M. Titanium dioxide nanoparticles exhibit genotoxicity and impair DNA repair activity in A549 cells, Nanotoxicology. 6, 501-513 (2012).
62. Bahadar H, Maqbool F, Niaz K, Abdollahi M. Toxicity of nanoparticles and an overview of current experimental models, Iran. Biomed. J. 20, 1 (2016).
63. Wang J, Zhou G, Chen C, Yu H, Wang T, Ma Y, Jia G, Gao Y, Li B, Sun J, Li Y. Acute toxicity and biodistribution of different sized titanium dioxide particles in mice after oral administration, Toxicol. Lett. 168, 176-185 (2007).
64. Mano SS, Kanehira K, Sonezaki S, Taniguchi A. Effect of polyethylene glycol modification of TiO2 nanoparticles on cytotoxicity and gene expressions in human cell lines, Int. J. Mol. Sci. 13, 3703-3717 (2012).
65. Tedja R, Soeriyadi AH, Whittaker MR, Lim M, Marquis C, Boyer C, Davis TP, Amal R. Effect of TiO 2 nanoparticle surface functionalization on protein adsorption, cellular uptake and cytotoxicity: the attachment of PEG comb polymers using catalytic chain transfer and thiol–ene chemistry, Polym. Chem. 3, 2743-2751 (2012).

66. Warheit DB, Donner EM. Risk assessment strategies for nanoscale and fine-sized titanium dioxide particles: Recognizing hazard and exposure issues, Food Chem. Toxicol. 85, 38-47 (2015).
67. Jones K, Morton J, Smith I, Jurkschat K, Harding AH, Evans G. Human in vivo and in vitro studies on gastrointestinal absorption of titanium dioxide nanoparticles, Toxicol. Lett. 233, 95-101 (2015).
68. Wadhwa S, Rea C, O'Hare P, Mathur A, Roy SS, Dunlop PS, Byrne JA, Burke G, Meenan B, McLaughlin JA. Comparative in vitro cytotoxicity study of carbon nanotubes and titania nanostructures on human lung epithelial cells, J. Hazard. Mater. 191, 56-61 (2011).
69. Maurizi L, Papa AL, Boudon J, Sudhakaran S, Pruvot B, Vandroux D, Chluba J, Lizard G, Millot N. Toxicological risk assessment of emerging nanomaterials: cytotoxicity, cellular uptake, effects on biogenesis and cell organelle activity, acute toxicity and biodistribution of oxide nanoparticles, Unraveling the Safety Profile of Nanoscale Particles and Materials-From Biomedical to Environmental Applications. 21, 17-36 (2018).
70. Magrez A, Horváth L, Smajda R, Salicio V, Pasquier N, Forro L, Schwaller B. Cellular toxicity of TiO2-based nanofilaments. ACS Nano. 3, 2274-2280 (2009).
71. Pan R, Liu Y, Chen W, Dawson G, Wang X, Li Y, Dong B, Zhu Y. The toxicity evaluation of nano-trititanate with bactericidal properties in vitro, Nanotoxicology. 6, 327-373 (2012).
72. Entezari M, Ghanbary F. Toxicity of Manganese Titanate on Rat Vital Organ Mitochondria, Iran. J. Pharm. Res. 18, 713 (2019).
73. Abdelgied M, El-Gazzar AM, Alexander DB, Alexander WT, Numano T, Iigou M, Naiki-Ito A, Takase H, Abdou KA, Hirose A, Taquahashi Y. Pulmonary and pleural toxicity of potassium octatitanate fibers, rutile titanium dioxide nanoparticles, and MWCNT-7 in male Fischer 344 rats, Arch. Toxicol. 93, 909-920 (2019).
74. Catalan-Figueroa J, Palma-Florez S, Alvarez G, Fritz HF, Jara MO, Morales JO. Nanomedicine and nanotoxicology: the pros and cons for neurodegeneration and brain cancer, Nanomedicine. 11, 171-187 (2016).
75. Krawczyńska A, Dziendzikowska K, Gromadzka-Ostrowska J, Lankoff A, Herman AP, Oczkowski M, Królikowski T, Wilczak J, Wojewódzka M, Kruszewski M. Silver and titanium dioxide nanoparticles alter oxidative/inflammatory response and renin–angiotensin system in brain, Food Chem Toxicol. 85, 96-105 (2015).
76. Geraets L, Oomen AG, Krystek P, Jacobsen NR, Wallin H, Laurentie M, Verharen HW, Brandon EF, de Jong WH. Tissue distribution and elimination after oral and intravenous administration of different titanium dioxide nanoparticles in rats, Part Fibre Toxicol. 11, 1-21 (2014).
77. Landsiedel R, Fabian E, Ma-Hock L, Wohlleben W, Wiench K, Oesch F, van Ravenzwaay B. Toxico-/biokinetics of nanomaterials, Arch. Toxicol. 86, 1021-1060 (2012).
78. Kamal N, Zaki AH, El-Shahawy AA, Sayed OM, El-Dek SI. Changing the morphology of one-dimensional titanate nanostructures affects its tissue distribution and toxicity, Toxicol. Ind. Health. 36, 272-286 (2020).

79. Kamal N, Zaki AH, El-Shahawy AA, Sayed OM, El-Dek SI. Changing the morphology of one-dimensional titanate nanostructures affects its tissue distribution and toxicity. Toxicol Ind Health. 36, 272-286 (2020).
80. Van Ravenzwaay B, Landsiedel R, Fabian E, Burkhardt S, Strauss V, Ma-Hock L. Comparing fate and effects of three particles of different surface properties: nano-TiO2, pigmentary TiO2 and quartz, Toxicol. Lett. 186, 152-159 (2009).
81. Kong R, Sun Q, Cheng S, Fu J, Liu W, Letcher RJ, Liu C. Uptake, excretion and toxicity of titanate nanotubes in three stains of free-living ciliates of the genus Tetrahymena, Aquat. Toxicol. 233, 105790 (2021).
82. Sipos B, Pintye-Hódi K, Kónya Z, Kelemen A, Regdon jr G, Sovány T. Physicochemical characterisation and investigation of the bonding mechanisms of API-titanate nanotube composites as new drug carrier systems, Int. J. Pharm. 518, 119-129 (2017).
83. Singh M, Lara SO, Tlali S. Effects of size and shape on the specific heat, melting entropy and enthalpy of nanomaterials, J. Taibah Univ. Sci. 11, 922-929 (2017).
84. Hamidi S, Jouyban A. Solubility of atenolol in ethanol+ water mixtures at various temperatures, J. Serbian Chem. Soc. 80, 695-704 (2015).
85. Meot-Ner M. The ionic hydrogen bond. 4. Intramolecular and multiple bonds. Protonation and complexes of amides and amino acid derivatives, J. Am. Chem. Soc. 106, 278-283 (1984).
86. Johnston A, Florence AJ, Shankland N, Kennedy AR, Shankland K, Price SL. Crystallization and crystal energy landscape of hydrochlorothiazide, Cryst. Growth Des. 7, 705-712 (2007).
87. Saini A, Chadha R, Gupta A, Singh P, Bhandari S, Khullar S, Mandal S, Jain DS. New conformational polymorph of hydrochlorothiazide with improved solubility, Pharm Dev Technol. 21, 611-618 (2016).
88. Srinivasan B, Kolli AR, Esch MB, Abaci HE, Shuler ML, Hickman JJ. TEER measurement techniques for in vitro barrier model systems, J. Lab. Autom. 20, 107–126 (2015).

ACKNOWLEDGEMENTS

I would like to express my special appreciation to my supervisor, Prof. Dr. **Tamás Sovány,** not just for introducing me to the topic, but also for his guidance and unending support along the way. Your expertise was invaluable and key to formulating the research and you have been a tremendous mentor for me, always there to give me guidance and push me when I was ready to stop. It was my honor and great fortune to have you as my supervisor.

I would like to express my sincere gratitude to my supervisor and team leader Prof. Dr. **Géza Regdon jr**. for the continuous support of my PhD study, for his patience, motivation, kindness and for being our spiritual father.

I would like to show my great appreciation to Prof. Dr. **Zoltán Kónya**, Vice-Rector for Scientific Affairs & Innovation and Head of the Department of Applied & Environmental Chemistry for his unconditional support since the very beginning of my PhD journey. It is not only about science, opened labs and the unlimited use of resources, but also about all the generosity, precious time given, understanding, and additional mentoring. It was the greatest privilege to have your support and guidance throughout my PhD.

I am also thankful to Prof. Dr. **Ildikó Csóka**, Head of the Institute of Pharmaceutical Technology and Regulatory Affairs for providing me with the opportunity to work in the department.

I am indebted to Prof. Dr. **Wolfgang Frieß**, Head of the Department of Pharmacy – Center for Drug Research, Pharmaceutical Technology and Biopharmaceutics in Ludwig Maximilian University of Munich for the fruitful collaboration, kindness and humanity. I will always remember Prof. Frieß and his exceptional team who made me feel at home, surrounded me with love and ensured that I enjoyed my stay in Munich.

I am glad to acknowledge Prof. Dr. **Piroska Szabó-Révész** for her kindness and exceptional presence and Prof. Dr. **Klára Pintye-Hódi** for her support, kindness and valuable advice in my research work.

I express my kindest gratitude to Dr. **Katalin Kristó** for her support, kind presence and sweet personality.

Many thanks to **László Nagy**, **Ildikó Vígh** and **Gabriella Molnár** for their technical assistance in my experimental work and for being lovely friends with me.

Getting through my dissertation required more than just academic support; my deep and sincere gratitude to my family for their continuous and unparalleled love, help and support.

- To my father **Ali Ranjous**: My first man who taught me that ethics is above education and helping people is a duty, not honorable. Every act of kindness I have done to anyone goes to you Dad.
- To my mother **Raifa Ranjous**: My first teacher who taught me how to carry a pencil and write. My first and only lady to whom I will always look up to. Thanks for your prayers and for the delicious food that you prepared with your love.
- To my architect brother **Yamen Ranjous**: To the noble man who everyone holds in high esteem for his morals and creativity. Architecture was lifeless before your magic touches revived it.
- To my pediatrician sister **Yara Ranjous**: You are the reason that makes me believe angels exist. How can one person have all that beauty, kindness, generosity and intelligence!
- To my dentist brother **Yazan Ranjous**: You have been my guardian angel since we were children when we used to share the same study table and you looked after me. Now fate brought you to Germany to be close to me during my studies in Hungary and to be always and forever the reason to draw laughter on my face and in my heart.
- To my beautiful angel niece **Amelie Ranjous**: You overwhelmed our heart with love, beauty and happiness.
- From the bottom of my heart, I would like to say a big thank you to **Robert Holmes**. No words can describe your humanity and great personality. Thanks for the true friendship, the support and for wiping away my tears.
- My sincere thanks go to **Krisztina Ludasi** who opened both her heart and home to me when I was new in the city. Life would be better if everyone was like you.

- Many thanks to all my **friends** in **Syria**, in the **Department of Applied & Environmental Chemistry** and in the **Szeged Language Swap** for their support and love.
- Finally, to my beloved **Syria** in the hope of a fast recovery.

ANNEX
Related articles

ELSEVIER

feature

Standpoint on the priority of TNTs and CNTs as targeted drug delivery systems

Yasmin Ranjous, Géza Regdon Jr., Klára Pintye-Hódi and Tamás Sovány, t.sovany@pharm.u-szeged.hu

Conventional drug delivery systems have limitations according to their toxicity and poor solubility, bioavailability, stability, and pharmacokinetics (PK). Here, we highlight the importance of functionalized titanate nanotubes (TNTs) as targeted drug delivery systems. We discuss the differences in the physicochemical properties of TNTs and carbon nanotubes (CNTs) and focus on the use of functionalization to improve their characteristics. TNTs are promising materials for drug delivery systems because of their superb properties compared with CNTs, such as their processability, wettability, and biocompatibility. Functionalization improves nanoparticles (NPs) via their surface modification and enables them to achieve the targeted therapy.

Introduction

Conventional drugs often have poor solubility, PK, biopharmaceutical properties, and stability or cause toxicity [1]. By contrast, nanotechnology-based drug delivery systems can improve the solubility, absorption, permeation, retention time, and bioavailability of drug molecules in target tissues, as well as improving their stability and, therefore, enhancing the shelf-life and acceptability of drugs by increasing either their uptake efficacy or patient compliance [2].

Nanosized delivery systems can be internalized by cells more effectively compared with micro-sized particles. In addition, NPs can be formulated in various shapes, sizes, and compositions, and can be modified physicochemically and functionally to obtain specific properties depending on the requirements of both the drug molecule and the targeted organ [1]. Nanotubes have an ideal inner diameter of 5–6 nm for loading with large biological molecules, with a surface area five times higher than that of other NPs. Furthermore, cell internalization is higher in the case of tubular NPs compared with their spherical counterparts (H.P. Kulkarni, PhD thesis, University of North Carolina at Chapel Hill, 2008).

The first nanotubes to be discovered were CNTs. The first synthesis method was described by Lijima in 1991, whereas TNTs were first synthesized by Hoyer via template-assisted synthesis in 1996 (reviewed in Ref. [3]). Nevertheless, over the past decades, numerous synthesis routes with various advantages and disadvantages have been developed (Tables 1 and 2).

Structure and classification

Although both CNTs and TNTs have a tubular structure, there are general differences in their structure. CNTs are allotropes of carbon made from graphene/graphite and are rolled up into concentric cylinders with various wall numbers, on which their classification is based.

Single-walled CNTs (SWNTs) have a diameter of 1 nm and length up to centimeters, prepared by rolling a single graphene sheet to form a cylinder. The conducting properties of SWNTs depend on the wrapping nature [10], which is represented by chiral vectors (n, m). A zigzag structure is obtained when $m = 0$, an armchair is obtained when $n=m$, and a chiral structure is obtained when m lies between the zigzag and the armchair structure values.

Although double-walled CNTs (DWNTs) generally have the same morphology and properties as SWNTs [11], they also exhibit several advantages, such as significantly improved resistance to chemicals, the same thermal and electrical stability as multiwalled CNTs (MWNTs), but the same flexibility as SWNTs [12].

MWNTs have a diameter from 2 nm to 100 nm and a length of tens of microns. They have two

https://doi.org/10.1016/j.drudis.2019.05.019

TABLE 1

Comparison of CNT preparation methods

Method	Product	Advantages	Disadvantages	Refs
Arc discharge	SWNTs 0.6–1.4 nm in diameter or; MWNTs with 1–3 nm inner and 10 nm outer diameter	Upscalable for volume production; nanotube diameter distribution can vary; yield up to 90%	Solid graphite source required; requires high temperature; SWNTs only obtained with use of metal	[4]
Laser ablation	SWNTs 1–2 nm in diameter and 5–20 μm long, or fullerenes	High-quality nanotubes; yield up to 70%	Solid graphite source required; not suitable for manufacture of MWNTs because of short length	[5]
Chemical vapor deposition (CVD)	SWNTs 0.6–4 nm in diameter or MWNTs 10–240 nm in diameter	Distinguished configuration and positional control	Two-step method; typical yield is 30%; often riddled with defects	[6]
Plasma-enhanced CVD	SWNTs or MWNTs	No solid graphite source required	Complicated process	[6]
Alcohol catalytic CVD	SWNTs 1 nm in diameter	SWNTs produced on large scale and at low cost	Obstacles in creating high-purity SWNTs	[6]
Hydrothermal Methods	MWNTs with 10–100 nm inner and 50–150 nm outer diameter nanorods, nanowires, nanobelts and nano-onions	Starting materials stable at ambient temperature; low temperature (150–180 °C) required; no hydrocarbon or carrier gas required		[7]

TABLE 2

Comparison of TNT preparation methods

Method	Advantages	Disadvantages	Refs
Electrochemical treatment	Self-organized TNT layers with large (100 nm) diameter; suitable for surface modification of Ti implants	Length varies (2–101 μm); not suitable for many biomedical applications because of size and potential clearance by reticuloendothelial system	[8]
Template-assisted synthesis	Variable (50–400 nm) diameter based on template pore size		[9]
Hydrothermal treatment	Small (5–10 nm) diameter and 100–1000 nm length; variable dimensions, porosity and specific surface depending on temperature, NaOH concentration, sonication and acidic post-treatment	Strongly agglomerated TNTs, which need to be dispersed before bioapplication; nanosheets result as byproducts (10% of batch)	[8]

structural models: the 'Russian Doll' model, when graphite sheets are ordered in concentric cylinders (Fig. 1), and the 'Parchment' model [11], when a single sheet of graphite is rolled in around itself. The layers have different chiralities with inconsiderable interlayer electronic coupling, and can shift randomly between metallic and semiconducting varieties. The main advantage of MWNTs is that their stiffness is higher than that of SWNTs, especially during compression [12]. The length-to-diameter ratio of MWNTs is >1 000 000 given that they are nanometers in diameter and several millimeters in length [3].

By contrast, TNTs are rolled up into a spiral (Fig. 1). with an inner cavity of ~4 nm and have an amorphous or crystalline structure depending on the specific electrochemical parameters [8]. The TNTs obtained after anodization are amorphous and not photoactive, whereas high temperature annealing converts amorphous TNTs into a crystalline form (anatase or rutile) and, hence, broadens their application range. TNTs are classified according to the synthesis parameters used to prepare TNTs, such as with template-assisted synthesis, hydrothermal treatments, or electrochemical treatments (H.P. Kulkarni, PhD thesis, University of North Carolina at Chapel Hill, 2008), which cause variations in their physical features (e.g., length, and inner diameter and outer diameter distributions).

Comparison of the physicochemical properties

CNTs have highly hydrophobic surfaces because they preserve the apolar characteristics of native graphene/graphite nanosheets and are insoluble in aqueous solutions [13], where the surface charge of CNTs is a function of the pH of the solution [14]. However, their solubility can be enhanced by functionalization [12], which can also facilitate their movement in the body and reduce both the blockage of body organ pathways and toxicity, partially by hindering the accumulation of highly apolar molecules in tissue. Nevertheless, the grade of toxicity (*in vivo* and *in vitro*) is determined by diverse factors, such as size, shape, purity, surface chemistry, and the existence of transition metal catalysts. Furthermore, it appears that the effect of CNTs on organs is related to the administration route used [15]. Intravenous, oral, and dermal administration of CNTs can cause only mild symptoms, whereas inhalation can result in severe inflammation and toxicity to the respiratory system. By contrast, another study reported that no significant lung inflammation or tissue damage was observed following direct inhalation of CNTs.

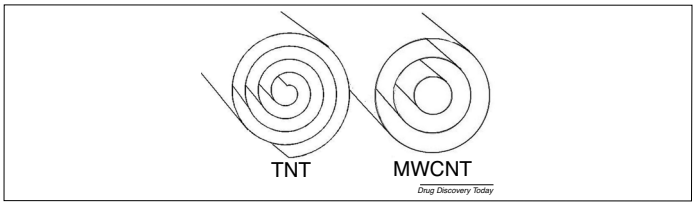

FIGURE 1

Schematic representation of the structural differences between titanate nanotubes (TNTs) and multiwalled carbon nanotubes (MWCNTs).

By contrast, TNTs display strong hydrophilicity because of their partially hydroxylated surface, which causes a negative ζ-potential (after washing until pH = 6) that, when combined with hydrogen bonds, causes superior wettability [16] but often leads to the agglomeration of the particles, especially in dry forms [8]. Their hydrophilicity is also supported by the capillary effect, resulting in the quick penetration of water droplets into the tube pores, and by their crystallinity, given that the amorphous, mixed crystalline phase shows high polarity because of the O–Ti–O bonds and to the extensive presence of hydroxyl groups on the TNT surface. Furthermore, the structure of TNTs also influences the contact angle, which decreases with increases in both tube and pore diameters and with increasing anodization voltage or thermal treatment up to 450 °C; however, beyond 450 °C, their hydrophilicity decreases because of the detachment of hydroxyl groups from the surface [17]. The high surface energy and polarity causes good wettability and, hence, improved cell adhesion. Therefore, TNTs showed extremely good biocompatibility. Bone cell adhesion and differentiation were improved by the use of TNT-covered implants and were proven to be better than those with a pure Ti surface. TNTs were also nontoxic when internalized by cells [18–20]; thus, they appear to have good applicability for therapeutic use in the clinic [21].

Despite their different surface characteristics, CNTs and TNTs exhibit considerable similarities regarding their impressive mechanical, electrical, and optical properties. Nanotubular structures usually have good mechanical properties. In CNTs, the covalent bonds between carbon atoms lead to high tensile strength (up to 63 GPa) and Young's modulus of elasticity (1–1.8 TPa depending on the diameter and the chirality of the tube) [3]. Therefore, SWNTs are stronger than steel by 10 to 100 times per unit weight. By contrast, MWNTs have lower Young's modulus values than SWNTs because stress is only supported by the outer graphite shelf on account of weak intertube cohesion. Similarly, TNTs exhibit high, but one grade lower Young's modulus (230 GPa) and tensile strength (680 MPa) compared with SWNTs. Nevertheless, these values still reflect impressive mechanical properties, supported by the results of Sipos *et al.*, who reported that TNTs and their composites formed with various drugs showed supreme flowability, compressibility, and compactibility compared with crystalline APIs, thus proving their superior processability [22–24]. In terms of their electrical behavior, CNTs display semiconducting or metallic resistance, capacitance, and inductance properties because of their electronic structure and symmetry of graphene [12]. SWNTs can be either semiconducting or metallic, whereas MWNTs are semiconducting. The electrical conductivity of self-organized TNTs is based on their crystalline structure and is tunable with the annealing temperature, because when the amorphous material converts into anatase at 300 °C, it results in significantly higher conductivity, whereas the conversion of anatase into the more resistive rutile above 500 °C reduces the conductivity [25]. In terms of their optical properties, both CNTs and TNTs show optical absorbance: the absorbance of CNTs is in near-infrared (NIR) zone [12], whereas TNTs display wider photo absorption properties, although not as good as TiO_2 NPs. However, when rare earth ions (Pr^{31}, Er^{31}, Nd^{31}, and Yb^{31}) were intercalated into TNTs, higher photoluminescence emission was observed compared with pristine Na-TNTs [26]. Overall, these remarkable properties make CNTs and TNTs an ideal target for a range of diagnostic, biomedical, or pharmaceutical applications.

Applications

The high binding capacity and unique physicochemical, especially electrical properties of nanotubes can be well utilized in specific molecule recognition and other diagnostic applications. CNTs can be used as biosensors to diagnose diseases, record the pulse and temperature of a patient, and measure blood glucose, or other biomolecules, such as H_2O_2, organophosphate pesticides, or cancer markers, in diagnosis and treatment [12,27–29]. In addition, their good biocompatibility and mechanical properties also make nanotubular structures suitable for tissue-engineering applications. CNTs can improve the mechanical strength of implanted catheters and, hence, reduce thrombus formation in cardiovascular surgeries [12]. CNT-coated polyurethane has high interconnected porosity, bioactivity, and nanostructured surface topography. Thus, CNTs can be used as bioactive scaffolds in bone tissue engineering and provide new properties, such as electrical conductivity, to these scaffolds [30], or, when filled with calcium, they can be used directly as a bone substitute, with improved mechanical properties because of their high tensile strength [3]. Consequently, they can help in directing cell growth [12]. Correspondingly, TNT coatings on scaffolds reinforce cell growth on the biodegradable photopolymer scaffolds [31] and also promote bone formation by hastening osteoblast growth by 300–400% compared with non-anodized Ti surfaces [32]. This effect was further improved when TNTs were coated with biocompatible polymer films comprising chitosan and poly(lactic-co-glycolic acid), when superior osteoblast adhesion and cell proliferation were achieved, compared with uncoated TNTs [33].

Given their unique characteristics, such as their hollow monolithic structure, nanoneedle shape, considerable molecule-binding capacity and versatile binding mechanisms, nanotubes are also ideal carriers in other biomedical and pharmaceutical applications. Two different methods exist for binding: wrapping, when drugs and biological molecules are attached to the surface through functional groups; and filling, when drugs and biological molecules are loaded inside CNTs [34].

CNTs display immunogenicity and devised antibody responses linked to viral protein VP1 of foot-and-mouth disease virus (FMDV), which could be utilized for the stimulation of the immune system [3]. The high RNA binding and internalization capacity also make CNTs suitable for cytoplasm or cell core targeting and valuable as vectors to transfer genes and drugs into cells to cure cancer and various genetic disorders [35]. However, SWNTs are more useful compared with MWNTs because of their 1D structure, efficient drug-loading capacity, and large surface area [36]. CNTs conjugated to small interfering (si)RNA molecules were successful in silencing the expression of CD4 cell surface receptors and CXCR4 co-receptors, thus inhibiting the infection of T cells by HIV [37]. Drug-embedded CNTs can also be utilized to kill viruses in viral ulcers without antibody production against the drug, because viruses present no intrinsic immunogenicity for CNTs [38]. CNTs can carry streptavidin and cytochrome C into the cell cytoplasm via the endocytosis pathway [12] and showed high selectivity to kill cancer cells after internalization, achieved by hyperthermia because of their thermal conductivity [39]. However, MWCTs are more suitable than are SWCTs for thermal cancer treatment given that MWNTs absorb NIR radiation faster than do SWNTs [40].

Nevertheless, CNTs can be applied for drug delivery and targeting without external stimulation because the SWCNT-anticancer drug complex increases blood circulation time, enhancing permeability and the retention effect by tumor cells [41], as shown by the successful delivery of amphotericin B [42], the successful delivery and retention of polyphosphazene platinum to the brain [43], the successful oral administration of erythropoietin (EPO) [43] and the slow release of cisplatin in an aqueous

environment to terminate the growth of human lung cancer cells [44].

Based on their physicochemical properties, TNTs offer fewer opportunities to attach drugs or other molecules; however, based on their unique properties, such as biocompatibility, mechanical strength, and chemical resistivity, they are proposed to be ideal materials for the development of various medical implants and devices. Thus, TNTs have so far been applied mainly in dentistry, orthopedics, and cardiovascular surgery [45].

Functionalization of TNTs and CNTs

Functionalization is the attaching of appropriate molecules to the nanostructure surface to render them soluble in water, reduce toxicity, increase biocompatibility [46], achieve targeted drug delivery, obtain selective binding to the desired epitope, achieve controlled drug release, facilitate cellular internalization, enhance biodistribution, and improve biofluid circulation. Many types of functionalization molecule have been used, such as polyethylene glycol (PEG), polyvinylpyrrolidone (PVP), cellulose, polypeptides, dextran, and silica [2].

CNTs can be functionalized covalently or noncovalently on the tips and side walls, although CNT tips have a higher functionalization affinity compared with the side walls [46]. Noncovalent functionalization, including Van der Waals interactions, π–π interactions, and hydrophobic interactions, causes minimal damage to the CNT surface and maintains the aromatic structure and, consequently, the electronic characteristics of CNTs. However, the disadvantage is that this kind of functionalization is not appropriate for targeted drug delivery applications because of the weak forces formed [47]. By contrast, covalent functionalization of CNTs can be achieved via oxidizing them by strong acids, such as nitric and sulfuric acids [48]. Hence, the forming of carboxylic acid groups because of the high negative charge increases the hydrophilicity, water solubility, and biocompatibility of CNTs [49]. By contrast, the disadvantage is that covalent functionalization damages CNT side walls and, thus, CNTs cannot be used in some applications, such as imaging [37]. Nevertheless, the presence of carboxylic and other oxygen-containing groups on the surface of CNTs also allows the covalent attachment of functional molecules [50]. The covalent surface functionalization of CNTs with amine-terminated PEG stabilizes CNT dispersions in various media and reduces deleterious effects on cultured cells [51], and oxidation debris (i.e., the breaking CNTs during oxidation or oxidizing carbonaceous nontubular structures in pristine CNT samples).

Similarly, the surface characteristics, such as the negative charge at physiological pH caused by the presence of hydroxyl groups on their surface above their isoelectric point (pH 3.7), enable TNTs to react with a variety of functional molecules [52]. The functionalization of TNTs improves their stability for vectorization applications and enables them to carry therapeutic molecules [53]. Tables 3 and 4 detail methods for the functionalization of CNTs and TNTs, respectively.

TABLE 3

Functionalization possibilities of CNTs

Reagent(s)	Aim of functionalization/grafting	Refs
Nitric acid (HNO_3)	Carboxylic groups covered MWNTs; increase solubility	[54]
$NH_2(CH_2CH_2O)_2–CH_2CH_2NH_2$	NH_2 covering of MWNTs; increase solubility; decrease aggregation; decrease cytotoxic effects	[55]
Second-generation poly (amidoamine) dendrimer (G_2-PAMAM)	Increase surface binding ability of DNA probe by supplying large number of amino groups	[56]
Folate moiety	Selective destruction of cancer cells labeled with folate receptor tumor markers; NIR-triggered cell death without harming receptor-free normal cells	[39]
Phospholipid-PEG2000-NH_2	Photothermal cancer treatment in mice by NIR irradiation	[51]
HNO_3 and salicylaldehyde	Reduce reaction step number and reaction time	[50]
HNO_3 and $H2SO_4$ mixture; 1-(3-dimethylaminopropyl)-3-ethylcarbodiimide hydrochloride; *N*-hydroxysuccinimide; P-glycoprotein antibody	Specific recognition of multidrug-resistant human leukemia cells (K562R)	[57]

TABLE 4

Functionalization possibilities of TNTs

Reagent(s)	Aim of functionalization/grafting	Res
Dopamine; Tris buffer; bone morphogenetic protein 2 (BMP_2)	Enhance bone osseointegration	[58]
3-isocyanatopropyltriethoxy; PEG; polyethylene imine (PEI)	Enhance TNT dispersion in water and reactivity	[53]
Allyltriethoxysilane; propyltriethoxysilane	Form stable suspensions in tetrahydrofuran (THF)	[59]
Antimicrobial peptides (HHC-36)	Prevent formation of biofilms (based on bactericide and bacteriostatic effect)	[60]
3-aminopropyltriethoxysilane; RGD peptide	Promote initial attachment and proliferation of human mesenchymal stem cells (hMSCs)	[61]
KRSR	Increase osteogenic differentiation and pre-osteoblast adhesion and spread on TNT surface	[62]
N,*N*-carbonyl diimidazole; 11-hydroxy-undecylphosphonic acid; EGF and BMP_2 growth factors	Increasing number and activity of MSCs	[63]
Gelatin-stabilized gold NPs	Improve MC3T3-E1 osteoblast cell adhesion and propagation (achieved)	[64]
Chitosan	Achieve sustained release of loaded drug (selenium or quercetin) from TNTs	[65,66]

Concluding remarks

Drug delivery devices based on nanotubular structures are ideal for modern theranostic applications because of their advantageous properties. However, they can bear the risk of toxicity attributable to their size, surface charge, chemical composition, chemical reactivity, chemical structure, crystal structure, shape, solubility, and degree of agglomeration. Moreover, nanomaterials can cause oxidative stress and damage phagocytosis inside the cells, reduce cell viability, and suppress cell proliferation by producing reactive oxygen species or remaining in the body because of their ability to evade the reticuloendothelial system.

Despite many promising results and numerous advantages, pristine CNTs are insoluble in water and most solvents; thus, they cannot be used immediately in biomedical applications. Furthermore, they bear a considerable risk of toxicity and carcinogenicity because they accumulate in the human body because of their strongly hydrophobic nature and residual metal catalysts, which increases their ability to produce O^{2-} anions, lipid peroxidation, or physical blockage generated from agglomeration at high doses, given that CNTs also have a strong electrostatic attraction.

By contrast, TNTs have exhibited promising toxicological profiles and good biocompatibility in numerous studies and a vital affinity for bone cell adhesion and differentiation, which allows their use in dentistry, orthopedics, and cardiovascular surgery. Therefore, and as a result of their tubular structure, CNT-similar chemical resistivity, mechanical strength, and electron mobility, TNTs might be promising alternatives for developing medical implants and devices. Nevertheless, despite these advantages, TNTs, especially hydrothermally synthetized free TNTs, are poorly studied in terms of their use in drug delivery applications, possibly because of their hydrophilic nature, which improves their biocompatibility and decreases the risk of adverse effects, but also acts negatively on their absorption and cell internalization properties. Thus, functionalization might be key to improving their applicability, given that the range of possibilities is almost as wide as for CNTs. Noncovalent bindings based on van der Waals forces, hydrogen bonds or π–π interactions are easily achievable, which maintain the aromatic structure and electronic characteristics; obtaining covalent functionalization with ether- or esterification of the free surface -OH groups is also possible. With the selection of the appropriate functional groups, the surface properties and, therefore, their absorption and internalization capacity could be improved without the considerable elevation of the risk of toxicity. Furthermore, their similar mechanical, electrical, and optical parameters could provide the same level of processability and range for external stimuli-adjusted targeting possibilities as CNTs.

In terms of their low toxicity and advantageous physicochemical properties, the further investigation, use, and application of hydrothermally synthetized TNTs is recommended for the development of new advanced drug delivery systems.

References

1 Suri, S.S. *et al.* (2007) Nanotechnology-based drug delivery systems. *J. Occup. Med. Toxicol.* 2, 16
2 Raliya, R. *et al.* (2016) Perspective on nanoparticle technology for biomedical use. *Curr. Pharma. Des.* 22, 2481–2490
3 Mahajan, D. (2017) Carbon nanotubes: a review on synthesis, electrical and mechanical properties and applications. *Asian J. Appl. Sci. Technol.* 1, 15–20
4 Ebbesen, T. and Ajayan, P. (1992) Large-scale synthesis of carbon nanotubes. *Nature* 358, 220
5 Sivaram, A. (2004) Laser ablation process for single-walled carbon nanotube production. *J. Nanosci. Nanotechnol.* 4, 317–325
6 Khurshed, A. *et al.* (2016) Synthesis of carbon nanotubes by catalytic chemical vapour deposition: a review on carbon sources, catalysts and substrates. *Mater. Sci. Semicond. Process.* 41, 67–82
7 Gogotsi, Y. and Libera, J.A. (2000) Hydrothermal synthesis of multiwall carbon nanotubes. *J. Mater. Res.* 15, 2591–2594
8 Boudon, J. *et al.* (2014) Titanate nanotubes as a versatile platform for nanomedicine. In *Nanomedicine* (Seifalian, A., ed.), pp. 403–429, One Central Press, Altricham, UK
9 Rørvik, P.M. *et al.* (2009) Template-assisted synthesis of PbTiO3 nanotubes. *J. Eur. Ceram. Soc.* 29, 2575–2579
10 Odom, T.W. *et al.* (1998) Atomic structure and electronic properties of single-walled carbon nanotubes. *Nature* 391, 62–64
11 Mamedov, A.A. *et al.* (2002) Molecular design of strong single-wall carbon nanotube/polyelectrolyte multilayer composites. *Nat. Mater.* 1, 190–194
12 Kumar, S.P. *et al.* (2012) Pharmaceutical application of carbon nanotube-mediated drug delivery system. *Int. J. Pharm. Sci. Nanotechnol.* 5, 1685–1696
13 Liu, Z. *et al.* (2009) Carbon nanotubes in biology and medicine: *in vitro* and *in vivo* detection, imaging and drug delivery. *Nano Res.* 2, 85–120
14 Dezfoli, A.R.A. *et al.* (2013) Structural properties of water around uncharged and charged carbon nanotubes. *Kor. J. Chem. Eng.* 30, 693–699
15 Smart, S.K. *et al.* (2006) The biocompatibility of carbon nanotubes. *Carbon* 44, 1034–1047
16 Wang, F. *et al.* (2013) Bioinspired micro/nano fabrication on dental implant–bone interface. *Appl. Surf. Sci.* 265, 480–488
17 Indira, K. *et al.* (2015) A review on TiO2 nanotubes: influence of anodization parameters, formation mechanism, properties, corrosion behavior, and biomedical applications. *J. Bio. Tribo. Corr.* 1, 28
18 Papa, A.-L. *et al.* (2012) Titanate nanotubes: towards a novel and safer nanovector for cardiomyocytes. *Nanotoxicology* 7, 1131–1142
19 Mirjolet, C. *et al.* (2013) The radiosensitization effect of titanate nanotubes as a new tool in radiation therapy for glioblastoma: a proof-of-concept. *Radiother. Oncol.* 108, 136–142
20 Fenyvesi, F. *et al.* (2014) Investigation of the cytotoxic effects of titanate nanotubes on Caco-2 cells. *AAPS PharmSciTech* 15, 858–861
21 Wang, Q. *et al.* (2016) TiO2 nanotube platforms for smart drug delivery: a review. *Int. J. Nanomedicine* 11, 4819–4834
22 Matsuno, R. *et al.* (2004) Polystyrene-and poly (3-vinylpyridine)-grafted magnetite nanoparticles prepared through surface-initiated nitroxide-mediated radical polymerization. *Macromolecules* 37, 2203–2209
23 Sipos, B. *et al.* (2017) Comparative study on the rheological properties and tablettability of various APIs and their composites with titanate nanotubes. *Powder Technol.* 321, 419–427
24 Sipos, B. *et al.* (2018) Investigation of the compressibility and compactibility of titanate nanotube–API composites. *Materials* 11, 2582
25 Tighineanu, A. *et al.* (2010) Conductivity of TiO2 nanotubes: Influence of annealing time and temperature. *Chem. Phys. Lett.* 494, 260–263
26 Marques, T.M.F. *et al.* (2017) Photoluminescence enhancement of titanate nanotubes by insertion of rare earth ions in their interlayer spaces. *J. Nanomater.* 2017, 3809807
27 Bandaru, P.R. (2007) Electrical properties and applications of carbon nanotube structures. *J. Nanosci. Nanotechnol.* 7, 1239–1267
28 Zhang, M. and Gorski, W. (2005) Electrochemical sensing platform based on the carbon nanotubes/redox mediators-biopolymer system. *ACC Chem. Res.* 127, 2058–2059
29 Liu, G. and Lin, Y. (2006) Biosensor based on self-assembling acetylcholinesterase on carbon nanotubes for flow injection/amperometric detection of organophosphate pesticides and nerve agents. *Anal. Chem.* 78, 835–843
30 Harrison, B.S. and Atala, A. (2007) Carbon nanotube applications for tissue engineering. *Biomaterials* 28, 344–353
31 Minagar, S. *et al.* (2013) Cell response of anodized nanotubes on titanium and titanium alloys. *J. Biomed. Mater. Res. A* 101, 2726–2739
32 Yamamoto, A. *et al.* (1998) A new technique for direct measurement of the shear force necessary to detach a cell from a material. *Biomaterials* 19, 871–879
33 Gulati, K. *et al.* (2012) Biocompatible polymer coating of titania nanotube arrays for improved drug elution and osteoblast adhesion. *Acta Biomater.* 8, 449–456
34 Sahoo, N.G. *et al.* (2011) Functionalized carbon nanomaterials as nanocarriers for loading and delivery of a poorly water-soluble anticancer drug: a comparative study. *Chem. Commun.* 47, 5235–5237
35 Kam, N.W.S. *et al.* (2005) Functionalization of carbon nanotubes via cleavable disulfide bonds for efficient intracellular delivery of siRNA and potent gene silencing. *J. Am. Chem. Soc.* 127, 12492–12493
36 Madani, S.Y. *et al.* (2011) A new era of cancer treatment: carbon nanotubes as drug delivery tools. *Int. J. Nanomedicine* 6, 2963–2979
37 Liu, Z. *et al.* (2009) Preparation of carbon nanotube bioconjugates for biomedical applications. *Nat. Protoc.* 4, 1372–1381

38 Pantarotto, D. *et al.* (2003) Immunization with peptide-functionalized carbon nanotubes enhances virus-specific neutralizing antibody responses. *Chem. Biol.* 10, 961–966
39 Kam, N.W.S. *et al.* (2005) Carbon nanotubes as multifunctional biological transporters and near-infrared agents for selective cancer cell destruction. *Proc. Natl. Acad. Sci. U. S. A.* 102, 11600–11605
40 Hirsch, L.R. *et al.* (2003) Nanoshell-mediated near-infrared thermal therapy of tumors under magnetic resonance guidance. *Proc. Natl. Acad. Sci. U. S. A.* 100, 13549–13554
41 Liu, Z. *et al.* (2008) Drug delivery with carbon nanotubes for *in vivo* cancer treatment. *Cancer Res.* 68, 6652–6660
42 Barroug, A. and Glimcher, M.J. (2002) Hydroxyapatite crystals as a local delivery system for cisplatin: adsorption and release of cisplatin in vitro. *J. Orthop. Res.* 20, 274–280
43 Pai, P. *et al.* (2006) Pharmaceutical applications of carbon tubes and nanohorns. *Pharm. Res.* 1, 11–15
44 Ajima, K. *et al.* (2005) Carbon nanohorns as anticancer drug carriers. *Mol. Pharm.* 2, 475–480
45 Rahman, Z.U. *et al.* (2016) Electrochemical & osteoblast adhesion study of engineered TiO 2 nanotubular surfaces on titanium alloys. *Mater. Sci. Eng. C* 58, 160–168
46 Prato, M. *et al.* (2007) Functionalized carbon nanotubes in drug design and discovery. *ACC Chem. Res.* 41, 60–68
47 Liu, Z. *et al.* (2007) Supramolecular chemistry on water-soluble carbon nanotubes for drug loading and delivery. *ACS Nano.* 1, 50–56
48 Klumpp, C. *et al.* (2006) Functionalized carbon nanotubes as emerging nanovectors for the delivery of therapeutics. *Biochim. Biophys. Acta Biomembr.* 1758, 404–412
49 Nagasawa, S. *et al.* (2000) Effect of oxidation on single-wall carbon nanotubes. *Chem. Phys. Lett.* 328, 374–380
50 Wang, Y. *et al.* (2005) Microwave-induced rapid chemical functionalization of single-walled carbon nanotubes. *Carbon* 43, 1015–1020
51 Moon, H.K. *et al.* (2009) *In vivo* near-infrared mediated tumor destruction by photothermal effect of carbon nanotubes. *ACS Nano* 3, 3707–3713
52 Papa, A.-L. *et al.* (2011) Synthesis of titanate nanotubes directly coated with USPIO in hydrothermal conditions: a new detectable nanocarrier. *J. Phys. Chem. C* 115, 19012–19017
53 Papa, A.-L. *et al.* (2015) Dispersion of titanate nanotubes for nanomedicine: comparison of PEI and PEG nanohybrids. *Dalton Trans.* 44, 739–746
54 Chen, C.-C. *et al.* (2007) Modification of multi-walled carbon nanotubes by microwave digestion method as electrocatalyst supports for direct methanol fuel cell applications. *Electrochem. Comm.* 9, 159–163
55 Coccini, T. *et al.* (2010) Effects of water-soluble functionalized multi-walled carbon nanotubes examined by different cytotoxicity methods in human astrocyte D384 and lung A549 cells. *Toxicology* 269, 41–53
56 Zhu, N. *et al.* (2010) Sensitive impedimetric DNA biosensor with poly (amidoamine) dendrimer covalently attached onto carbon nanotube electronic transducers as the tether for surface confinement of probe DNA. *Biosens. Bioelectron.* 25, 1498–1503
57 Li, R. *et al.* (2010) P-glycoprotein antibody functionalized carbon nanotube overcomes the multidrug resistance of human leukemia cells. *ACS Nano.* 4, 1399–1408
58 Lai, M. *et al.* (2011) Surface functionalization of TiO2 nanotubes with bone morphogenetic protein 2 and its synergistic effect on the differentiation of mesenchymal stem cells. *Biomacromolecules* 12, 1097–1105
59 Byrne, M.T. *et al.* (2007) Chemical functionalisation of titania nanotubes and their utilisation for the fabrication of reinforced polystyrene composites. *J. Mater. Chem.* 17, 2351–2358
60 Kazemzadeh-Narbat, M. *et al.* (2013) Multilayered coating on titanium for controlled release of antimicrobial peptides for the prevention of implant-associated infections. *Biomaterials* 34, 5969–5977
61 Oh, S. *et al.* (2013) Effect of RGD peptide-coated TiO 2 nanotubes on the attachment, proliferation, and functionality of bone-related cells. *J. Nanomater.* 2013, 965864
62 Oliveira, W.F. *et al.* (2017) Functionalization of titanium dioxide nanotubes with biomolecules for biomedical applications. *Mater. Sci. Eng. C* 81, 597–606
63 Bauer, S. *et al.* (2011) Covalent functionalization of TiO 2 nanotube arrays with EGF and BMP-2 for modified behavior towards mesenchymal stem cells. *Integr. Biol.* 3, 927–936
64 Neupane, M.P. *et al.* (2011) Titania nanotubes supported gelatin stabilized gold nanoparticles for medical implants. *J. Mater. Chem.* 21, 12078–12082
65 Chen, X. *et al.* (2013) Fabrication of selenium-deposited and chitosan-coated titania nanotubes with anticancer and antibacterial properties. *Coll. Surf. B: Biointerfaces* 103, 149–157
66 Mohan, L. *et al.* (2016) Drug release characteristics of quercetin-loaded TiO_2 nanotubes coated with chitosan. *Int. J. Biol. Macromolecul.* 93, 1633–1638

Yasmin Ranjous
Géza RegdonJr.
Klára Pintye-Hódi
Tamás Sovány*

University of Szeged, Institute of Pharmaceutical Technology and Regulatory Affairs, H-6720, Eötvös u. 6, Szeged, Hungary

*Corresponding author.

nanomaterials

MDPI

Article

Optimization of the Production Process and Product Quality of Titanate Nanotube–Drug Composites

Yasmin Ranjous [1], Géza Regdon Jr. [1], Klára Pintye-Hódi [1], Tamás Varga [2], Imre Szenti [2], Zoltán Kónya [2,3] and Tamás Sovány [1,*]

[1] Institute of Pharmaceutical Technology and Regulatory Affairs, University of Szeged, Eötvös u. 6., H-6720 Szeged, Hungary; yasmin.ranjous@pharm.u-szeged.hu (Y.R.); geza.regdon@pharm.u-szeged.hu (G.R.J.); klara.hodi@pharm.u-szeged.hu (K.P.-H.)

[2] Department of Applied and Environmental Chemistry, University of Szeged, Rerrich Béla tér 1., H-6720 Szeged, Hungary; tamas.varga@chem.u-szeged.hu (T.V.); imre.szenti@chem.u-szeged.hu (I.S.); konya@chem.u-szeged.hu (Z.K.)

[3] Reaction Kinetics and Surface Chemistry Research Group, Hungarian Academy of Sciences-University of Szeged, Rerrich Béla tér 1, H-6720 Szeged, Hungary

* Correspondence: t.sovany@pharm.u-szeged.hu; Tel.: +36-62-545-576

Received: 17 September 2019; Accepted: 28 September 2019; Published: 2 October 2019

Abstract: Recently, there has been an increasing interest in the application of nanotubular structures for drug delivery. There are several promising results with carbon nanotubes; however, in light of some toxicity issues, the search for alternative materials has come into focus. The objective of the present study was to investigate the influence of the applied solvent on the composite formation of titanate nanotubes (TNTs) with various drugs in order to improve their pharmacokinetics, such as solubility, stability, and bioavailability. Composites were formed by the dissolution of atenolol (ATN) and hydrochlorothiazide (HCT) in ethanol, methanol, 0.01 M hydrochloric acid or in ethanol, 1M sodium hydroxide, dimethylformamide (DMF), dimethyl sulfoxide (DMSO), respectively, and then they were mixed with a suspension of TNTs under sonication for 30 min and vacuum-dried for 24 h. The structural properties of composites were characterized by SEM, TEM, FT-IR, differential scanning calorimetry (DSC), thermogravimetric (TG) analysis, and optical contact angle (OCA) measurements. Drug release was determined from the fast disintegrating tablets using a dissolution tester coupled with a UV–Vis spectrometer. The results revealed that not only the good solubility of the drug in the applied solvent, but also the high volatility of the solvent, is necessary for an optimal composite-formation process.

Keywords: atenolol; hydrochlorothiazide; titanate nanotubes; composite formation; solvent selection

1. Introduction

Oral administration is the main route of drug administration for a systemic effect [1]. Orally administered drugs should be released from the dosage form and dissolve before absorption. Thus, numerous attempts such as complexation, particle size reduction, solid state alternation, the application of soft gel technology, solid dispersions, using cosolvents or forming emulsions, microemulsions, micelles, polymeric micelles, liposomes, pharmaceutical salts, and pro-drugs have been made to increase the dissolution rate of the drugs in order to improve their bioavailability [2]. Particle size reduction is an easy and suitable approach to increase the dissolution rate and thus the absorption due to the increment in specific surface area [3]; however, the stabilization of particle size may be a critical issue in this approach.

Solid state dispersion is a particularly promising technique to enhance the solubility, dissolution rate, and bioavailability of poorly water-soluble drugs and to resolve the stability problems

of micronized/nanonized drugs, which are dispersed in an inert solid carrier or matrix either as fine particles or molecularly [4]. This technique has numerous advantages from many aspects, such as improved stability due to the probable interactions between the drug and carrier functional groups [5], the increment of glass transition temperature of the solid dispersion matrix [6] or the displacement of crystalline structure by an amorphous form [7,8], resulting in local solubility and wettability improvement of poorly soluble drugs [9], and suppression of drug precipitation from the supersaturated solution to achieve higher solubility and dissolution rate for the metastable drug polymorphs connected to the carrier [10]. Solid dispersions may be divided into multiple classes including solid solutions, drug–carrier complexes, glassy solutions or suspensions, simple eutectic mixtures, and amorphous drug precipitates in a crystalline carrier [11]. Solid state dispersions can be prepared with various methods including the fusion process, solvent method, fusion-solvent method, spray drying, lyophilization, hot-melt extrusion, the electrospinning method, supercritical fluid technology, and spraying on beads using a fluidized-bed coating system [2]. In the solvent method, the drug and the carrier are dissolved in a suitable solvent, which will later be evaporated at an elevated temperature or under vacuum. Then, supersaturation and simultaneous precipitation of the components happens, resulting in a solid residue. Afterwards, organic and/or toxic solvents should be completely removed under vacuum. For this purpose, many sensitive techniques can be used to detect the trace amounts of solvents, such as differential scanning calorimetry (DSC), thermogravimetric (TG) analysis, or differential thermal analysis (DTA) [2]. The upsides of this method are the ability to control drug particle size by monitoring the temperature and the solvent evaporation rate [3], the capability of evaporating solvents at a lower temperature, and reduced pressure for thermolabile drugs or for frozen systems [2]. The downsides of this method are the difficulty of choosing the appropriate solvent for both the drug and the carrier, since most of the carriers are hydrophilic while the drugs are hydrophobic [12], the necessity of complete solvent removal, especially if the solvents can plasticize the carrier [13], and the large volume of solvent required to dissolve both the drug and the carrier, which is not economical in some cases [2].

Conventional drugs have many limitations, such as restricted drug solubility, undesirable pharmacodynamics, side effects, short circulating time, and lack of selectivity [14–17]. Of the drugs currently on the market, 90% are hydrophobic and poorly soluble or insoluble in water, which restricts systemic delivery [18]. However, nanocarriers may improve solubility, absorption, permeation, and retention in the target tissues, as well as the bioavailability, circulation time, and stability of drug molecules [19]. Furthermore, they may protect various drug molecules from premature degradation in the body and show higher uptake efficiency in the target cells compared to normal cells [20]. Nanotubes not only have an exemplary inner diameter of 5–6 nm, which makes them able to contain therapeutic drugs and large biological molecules, but also a large surface area and distinct outside geometry, which enable them to be modified and multi-functionalized [21].

Titanate nanotubes (TNTs) have particularly appealing characteristics, such as hydrophilicity, biocompatibility, high surface area, stable tubular structures [22], controllable dimensions, tunable geometries, surface chemistry, and the ability to modulate drug release kinetics [23]. In addition, layered titanate nanostructures have been used in several industrial applications, such as pharmaceutics, energy storage, photocatalysis, electronics, paints, and coatings. Moreover, 1D titanate nanomaterials are receiving more scientific interest, evidenced by the fact that about one new paper is published daily, according to an ISI Web of Science topic search [23]. Furthermore, TNTs can be used as drug carriers since they can load a higher amount of drug compared to carbone nanotubes (CNTs) [24].

In a previous work, 70% ethanol solution was used as a solvent to prepare composites with various drugs [25]. The selected solvent was able to improve the poor aqueous solubility of diclofenac sodium, atenolol (ATN), and hydrochlorothiazide (HCT) [26–28] or improve the crystallization of the highly water-soluble diltiazem HCl, while providing uniform process conditions for better comparability. Nevertheless, the result revealed that the composite formation was suboptimal for ATN and HCT. According to our hypothesis, the suboptimal solubility of the drug in the solvent, the featured

crystal growth due to slow evaporation, and the intensive drug–solvent interactions may be possible explanations. The present study aims to optimize the composite formation of TNTs with atenolol (ATN) and hydrochlorothiazide (HCT), thus improving the solubility and bioavailability of the active pharmaceutical ingredients (APIs). These drugs have poor bioavailability due to different reasons. ATN belongs to the 3rd class of the Biopharmaceutical Classification System (BCS), so it has good solubility but poor permeability, which results in a lower than 50% absorption rate from the GI tract, especially if it is taken with food. HCT belongs to BCS class IV, so poor bioavailability is due to poor solubility and permeability. The successful binding of these drugs to an appropriate nanocarrier in nanocrystalline or especially in amorphous form may considerably increase their bioavailability. Therefore, the selection of the optimal solvents and process conditions is essential for such drugs.

2. Materials and Methods

The titanate nanotubes (TNTs), TNT-ATN (TiATN), and TNT-HCT (TiHCT) composites were prepared at the University of Szeged's Department of Applied and Environmental Chemistry following the general composite formation method described by Sipos et al. [25]. However, since composite formation was not completely successful in the previous study, the 70% ethanol solution was replaced with methanol (0.0168% water content) and 0.01 M aqueous solution of HCl (HCl 0.01 M) or with 1 M aqueous solution of sodium hydroxide (NaOH 1M), DMF (0.012% water content), and DMSO (0.027% water content) for the synthesis of TiATN and TiHCT, respectively. The water content of the solvents was determined with Karl–Fisher titration. The solvents were purchased from Molar Chemicals Ltd., Budapest, Hungary. In addition, since TNTs exhibit instability below pH 2, TNTs treated with HCl 0.01 M were prepared as a reference to detect if this solvent may cause any change in the properties of titanate nanotubes.

ATN and HCT were kindly supplied by TEVA Pharmaceuticals PLC, Debrecen, Hungary and Gedeon Richter PLC, Budapest, Hungary, respectively. The excipients used for tablets were Avicel PH 112 (FMC Biopolymer Inc., Philadelphia, PA, USA), Tablettose 70 (Meggle Pharma GmbH, Wasserburg am Inn, Germany), talc, and magnesium stearate (both from Molar Chemicals Ltd., Budapest, Hungary).

Hydrothermally synthetized TNTs were prepared by adding 120 g of NaOH in 300 mL of distilled water on a magnetic stirrer for a few minutes and then adding 75 g of TiO_2 for 15 min. After that, the mixture was put in the autoclave at 185 °C for 24 h then cooled at room temperature for 2 h, followed by cooling with cold water. TNTs were washed with distilled water under vacuum and by using filter No:4.

TNTs with HCl 0.01 M were prepared by adding 50 g of TNTs in 300 mL of HCl 0.01 M in an ultrasonic bath until a homogenous suspension was obtained. After that, 200 mL of HCl 0.01 M was added to the previous suspension on a magnetic stirrer and the mixture was dried in a dry oven for 24 h to remove the solvent.

A 1:1 ratio of TiATN–methanol and TiATN–HCl composites were prepared by adding 50 g of TNTs in 300 mL of methanol in an ultrasonic bath until a homogenous suspension was obtained and 50 g of atenolol in 200 mL of methanol on a magnetic stirrer. After that, the two mixtures were added to each other on the magnetic stirrer, and the final mixture was put in a vacuum distillation device until complete removal of the solvent.

To prepare a 1:1 ratio of TiHCT–NaOH composite, 50 g of TNTs were put in 1000 mL of NaOH 1 M in an ultrasonic bath to get a homogenous suspension, and 50 g of HCT was dissolved in 500 mL of NaOH 1 M on a magnetic stirrer until complete dissolution. Furthermore, the two prepared mixtures were added to each other on a magnetic stirrer until reaching homogeneity. After that, 130 mL of HCl 37% was added to neutralize the final mixture, which was washed with distilled water in a vacuum dryer until pH = 9 to eliminate the solvent. Finally, the obtained powder was dried in a dry oven for 24 h to get the required composites TiATN and TiHCT.

A 1:1 ratio of TiHCT–DMF and TiHCT–DMSO composites were prepared by adding 50 g of TNTs in 1000 mL of DMF in an ultrasonic bath and 50 g of HCT with 1000 mL of DMF on a magnetic stirrer.

Then, the two prepared mixtures were added to each other on a magnetic stirrer until a homogenous mixture was obtained, which was put in a vacuum distillation device to remove the solvent.

The morphology and size of the TNTs and composites were investigated by scanning electron microscope (SEM) (Hitachi 4700, Hitachi Ltd., Tokyo, Japan) and transmission electron microscope (TEM) (FEI Tecnai G2 20 X-TWIN, Hillsboro, OR, USA). The APIs, TNTs, and the composites were coated with a thin conductive gold layer by a sputter coating unit (Polaron E5100, VG Microtech, London, UK) for the SEM measurements. The images were taken at an accelerating voltage of 10.0 kV, the used air pressure was 1.3–13 mPa during the analyses. TEM images were taken at 100 kV of electron energy, and those images served to analyze the particle size of TNTs by using Image J 1.47 t (National Institute of Health, Bethesda, MD, USA) software.

To detect the interactions between the APIs and the TNTs, a Thermo Nicolet Avatar 330 FT-IR spectrometer (Thermo Fisher Scientific Ltd., Waltham, MA, USA) was used. Measurements were performed with a Transmission E.S.P. accessory by using 256 scans at a resolution of 4 nm and applying H_2O and CO_2 corrections. Results were evaluated with Spectragryph 1.2.8 software (Friedrich Menges, Obersdorf, Germany). For better comparability of the original spectra of ATN and HCT with the TiATN and TiHCT composites, respectively, the signal of TNTs was subtracted from the composite spectra and the spectra were normalized to the highest peak which belongs to C=O stretching.

The surface free energy of the prepared samples was determined with a DataPhysics OCA20 (DataPhysics Instruments GmbH, Filderstadt, Germany) optical contact angle tester by using the sessile drop method. Polar and apolar test liquid (water and diiodomethane) were used and dropped onto the surface of 13-mm-diameter tablets prepared with a Specac hydraulic press (Specac Ltd., Orpington, UK) at a pressure of 3 tons. Disperse (${\gamma_s}^D$) and polar (${\gamma_s}^P$) components of the total surface free energy (γ_s) of the solid were calculated according to Wu Equations (1) and (2).

$$(1 - \cos\Theta_1)\gamma_1 = 4(({\gamma_1}^D{\gamma_s}^D)/({\gamma_1}^D + {\gamma_s}^D)) + (({\gamma_1}^P{\gamma_s}^P)/({\gamma_1}^P + {\gamma_s}^P))), \quad (1)$$

$$(1 - \cos\Theta_2)\gamma_2 = 4(({\gamma_2}^D{\gamma_s}^D)/({\gamma_2}^D + {\gamma_s}^D)) + (({\gamma_2}^P{\gamma_s}^P)/({\gamma_2}^P + {\gamma_s}^P))), \quad (2)$$

where γ_1 is the surface tension of the first and γ_2 is the surface tension of the second liquid.

Polarity was calculated according to the following Equation (3):

$$\text{Polarity} = \text{У}s^P/\text{У}s \times 100. \quad (3)$$

The thermal behavior of TNTs, APIs, and composites was determined by thermogravimetric analysis (TGA) and differential scanning calorimetry (DSC) analysis. TGA and DSC tests were performed by a Mettler Toledo TGA/DSC1 simultaneous analyzer (Mettler-Toledo Ltd., Budapest, Hungary) in which the samples were heated steadily from 25 to 500 °C with a heating rate of 10 K/min, using nitrogen as purge gas. The mass of the samples was 10 ± 1 mg in a closed aluminum pan (100 µL). The curves were evaluated with STARe Software (Mettler-Toledo Ltd, Budapest Hungary). To compare the curves of the API, TNTs, and the composite, the results were normalized to sample weight and to the temperature of the reference pan.

Tablets containing APIs or API–TNT composites (Table 1) were formulated to study drug release. The powders were mixed with a Turbula mixer (Willy A. Bachofen Maschinenfabrik AG, Muttenz, Switzerland) for 8 min without magnesium stearate and for an additional 2 min with it. Tablets (300 mg) containing 50 mg of API were prepared with a Korsch EK0 eccentric tablet press (E. Korsch Maschinenfabrik GmbH, Berlin, Germany) instrumented with strain gauges and a displacement transducer using 10-mm-diameter flat punches and a 5 kN compression force for all compositions.

Table 1. Compositions of active pharmaceutical ingredient (API) and titanate nanotube (TNT)–API tablets.

Materials	API Tablets	TNT-API Tablets
API	16.7%	-
TNT–API	-	33.3%
Avicel PH 112	50.0%	39.5%
Tablettose	29.3%	23.2%
Talc	3.0%	3.0%
Mg stearate	1.0%	1.0%

Drug release was determined with an Erweka DT700 (Erweka GmbH, Heusenstamm, Germany) dissolution tester using the USP II method. Dissolution was applied at 37 °C using pH 1.2 enzyme-free artificial gastric juice as dissolution media. Samples of 5 mL were taken after 5 min, 10 min, 15 min, 30 min, 60 min, 90 min, and 120 min. The concentration of the released drug was measured with a ThermoScientific GENESYS 10S UV–Vis spectrophotometer (Thermo Fisher Scientific Ltd., Waltham, MA, USA), and the results were evaluated with Sigmaplot v12 (Systat Sofware Inc., San Jose, CA, USA) software.

3. Results

3.1. Properties of the TNTs

Hydrothermal synthesis produces TNTs with asymmetric, open-ended, and particular spiral cross-sectioned tubular structure [25]. The dimensions and surface characteristics of TNTs are sensitive to the synthesis conditions. Since the present work compares the properties of freshly synthetized TNTs and TNT–API composites with those from the previous work [25], the appropriate reproduction of the properties of the starting TNTs was essential.

According to TEM images (Figure 1a), TNTs were effectively prepared without nanowire formation. The obtained TNTs had an average length of 116.22 nm (SD ± 49.49 nm) and an average diameter of 10.99 nm (SD ± 10.15 nm), which considerably approaches the previously described results of Sipos et al. [25]. The SEM images (Figure 1b) also exhibited the characteristic aggregates of almost distinct and randomly oriented TNTs. Furthermore, the results of the contact angle measurements showed no significant difference in the surface characteristics of the new and the previous batch of TNTs (Table 2).

TNT–HCl samples were also prepared as a reference to investigate the effect of diluted 0.01 M HCl on the properties of TNTs (Figure 1c,d) since strong acidic media may induce the decomposition of the nanotubular structure. The dimensions of TNT–HCl were slightly smaller than TNTs, with an average length of 83.92 nm (SD ± 42.48 nm) and an average diameter of 8.78 nm (SD ± 1.76 nm). However, neither the surface characteristics (Table 2) nor the FT-IR spectrum (Figure 2) showed a significant difference from the results of the native TNTs. Thus, no considerable difference was expected in the behavior of TNT and TNT–HCl from the aspect of composite formation ability.

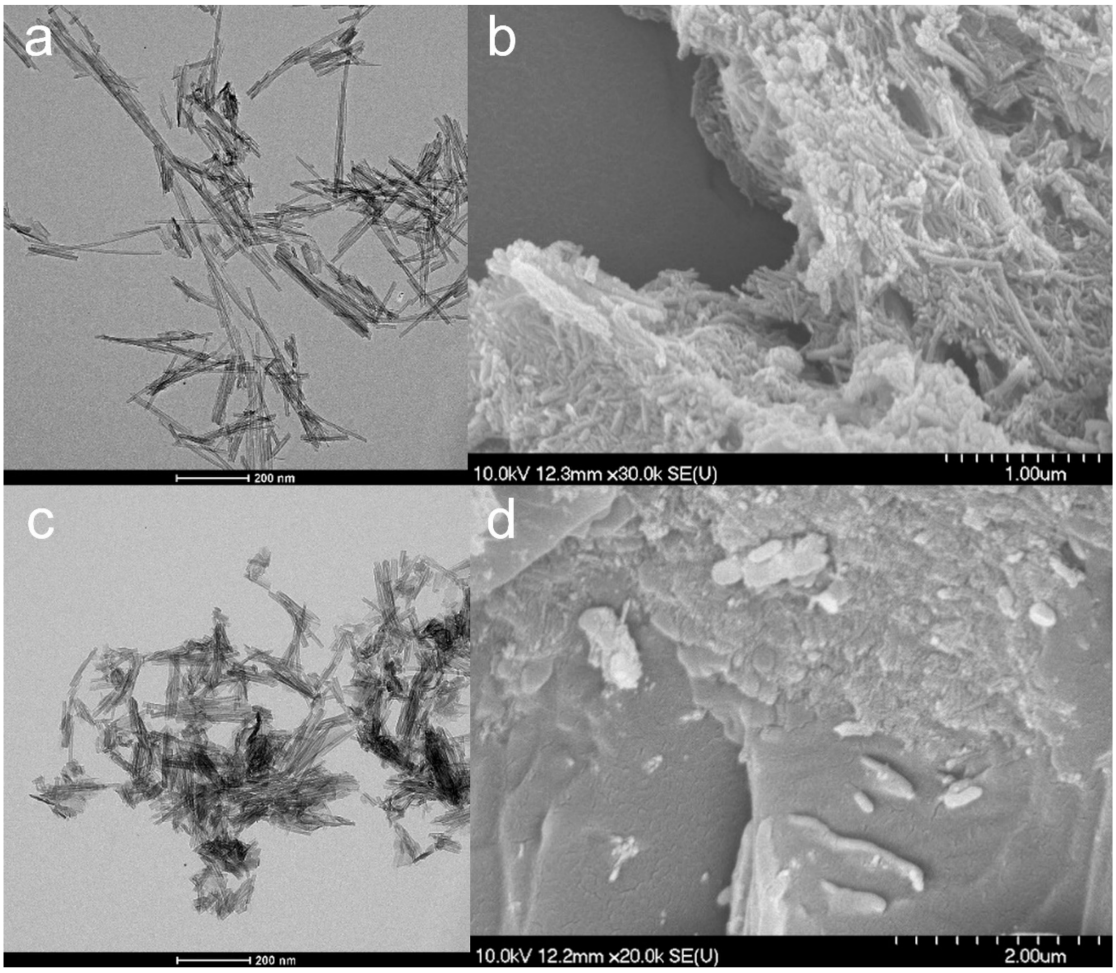

Figure 1. TEM (**a**,**c**) and SEM (**b**,**d**) micrographs of TNTs (**a**,**b**) and TNT–HCl 0.01 M (**c**,**d**).

Table 2. Surface free energy and polarity of TNTs, atenolol (ATN), hydrochlorothiazide (HCT), and their composites.

Material	γ_s (mJ/m^2)	SD	γ_s^{Disp} (mJ/m^2)	SD	γ_s^{Pol} (mJ/m^2)	SD	Polarity %
TNTs (previous)	80.72	±0.64	43.78	±0.54	36.94	±0.35	45.76
TNTs (current)	80.85	±1.18	44.55	±0.53	36.31	±1.04	44.90
TNT–HCl	78.63	±2.07	43.10	±0.27	35.53	±2.05	45.19
ATN	59.48	±3.99	36.70	±2.96	22.77	±2.68	38.20
TiATN–ethanol	60.14	±4.25	40.45	±1.48	19.68	±3.87	32.72
TiATN–methanol	58.04	±2.01	37.12	±1.19	20.92	±1.47	36.04
TiATN–HCl	68.37	±2.26	34.83	±0.05	33.54	±2.26	49.06
HCT	69.51	±2.71	43.33	±0.79	26.18	±2.59	37.60
TiHCT–ethanol	78.25	±0.86	44.65	±0.57	33.60	±0.64	42.93
TiHCT–NaOH 1M	77.54	±1.89	44.52	±0.80	33.02	±1.71	42.59
TiHCT–DMF	71.47	±2.63	42.53	±0.29	28.94	±2.63	40.49
TiHCT–DMS	73.92	±1.42	45.29	±0.08	28.63	±1.42	38.72

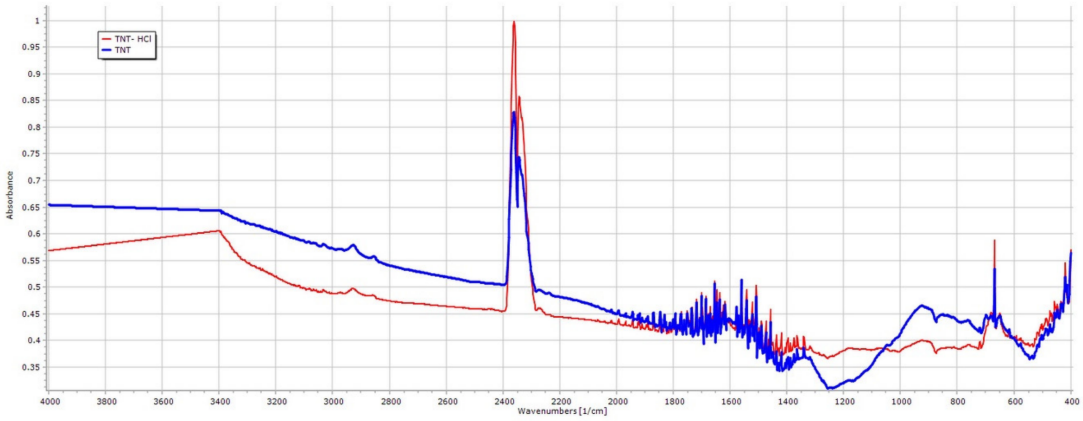

Figure 2. FT-IR spectra of TNTs and TNT–HCl 0.01 M.

3.2. *Effect of Various Solvents on Composite Formation with ATN*

SEM images (Figure 3) show that the composite formation was insufficient for TiATN–ethanol (Figure 3b) since the smooth-surfaced particles of crystalline ATN (Figure 3a) are clearly visible beside the aggregates of TNTs. In contrast, a strong surface coverage of ATN particles with TNTs may be observed in the micrographs of the TiATN–methanol sample (Figure 3c), indicating a stronger interaction but still insufficient composite formation between the drug and the carrier. A rough surface and highly ordered aggregations can be observed in TiATN–HCl (Figure 3d), which may indicate a more adequate composite formation and the accumulation of ATN nanocrystals on the surface of the composite without the existence of individual ATN crystals.

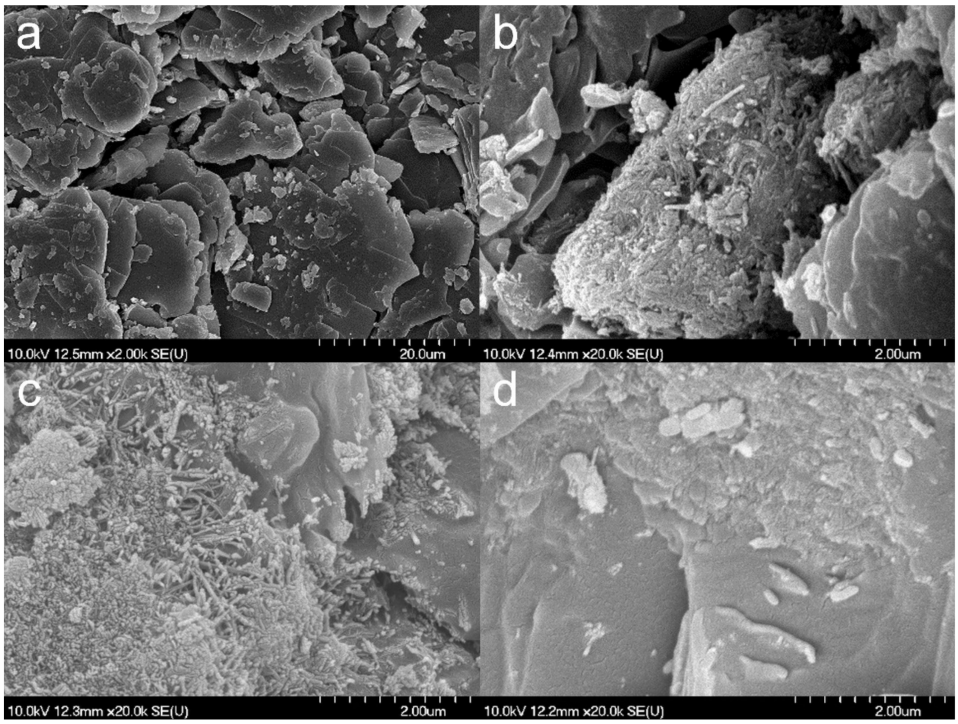

Figure 3. SEM micrographs of atenolol (**a**), TiATN–ethanol (**b**), TiATN–methanol (**c**), and TiATN–HCl 0.01 M (**d**).

Interestingly, the γ_s (Table 1) for TiATN–ethanol and TiATN–methanol were almost identical to ATN, which may indicate not pure TNTs but TNT–ATN composites aggregated to the surface of bigger ATN particles. However, the γ_s and polarity values for TiATN–HCl were distinctly different from

the pure ATN and TNTs, which may reflect not only a kind of interaction between NH_3^+ from ATN and the hydrophilic sites in TNTs enriching the hydrophobic regions in TNTs, but also a different particle-forming mechanism than in the case of other solvents, which leads to a different expected behavior during processing and use.

Nevertheless, the consequences drawn from the morphological investigations were only partially supported by the DSC/TG and FT-IR measurements. It is visible in Figure 4 that the DSC curve of ATN contains an endothermic and a broad exothermic peak. The sharp endothermic peak at 155.21 °C represents the fusion of the compound, and the exothermic peak describes its decomposition, which is supported by the TG curve of ATN. Similarly, TiATN–ethanol and TiATN–methanol composites have an endothermic peak at 161 °C and 159.84 °C, respectively. A decrease in the enthalpy of fusion was noticed from −154.795 Jg^{-1} in ATN to −74.97 Jg^{-1} and −50.71 Jg^{-1} in TiATN–ethanol and TiATN–methanol, respectively, which suggests that poor composite formation was achieved by using ethanol or methanol as solvent. Only a minor size reduction may be concluded in the case of TiATN–methanol. In contrast, the shift of the fusion temperature was higher in the TiATN–HCl composite, and the enthalpy of fusion significantly decreased to −40.55 Jg^{-1}, which may be explained by the stronger interactions and by the considerable particle size reduction of ATN [29], which was in accordance with the SEM images where less crystallization was observed. These results were also supported by the FT-IR spectra, which displayed no substantial differences between the spectra of ATN, TiATN–ethanol, and TiATN–methanol (Figure 5), whereas the appearance of a new peak at 1560 cm^{-1} indicating the protonation of the carbonamide group and wide low intensity peaks between 1900–2100 cm^{-1} and 2300–2500 cm^{-1} indicating the protonation of the secondary amino group were noticed in the spectrum of TiATN–HCl.

For better comparability, the spectra of ATN and its composites were normalized to the C=O stretching peak at 1637 cm^{-1} (Figure 5). The characteristic peaks of pure ATN at 2964 cm^{-1} (C–H stretching in CH_3), 2922 cm^{-1} (C–H stretching in CH_2), 2865.8 cm^{-1} (C–H stretching), 1614 cm^{-1} (conjugated C=C in the aromatic ring), and 885.9 cm^{-1} (C=CH_2 vibrations) did not show considerable differences, indicating that the C–C skeleton of the molecule is not affected by the composite formation process. However, the minor left-shift of the peak at 2800 cm^{-1} indicates the involvement of the secondary amino group in the drug carrier interactions in TiATN–HCl samples. A considerable decrease in the relative intensity at 3356 cm^{-1} can be noticed in TiATN–methanol and TiATN–HCl compared to ATN and TiATN–ethanol, which refers to the participation of the secondary –OH as a hydrogen donor in TNT–ATN conjugation. Furthermore, a similar decrease of the relative intensity of the peak at 3173 cm^{-1} may be observed for TiATN–methanol and TiATN–HCl, which indicates the participation of the carbonamide group in hydrogen bonding formation. The shift of the peak from 1637 cm^{-1} to 1650 cm^{-1} and 1659 cm^{-1} in TiATN–HCl and TiATN–ethanol samples, respectively, and the appearance of a peak at 1558 cm^{-1} in TIATN–HCl also supports the participation of the amide N as H donor and the C=O as H acceptor in the conjugation process. Moreover, the appearance of a new broad peak at around 2000 cm^{-1} indicates the formation of ATN chloride salt. The shift of the peak in TiATN–ethanol from 1382 cm^{-1} to 1385 cm^{-1}, belonging to the associated β-OH vibration, indicates the role of the secondary alcohol in the conjugation. Similar, but stronger shifts of the peaks belonging to the β–OH deformation vibration were also observed in TiATN–HCl, which indicates stronger association between TNTs and ATN in this sample.

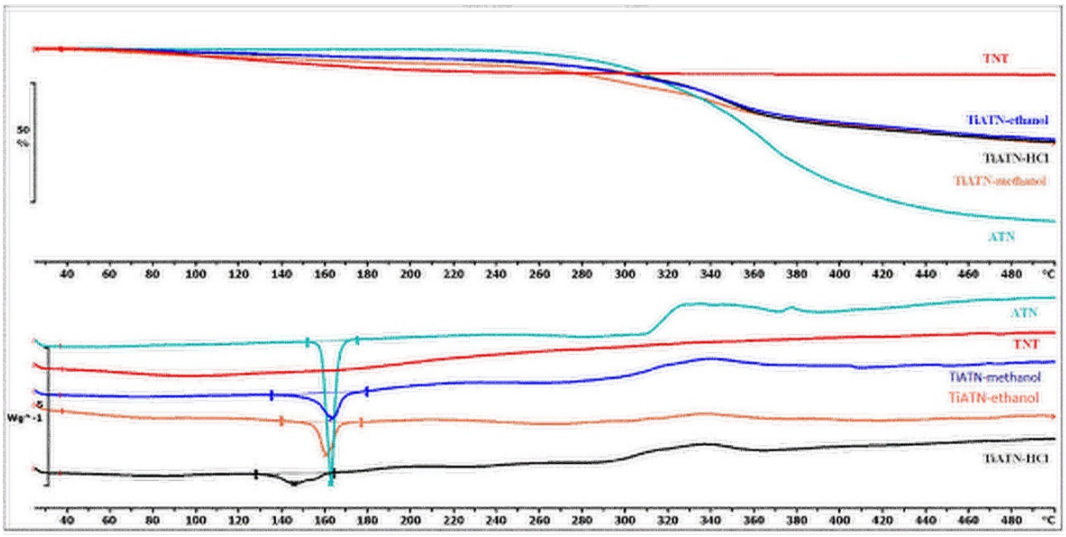

Figure 4. Differential scanning calorimetry (DSC) and thermogravimetric (TG) curves of TNT, ATN, TiATN–methanol, TiATN–ethanol, and TiATN–HCl.

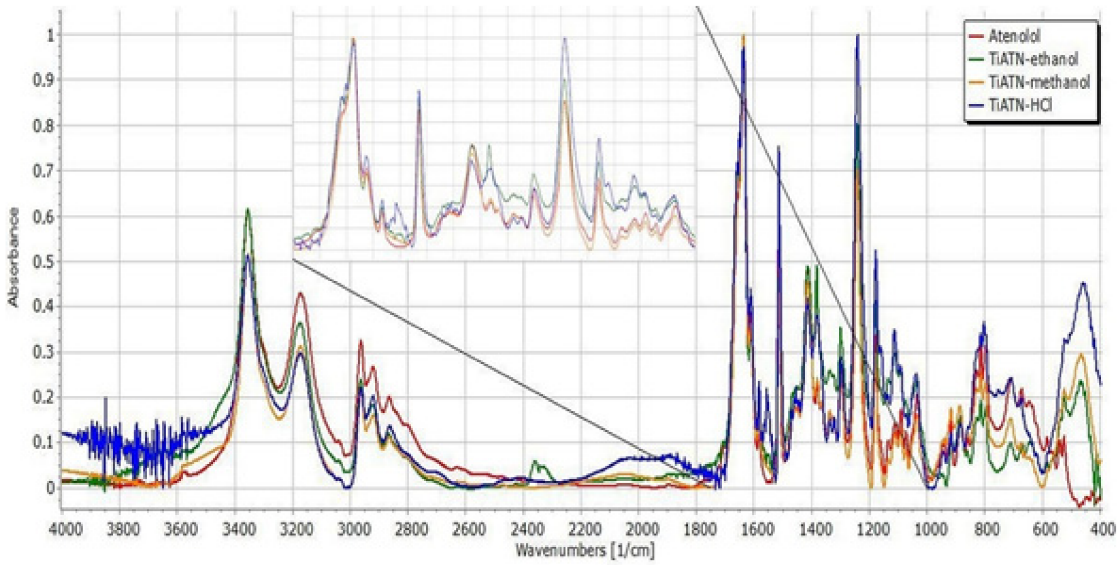

Figure 5. FT-IR spectra of atenolol, TiATN–ethanol, TiATN–methanol, and TiATN–HCl 0.01 M.

All of these data indicate considerable solvent-dependent differences in the formation process of TiATN composites. The surface characteristics and SEM images of TiATN ethanol samples indicate that ATN nanocrystals covered Ti nanotubes and also that bigger ATN crystals may be found in the system. This may be explained by the phenomenon that the highest solubility of ATN can be observed in the 70 *w*/*w*% ethanol solution [27]. The fast evaporation of the ethanol content during solvent removal may induce the fast supersaturation of the solution, which can result in intensive nanocrystal formation on the surface of TNTs as nuclei. On the other hand, the rest of the ATN may undergo a slower crystallization process due to the slower evaporation rate of and strong H-bond-based interactions with water. Similarly, the fast evaporation of the water-free methanol featured fast nanocrystal formation on the TNTs surface and resulted in stronger composites. Nevertheless, despite the slow evaporation rate, the strongest reaction between TNTs and ATN was achieved by using HCl 0.01 M as a solvent. This may be explained by the protonation of the carboxyl amide and secondary amino groups of ATN, which results in repulsion between ATN molecules and may increase their H-bonding strength in the presence of polyfunctional carriers such as TNTs [30]. These effects also lead to featured ATN–TNT

interactions, which result in an increased dissolution rate from the composites due the formation of stable nanocrystals on the carriers' surface (Figure 6).

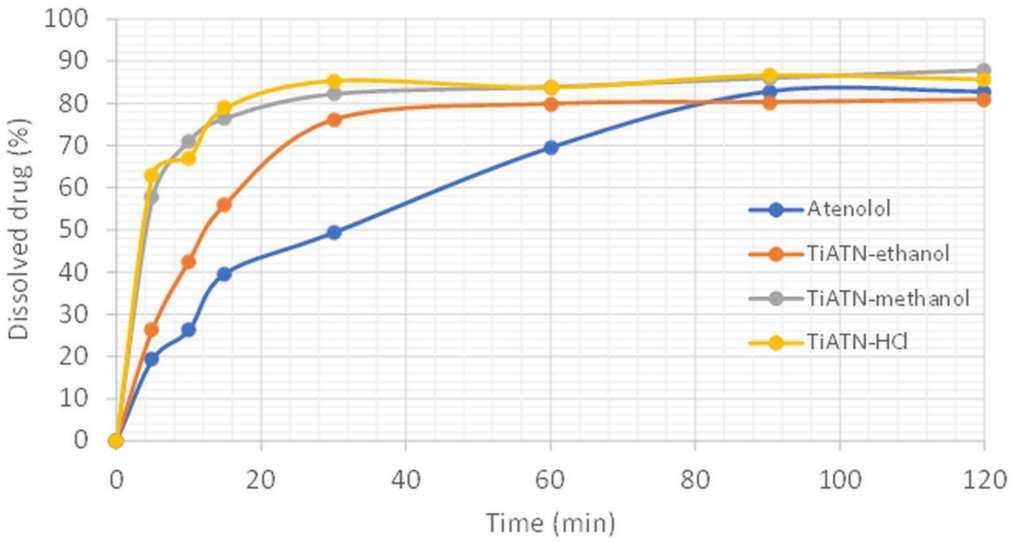

Figure 6. Dissolution study of TiATN composites in gastric juice (non-sink conditions).

3.3. Effect of Various Solvents on the Composite Formation with HCT

The SEM micrographs reveal a strong recrystallization of HCT (Figure 7a) from ethanol and NaOH (Figure 7b,c) with the appearance of HCT crystals covered by the composites. In contrast, in the case of TiHCT–DMF and TiHCT–DMSO (Figure 7d,e), no considerable recrystallization was observed and only strong compacts of TNTs with increased thickness are visible, which indicates an appropriate loading of the nanotubes with the API, which was also supported by the results of the OCA measurements (Table 1) and DSC analysis.

The OCA results revealed that γ_s and polarity values for TiHCT–ethanol and TiHCT–NaOH were higher compared to HCT due to the accumulation of TNTs on the surface of HCT crystals, whereas TiHCT–DMF and TiHCT–DMSO showed γ_s values similar to HCT due to the surface coverage of TNTs with HCT molecules.

The DSC curve of HCT reveals that the fusion of the API could be recognized near 270.67 °C, which was followed by a characteristic exothermic event near 320 °C, ascribed to the decomposition of the material (Figure 8). There was a slight shift in the melting peak in TiHCT–NaOH composites to 269.74 °C, which indicates poor composite formation from this solvent. This can be explained by the long evaporation time of the aqueous medium, which resulted in the domination of crystal growth and not the core formation. This effect is also strengthened by the deprotonation of the sulfonamide group, which decreases the H-bond-forming ability of HCT. A higher shift in the melting peak was noticed at 257.2 °C and 234.17 °C in TiHCT–ethanol and TiHCT–DMF, respectively; this reflects a stronger interaction when using ethanol and DMF. In the case of TiHCT–ethanol samples, the explanation may be the same as for ATN: that the fast evaporation of ethanol indicates nuclei formation, while the slow evaporation of water features the growth of HCT crystals. In contrast, despite the slower evaporation rate, an improved composite formation was expected for the water-free DMF and DMSO due to their aprotic nature, which induced the recrystallisation of HCT on the surface of TNTs as nuclei. The expectation was confirmed for DMF but interestingly, no fusion peak can be seen in the case of TiHCT–DMSO composites, which can be explained by the formation of amorphous HCT particles instead of nanocrystals. All these findings were in accordance with the results of the X-ray powder diffraction (XRPD) results (Figure 9).

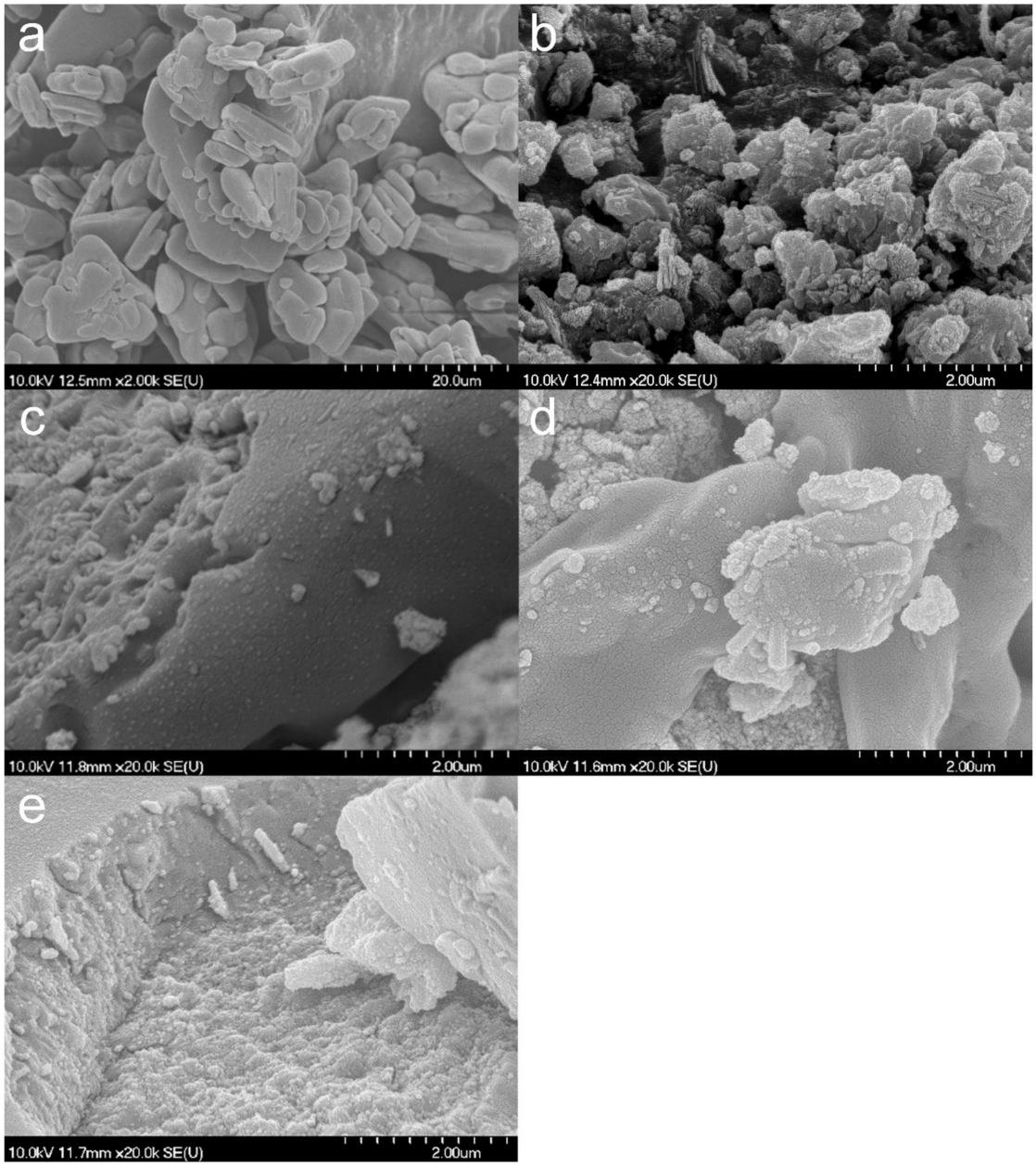

Figure 7. SEM micrographs of HCT (**a**), TiHCT–ethanol (**b**), TiHCT–NaOH (**c**), TiHCT–DMF (**d**), TiHCT–DMSO (**e**).

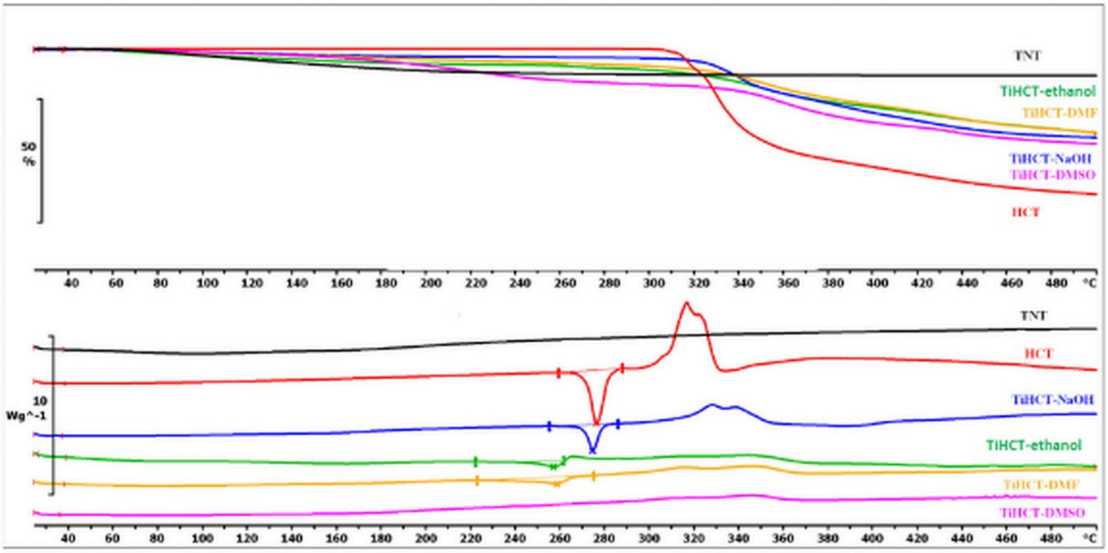

Figure 8. DSC and TG curves of TNT, HCT, TiHCT–ethanol, TiHCT–NaOH, TiHCT–DMF, and TiHCT–DMSO.

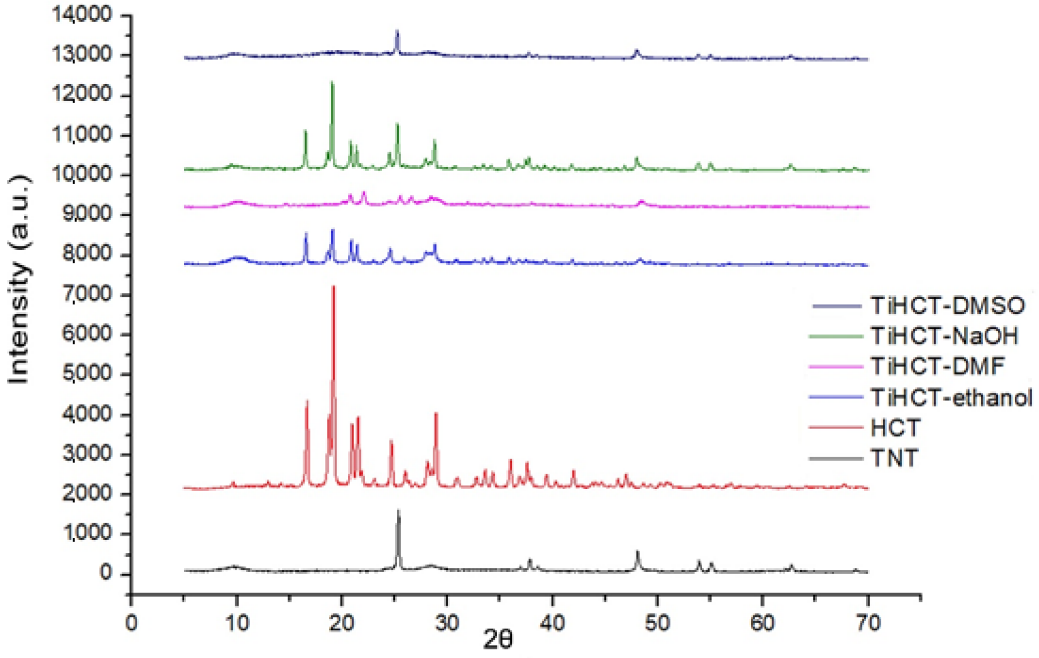

Figure 9. X-ray diffractograms of HCT and its composites.

It is clearly visible that the X-ray diffractogram of TiHCT–DMSO contains only the characteristic peaks of the crystalline TNTs, which clearly indicates that we were able to bond HCT to TNTs in an amorphous form, which is highly desirable to ensure an improved dissolution rate, while the other composites contained HCT in a (nano) crystalline form. Nevertheless, it is also notable that a new polymorphic form of HCT was recrystallized from DMF (the metastable Form II or DMF solvate instead of the starting stable form I) [31,32].

The spectra were normalized to the peak at 1319 cm^{-1} (Figure 10). The peaks at 3391 cm^{-1} belong to non-associated NH stretching, the right shift of this peak and that at 3269 cm^{-1} indicate the increasing strength of interactions between TNT and HCT in the order of TiHCT–ethanol, TiHCT–NaOH, TiHCT–DMF, and TiHCT–DMSO. The very strong association indicated by the merging of these peaks in the case of DMSO may also be due to the amorphous state of the drug in the composite. The slight

right-shift of the N–H bend signal at 1605 cm^{-1}, and the change in the intensity ratio of the peaks at 1555 cm^{-1} and 1538 cm^{-1} also indicate the participation of sulfonamide and secondary amino groups in the composite formation.

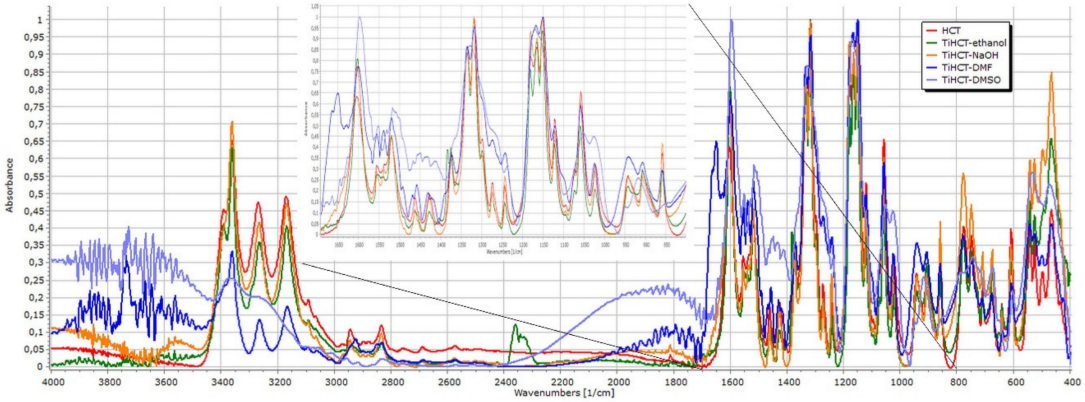

Figure 10. FT-IR spectra of HCT and its composites.

The minor modification of the C=N stretch signals between 1319–1375 cm^{-1} or the varying intensities in the 420–910 cm^{-1} region due to C–Cl stretching alteration and benzothiazidine ring skeletal vibration are also related to these interactions. Meanwhile, the left-shift and the merging of the peak triplet at 1182 cm^{-1}, 1058 cm^{-1}, and 1151 cm^{-1} indicate the involvement of S=O groups as hydrogen acceptors in the interactions.

The strength of interactions basically determined the dissolution rate of the drug from the composites. There was no significant difference in the dissolution rates of pure HCT and TiHCT–ethanol composites where the weakest interaction was observed (Figure 11). The increasing strength of the interactions resulted in a controlled dissolution rate, which was similar to that of diclofenac–TNT composites [25] and resulted in the switch of release kinetics from first order to power law model described by Korsmeyer and Peppas. The most considerable elongation of drug release was observed in the case of TiHCT–DMSO, despite the amorphous state of the drug, which may assume an increased release rate due to the lack of a crystal lattice. It is also notable that the decrease in the release rate of TiHCT–NaOH was higher than expected, which may be due to the large size of the HCT particles due to the slow recrystallization of the drug from the solvent.

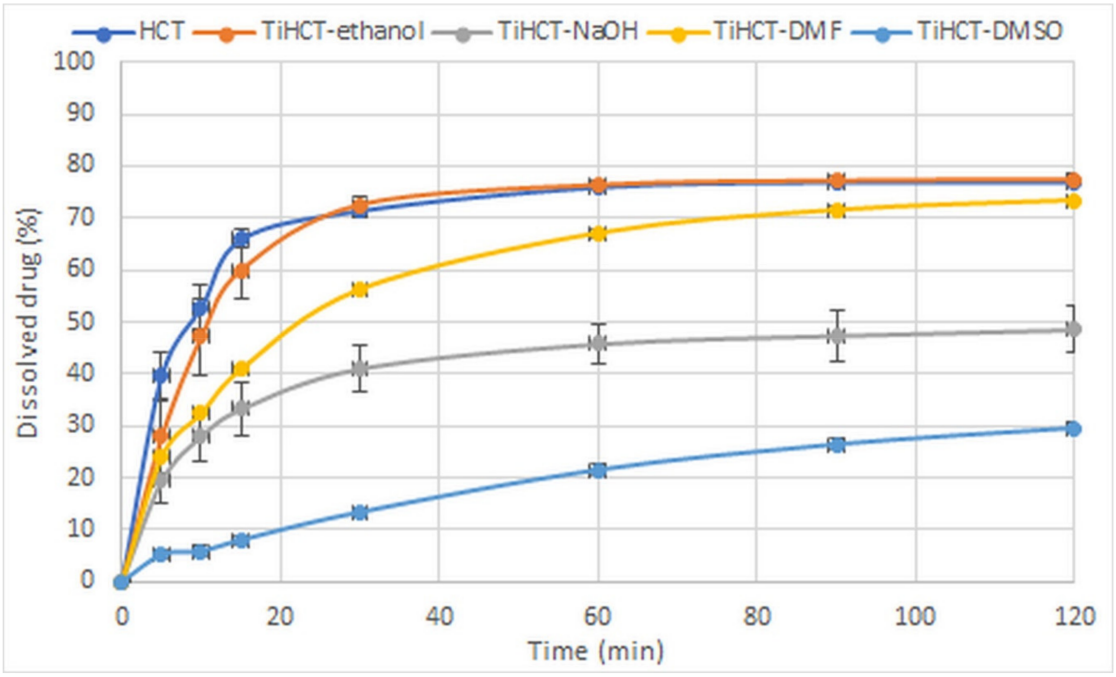

Figure 11. Dissolution study of TiHCT composites in gastric juice (non-sink conditions).

4. Discussion

Based on these results, it may be concluded that choosing the appropriate solvent is essential from the aspect of composite formation efficacy. The solubility of the API in the selected solvent is important as regards process performance and economy, but its volatility and protic/aprotic nature seems to be more important from the aspect of the strength and quality of composites. ATN exhibits good solubility in 70 *w*/*w*% ethanol solution, methanol, and HCl 0.01 M. The Janus-faced properties of the TiATN–ethanol sample may be explained by the fast supersaturation of the solution as a result of the fast evaporation of the ethanol content followed by the slower removal speed of water, which induced the concentration of ATN molecules and featured the formation of ATN–ATN bonds instead of ATN–TNT ones. This latter effect was not observed during the fast removal of water-free methanol, while in the case of 0.01 M HCl solution, the repulsive effect between protonated ATN molecules prohibited the formation of ATN–ATN interactions despite the slower solvent removal speed. The featured drug–carrier interactions and the stabilization of the drug in the nanocrystalline state highly improved the dissolution rate from the TiATN composites.

In contrast, the results with HCT were not so obvious. HCT was dissolved in 70 *w*/*w*% ethanol solution and NaOH 1 M as an analog of the experiments with ATN. However, the quality of the TiHCT–NaOH composites was below expectations, which may be explained by the strong interaction between the drug and the solvent, which may lead to the deprotonation of the drug molecule and may decrease the intensity of drug–carrier interactions within the composites. To eliminate this effect, a pair of aprotic solvents was applied, and DMF and DMSO were successful in forming the TiHCT composites since H-bonding was featured between HCT and TNTs due to the lack of drug–solvent interactions. Nevertheless, it is notable that despite the stabilized nanocrystalline form or HCT "recrystallizing" from DMSO in an amorphous form, the very strong drug–carrier interactions resulted in an extended release of the drug from the composites.

In conclusion, the selection of a highly volatile aprotic solvent may be the best way for the preparation of strong TNT–API composites, but the use of protic solvents could also be advantageous if it results in the protonation of the drug molecule. Nevertheless, care must be taken regarding the strength of drug–carrier interactions since they may influence the detachment of the drug and therefore

exhibit considerable influence on the characteristics of the products, determining processability, release rate, and behavior in a biological environment.

Author Contributions: Conceptualization, T.S. and Z.K.; methodology, T.S.; formal analysis, Y.R. and T.S.; investigation, Y.R., I.S., T.V., and G.R.J.; resources, Z.K.; writing—original draft preparation, Y.R.; writing—review and editing, T.S., K.P.-H., G.R.J., and Z.K.; supervision, T.S. and Z.K.

Funding: This research received no external funding.

Acknowledgments: The authors would like to thank the valuable contribution of László Nagy in the synthesis of titanate nanotubes and composites.

Conflicts of Interest: The authors declare no conflict of interest.

References

1. Shukla, A.K.; Bishnoi, R.S.; Dev, S.K.; Kumar, M.; Fenin, V. Biopharmaceutical Classification System: Tool based prediction for drug dosage formulation. *Adv. Pharm. J.* **2017**, *2*, 204–209.
2. Kumar, P.; Singh, C. A study on solubility enhancement methods for poorly water soluble drugs. *Am. J. Pharmacol. Sci.* **2013**, *1*, 67–73. [CrossRef]
3. Habib, M.J. *Pharmaceutical Solid Dispersion Technology*; CRC Press: Washington, DC, USA, 2000.
4. Joshi, H.N.; Tejwani, R.W.; Davidovich, M.; Sahasrabudhe, V.P.; Jemal, M.; Bathala, M.S.; Varia, S.A.; Serajuddin, A.T. Bioavailability enhancement of a poorly water-soluble drug by solid dispersion in polyethylene glycol–polysorbate 80 mixture. *Int. J. Pharmaceut.* **2004**, *269*, 251–258. [CrossRef] [PubMed]
5. Konno, H.; Taylor, L.S. Influence of different polymers on the crystallization tendency of molecularly dispersed amorphous felodipine. *J. Pharm. Sci.* **2006**, *95*, 2692–2705. [CrossRef] [PubMed]
6. Van den Mooter, G.; Wuyts, M.; Blaton, N.; Busson, R.; Grobet, P.; Augustijns, P.; Kinget, R. Physical stabilisation of amorphous ketoconazole in solid dispersions with polyvinylpyrrolidone K25. *Eur. J. Pharm. Sci.* **2001**, *12*, 261–269. [CrossRef]
7. Leuner, C.; Dressman, J. Improving drug solubility for oral delivery using solid dispersions. *Eur. J. Pharm. Biopharm.* **2000**, *50*, 47–60. [CrossRef]
8. Yu, L. Amorphous pharmaceutical solids: Preparation, characterization and stabilization. *Adv. Drug Deliv. Rev.* **2001**, *48*, 27–42. [CrossRef]
9. Verheyen, S.; Blaton, N.; Kinget, R.; van den Mooter, G. Mechanism of increased dissolution of diazepam and temazepam from polyethylene glycol 6000 solid dispersions. *Int. J. Pharmaceut.* **2002**, *249*, 45–58. [CrossRef]
10. Martınez-Oharriz, M.; Martın, C.; Goni, M.; Rodrıguez-Espinosa, C.; Tros-Ilarduya, M.; Zornoza, A. Influence of polyethylene glycol 4000 on the polymorphic forms of diflunisal. *Eur. J. Pharm. Sci.* **1999**, *8*, 127–132. [CrossRef]
11. Chiou, W.L.; Riegelman, S. Pharmaceutical applications of solid dispersion systems. *J. Pharm. Sci.* **1971**, *60*, 1281–1302. [CrossRef]
12. Nelson, E.; Knoechel, E.; Hamlin, W.; Wagner, J. Influence of the absorption rate of tolbutamide on the rate of decline of blood sugar levels in normal humans. *J. Pharm. Sci.* **1962**, *51*, 509–514. [CrossRef] [PubMed]
13. Lin, S.L.; Lachman, L.; Swartz, C.; Huebner, C. Preformulation investigation I: Relation of salt forms and biological activity of an experimental antihypertensive. *J. Pharm. Sci.* **1972**, *61*, 1418–1422. [CrossRef] [PubMed]
14. Losic, D.; Simovic, S. Self-ordered nanopore and nanotube platforms for drug delivery applications. *Exp. Op. Drug Deliv.* **2009**, *6*, 1363–1381. [CrossRef] [PubMed]
15. Aw, M.S.; Kurian, M.; Losic, D. Non-eroding drug-releasing implants with ordered nanoporous and nanotubular structures: Concepts for controlling drug release. *Biomaterial. Sci.* **2014**, *2*, 10–34.
16. Mainardes, R.M.; Silva, L.P. Drug delivery systems: Past, present, and future. *Curr. Drug Target.* **2004**, *5*, 449–455. [CrossRef]
17. Fahr, A.; Liu, X. Drug delivery strategies for poorly water-soluble drugs. *Exp. Op. Drug Deliv.* **2007**, *4*, 403–416. [CrossRef] [PubMed]
18. Wolinsky, J.B.; Colson, Y.L.; Grinstaff, M.W. Local drug delivery strategies for cancer treatment: Gels, nanoparticles, polymeric films, rods, and wafers. *J. Control. Rel.* **2012**, *159*, 14–26. [CrossRef]

19. Pison, U.; Welte, T.; Giersig, M.; Groneberg, D.A. Nanomedicine for respiratory diseases. *Eur. J. Pharmacol.* **2006**, *533*, 341–350. [CrossRef]
20. Wang, S.; Su, R.; Nie, S.; Sun, M.; Zhang, J.; Wu, D.; Moustaid-Moussa, N. Application of nanotechnology in improving bioavailability and bioactivity of diet-derived phytochemicals. *J. Nutr. Biochem.* **2014**, *25*, 363–376. [CrossRef]
21. Kulkarni, H.P. Synthesis and Applications of Titania Nanotubes: Drug Delivery and Ionomer Composites. Ph.D. Thesis, University of North Carolina, Chapel Hill, NC, USA, 2008.
22. Gulati, K.; Ramakrishnan, S.; Aw, M.S.; Atkins, G.J.; Findlay, D.M.; Losic, D. Biocompatible polymer coating of titania nanotube arrays for improved drug elution and osteoblast adhesion. *Acta Biomater.* **2012**, *8*, 449–456. [CrossRef]
23. Wang, Q.; Huang, J.-Y.; Li, H.-Q.; Zhao, A.Z.-J.; Wang, Y.; Zhang, K.-Q.; Sun, H.-T.; Lai, Y.-K. Recent advances on smart TiO2 nanotube platforms for sustainable drug delivery applications. *Int. J. Nanomed.* **2017**, *12*, 151.
24. Lai, S.; Zhang, W.; Liu, F.; Wu, C.; Zeng, D.; Sun, Y.; Xu, Y.; Fang, Y.; Zhou, W. TiO_2 nanotubes as animal drug delivery system and in vitro controlled release. *J. Nanosci Nanotechnol.* **2013**, *13*, 91–97.
25. Sipos, B.; Pintye-Hódi, K.; Kónya, Z.; Kelemen, A.; Regdon, G., Jr.; Sovány, T. Physicochemical characterisation and investigation of the bonding mechanisms of API-titanate nanotube composites as new drug carrier systems. *Int. J. Pharmaceut.* **2017**, *518*, 119–129. [CrossRef] [PubMed]
26. Saei, A.A.; Jabbaribar, F.; Fakhree, M.A.A.; Acree, W.E., Jr.; Jouyban, A. Solubility of sodium diclofenac in binary water + alcohol solvent mixtures at 25 °C. *J. Drug Del. Sci. Tech.* **2008**, *18*, 149–151. [CrossRef]
27. Hamidi, S.; Jouyban, A. Solubility of atenolol in ethanol + water mixtures at various temperatures. *J. Serb. Chem. Soc.* **2015**, *80*, 695–704. [CrossRef]
28. Wang, S.; Xi, S.; Qu, Y.; Wang, J. Measurement and Correlation of Solubility of Hydrochlorothiazide in Monosolvents and Binary Solvent Mixtures from 283.15 to 323.15 K. *J. Chem. Eng. Data* **2019**, *64*, 3128–3138. [CrossRef]
29. Singh, M.; Lara, S.; Tlali, S. Effects of size and shape on the specific heat, melting entropy and enthalpy of nanomaterials. *J. Taibah Univ. Sci.* **2017**, *11*, 922–929. [CrossRef]
30. Meot-Ner, M. The ionic hydrogen bond 4. Intramolecular and multiple bonds. Protonation and complexes of amides and amino acid derivatives. *J. Am. Chem. Soc.* **1984**, *106*, 278–283. [CrossRef]
31. Johnston, A.; Florence, A.J.; Shankland, N.; Kennedy, A.R.; Shankland, K.; Price, S.L. Crystallization and Crystal Energy Landscape of Hydrochlorothiazide. *Cryst. Growth Des.* **2007**, *7*, 705–712. [CrossRef]
32. Saini, A.; Chadha, R.; Gupta, A.; Singh, P.; Bhandari, S.; Khullar, S.; Mandal, S.; Jain, D.D. New conformational polymorph of hydrochlorothiazide with improved solubility. *Pharm. Dev. Techn.* **2016**, *21*, 611–618. [CrossRef]

Evaluation of the permeability and in vitro cytotoxicity of functionalized titanate nanotubes on Caco-2 cell line

YASMIN RANJOUS[1], DÓRA KÓSA[2], ZOLTÁN UJHELYI[2], GÉZA REGDON JR.[1], KRISZTINA ANITA NAGY[3], IMRE SZENTI[3], ZOLTÁN KÓNYA[3,4], ILDIKÓ BÁCSKAY[2], TAMÁS SOVÁNY[1]*

[1]*University of Szeged, Institute of Pharmaceutical Technology and Regulatory Affairs, 6720, Szeged, Eötvös u 6., Hungary*
[2]*University of Debrecen, Department of Pharmaceutical Technology, 4010, Debrecen, Nagyerdei krt. 98, Hungary*
[3]*University of Szeged, Department of Applied and Environmental Chemistry, 6720, Szeged, Rerrich ter 1, Hungary*
[4]*MTA--SZTE Reaction Kinetics and Surface Chemistry, Research Group, 6720, Szeged, Rerrich ter 1, Hungary*

Corresponding author: Tamás Sovány, PhD
Email: sovany.tamas@szte.hu

Received: *19 April 2021* / ***Accepted:*** *18 May 2021*

Titanate nanotubes (TNTs) are promising vectors for drug delivery due to their unique physicochemical properties such as biocompatibility, mechanical strength, and chemical resistivity. However, considering their strong hydrophilicity, pristine TNTs exert very limited permeability through the intestinal cell layer. The aim of this study was to turn the surface characteristics and thus enhance the permeability of TNTs by functionalization. TNTs were functionalized with trichloro(octyl)silane (TCOS) and magnesium stearate (MgSt). Carbon content and surface free energy of the functionalized TNTs were detected to evaluate the effectiveness of functionalization, by using CHNS analytical and optical contact angle (OCA) measurements, respectively. Caco-2 cell line was applied to test the permeability and the cytotoxicity of the samples. Cytotoxicity was evaluated by using MTT assay. The results revealed that the surface characteristics of TNTs may be adjusted in a wider range with TCOS-TNT than with St, but the samples show higher toxicity. Silane functionalized TNTs may be safe up to 1 mg/ml, while St functionalized TNTs up to 2 mg/ml concentration. The preparation method of MgSt-TNT was also superior from the aspect of environmental safety. The permeability was suitable for samples with moderate hydrophobicity (aqueous contact angle 60-90°).

Keywords: *cytotoxicity; permeability; functionalization; titanate nanotubes; magnesium stearate; silane derivatives*

Introduction

Titanium dioxide nanoparticles (TiO_2 NPs) are one of the most commonly applied nanoparticles in various fields, such as building engineering, agriculture, food and cosmetic industry, environmental protection or medicine (1). TiO_2 NPs exist in three different structures: as anatase, rutile, and brookite (2) (Figure 1.), which differ in their crystal structure where the Ti-O bond length ranges are 1.931- 2.004 Å for rutile, 1.914- 2.005 Å for anatase and 1.850- 2.099 Å for brookite (3).

Despite that anatase is the most toxic form comparing to rutile and brookite (4), it has more industrial applications due to its photocatalytic activity (2). Moreover, the global market presented 117 various products in food and beverage field based on nanotechnology (5). It is allowed in USA to use TiO_2 NPs in foodstuff when its percentage does not exceed 1% of the total product weight (6). However, Europe is following the "quantum satis" concept (7). Furthermore, a child can take 2-4 times more TiO_2 NPs/ 1 kg of body weight (bw) per a day in comparison to an adult person, which was determined in Great Britain as 2–3 mg TiO_2/kg bw/day for children less than 10 years old, whereas adults can take about 1 mg TiO_2/kg bw/day(4). Nevertheless, the vast TiO_2 NPs applications in food industry resulted in diverse debates on their safety, regarding to toxicity considerations. TiO_2 NPs pigment is categorized as a prospective carcinogenic factor from group 2B by the International Agency for Research on Cancer (IARC)(8). In contrast, there is no matter of concern on the safety of E171 (titanium dioxide) in 2016 according to the European Food Safety Authority (EFSA)(7). Nevertheless, there are no adequate research data on the acceptable daily intake of TiO_2 NPs and the safety margin was determined as 2.25 mg TiO_2 NPs/kg bw/day built on tests involving animals (7).

TiO_2 NPs toxicity on human body has been connected mostly to apoptosis (9) and some studies displayed that TiO_2 NPs may cause DNA damage (10) and disturb glucose and lipid homeostasis in mice and rats. In addition, TiO_2 NPs may accumulate in the lungs, alimentary tract, liver, kidneys,

DOI: 10.33892/aph.2021.91.31-39

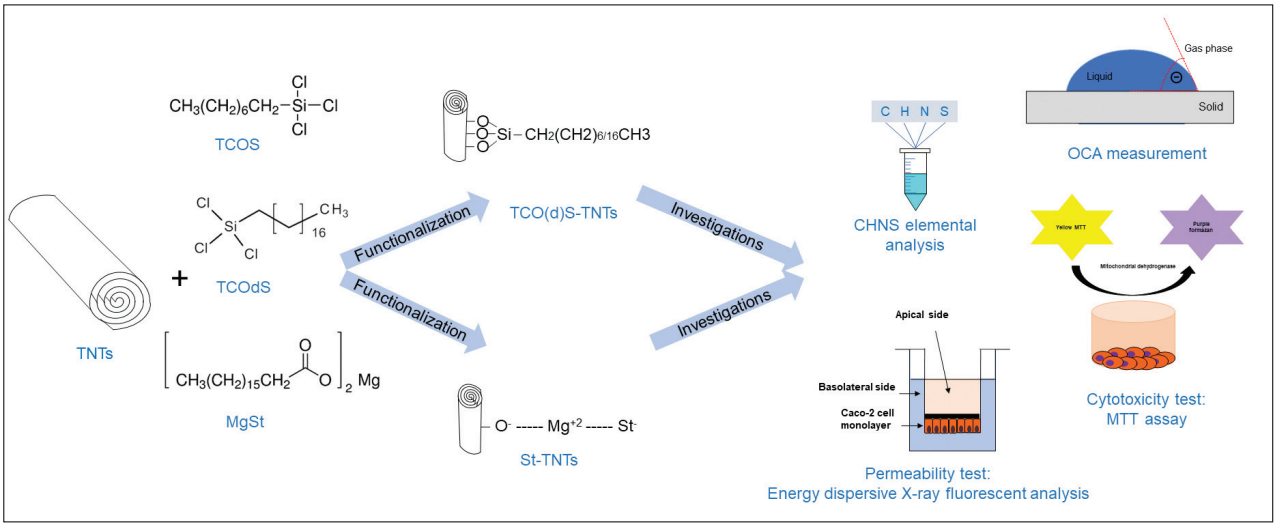

Graphical abstract

spleen, heart, and cardiac muscle after inhalation or oral exposure (11). Interestingly, the nanoparticle size influences their toxicity and accumulation in different organs in which the larger particles with 80 nm size are largely assembled in the liver whereas the smaller particles with 25 nm diameter can accumulate in the spleen and slightly in the lungs and kidneys after a one-time oral administration to mice (12).

TiO_2 NPs modification with polyethylene glycol (PEG) decreases the cytotoxicity and the induction of stress-related genes (13). Furthermore, the presence of PEG combining catalytic chain transfer and thiolene polymer layers around TiO_2 NPs leads to not only the reduction of protein adsorption onto their surface, but also the reduction of the size of aggregated particles and the alteration of particle surface chemistry that results in an increased cellular uptake and diminishment of cytotoxicity for both human lung epithelial cell lines A549 and NCI-H1299 (14).

The extent of TiO_2 NPs absorption from the gastro-intestinal tract (GIT) into systemic circulation depends on many factors such as species, type of nanoparticles, size, dispersability or particle charging (15). Recent studies indicated that TiO_2 NPs were barely transferred from the GIT into the blood circulation in humans and rats. Furthermore, there was no impact of the particle size on their absorption when administrating a single dose of TiO_2 NPs (5 mg/kg bw/day) with different particle sizes (15 nm/ 100 nm/ < 5000 nm), which may related to their hydrophilicity (16).

TiO_2 nanostructures have been reported to cause neurological risk after passing the blood–brain barrier (17, 18). Another studies reported the accumulation of TiO_2 nanostructures without metabolism in some organs such as the liver and spleen, and with a less degree in the brain, kidneys, lungs, GIT and heart (19, 20). Many factors play a role in the tissue distribution of TiO_2 nanostructures such as their morphology (21), size and surface charge (22, 23).

Different tissue distribution and toxicity profiles were demonstrated after a single and successive intravenous administration of TiO_2 nanotubes, rods, and ribbons in rats, in which nanotubes displayed the most toxic effect and the largest accumulation, following that nanorods and ribbons (21).

Ren et al, investigated the toxicity, uptake pathways and excretion of TNTs in three strains of free-living ciliates of the genus Tetrahymena which are a wild type strain (SB210) and two mutant strains (SB255, NP1) (24). The results revealed that TNTs caused cytotoxicity in high concentrations. Using 10 mg/l of TNTs for 120 min resulted in their accumulation in NP1 and SB255 in a higher or comparable percentage comparing to SB210, whereas using 10 mg/l of TNTs for 24 h caused a larger decline in cell density of NP1 (38.2 %) and SB255 (36.8 %) in comparison to SB210 (26.5 %) (24).

TNTs are of emerging interest amongst the TiO_2 derived nanomaterials since their nanotubular structure bears special advantages in various application fields (25). Therefore, they became promising alternatives of carbon-based nanotubes, especially since they showed no cytotoxicity in a 7 days incubation study on A549 lung epithelial cell

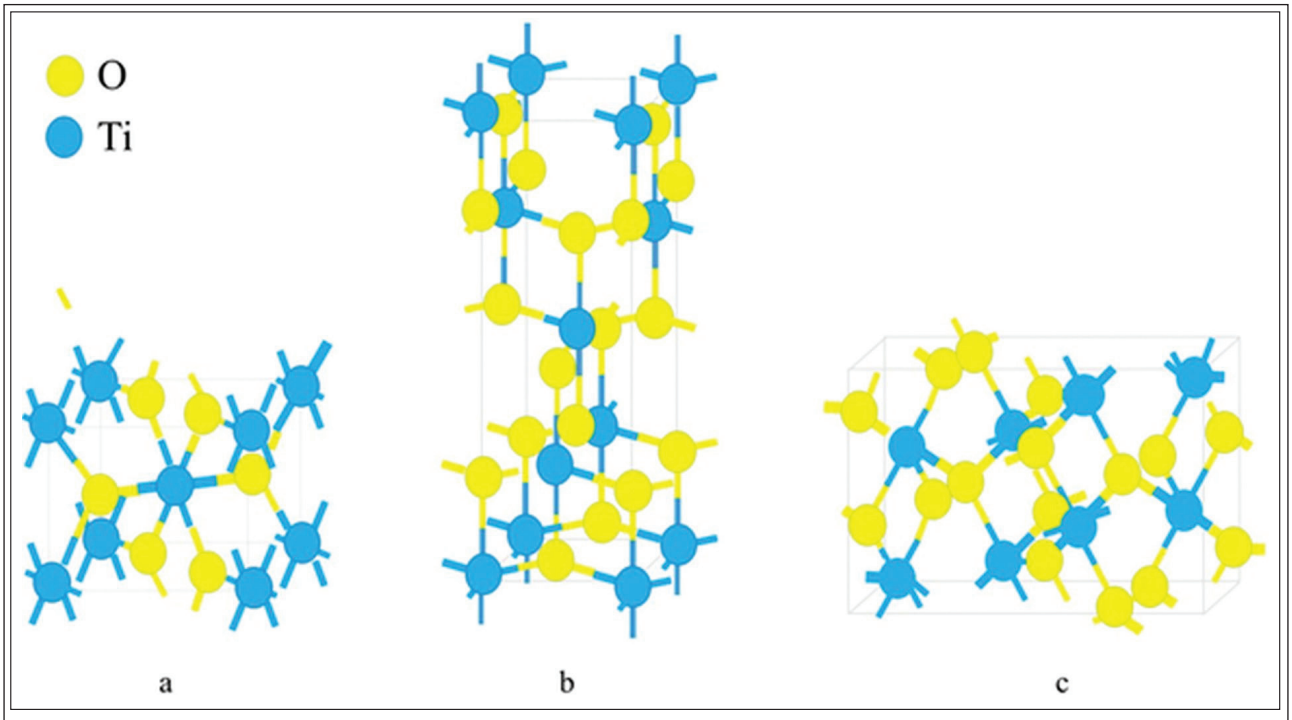

Figure 1 *The primitive unit cell of (a) rutile, (b) anatase and (c) brookite TiO_2.*

lines, in contrast with single-walled- and multi-walled carbon nanotubes (26). Similarly, no cytotoxicity was observed on Caco-2 cells up to 5 mg/ml concentration, so hydrothermally synthetized TNTs are promising vectors also for intestinal drug delivery, since they do not cause cytotoxicity in short-term treatment and no notable number of TNTs was identified. However, non-tubular high-density granules were detected on the surface of the endoplasmic reticulum in the treated cells and these granules were identified as TiO_2 NPs that passed into the Caco-2 monolayer (27). Nevertheless, it is notable that the surface charge and characteristics seems to play a key role in titanate cytotoxicity. Sodium titanate NaxTiOy+z exhibit low risk (26-28) from toxicological aspect, hydrogen titanate HxTiOy+z bears considerable risk of cytotoxic effects investigated on H596 human lung tumor cell line (28, 29) and on HEp-2 cells (30). Similar signs were observed in some mammalian cell lines investigating manganese or potassium titanate nanotubes and nanofibers possibly by the promoting of reactive oxygen species (31, 32).

The functionalization of nanomaterials is important to improve their surface characteristics and achieve the targeted drug delivery. TNTs have negative charge at physiological pH due to their partially hydroxylated surface, thus they can interact with different molecules (33). TNTs functionalization enhances their stability and increase their capacity as drug carriers (34). A variety of molecules have been used in TNTs functionalization such as using dopamine; tris buffer; bone morphogenetic protein 2 (BMP2) to improve the bone osseointegration, allyltriethoxysilane; propyltriethoxysilane to achieve stable suspensions in tetrahydrofuran (THF), and chitosan to control the drug release; PEG or polyethylene imine (PEI) to improve the dispersion and reactivity of TNTs in water, antimicrobial peptides (HHC-36) to stop the biofilms formation, and 3-aminopropyltriethoxysilane or RGD peptide to enhance the human mesenchymal stem cells (hMSCs) attachment and proliferation (25). The aim of present study was to develop functionalized TNTs with tailored surface characteristics for drug delivery applications and investigate how the functionalization of the highly hydrophilic TNTs will increase their hydrophobicity and may influence their toxicity profile and their absorption from the gastro-intestinal tract.

Materials and Methods:

The pristine sodium trititanate ($Na_2Ti_3O_7$) nanotubes (Na-TNTs) were prepared at the following the general method described by Sipos et al. (35), by dissolving 120 g of sodium hydroxide (NaOH) in 300 mL of distilled water on a magnetic stirrer and then adding 75 g of TiO_2 (anatase) for 15 min. Following that, the mixture was moved to the au-

toclave that was put inside an oven at 185°C for 24 h, then cooled at room temperature for 2 h, followed by cooling with cold water. Then, TNTs were washed with distilled water using filter No:4 and under vacuum (35).

Trichloro octyl silane (TCOS) (Sigma-Aldrich, St. Louis, Missouri, United States) were attached to hydrogen trititanate ($H_2Ti_3O_7$) nanotubes (H-TNTs). H-TNTs were prepared by adding 50 g of the pristine Na-TNTs in 300 mL of HCl 0.01 M in an ultrasonic bath until a homogenous suspension was obtained. Following that, 200 mL of HCl 0.01 M was added to the previous suspension on a magnetic stirrer and the mixture was dried in a dry oven for 24 h to remove the solvent.

TOCS-TNTs were prepared by adding 0.5 g of H-TNTs to 15 mL of toluene in ultrasonic bath for 1 h until a homogenous suspension was obtained. After that, the suspension was heated at 80 °C in a condenser which was connected to nitrogen gas for 30 min. Then, TCOS was added to the previous system in different volumes, e.g. 1- 2- 10- 50- 100- 500- 1000 μL, covering the 0.001:1 - 2:1 molar ratios, respectively and mixed for one day. Finally, the functionalized TNTs were washed by hexane 8 times and dried in a drying oven at 80 °C (Sanyo Electric Co., Ltd, Osaka, Japan).

Mg-stearate (MgSt) functionalized TNTs were prepared in two step process. In the first step sodium ions of Na-TNTs were replaced with Mg by adding 100 g of Na-TNTs to 1L of 0.1M $MgCl_2$ solution on magnetic stirrer for 1 day. Then, the mixture was filtered by using glass filter No#4 under vacuum to obtain magnesium trititanate ($MgTi_3O_7$) nanotubes (Mg-TNTs). This procedure was repeated three times to make sure that no Na-TNTs are existing anymore. Then, Mg-TNTs were washed with distilled water 8 times under vacuum and by using glass filter No#4. After that, 10 g of Mg-TNTs were added to 200 ml of distilled water in ultrasonic bath for 30 min. Following that, the mixture was heated to 80 °C in a magnetic stirrer (Thermo Fisher Scientific, Waltham, MA, USA) and Na stearate (VWR International, Radnor, Pennsylvania, United States) was added in different (e.g. 0.001:1-0.1:1) molar ratios to this system for 1 night. Finally, St-TNTs were filtered by using filter No#4 under vacuum and dried in a drying oven.

The morphology of the different preparation of TNTs was investigated by scanning electron microscope (SEM) (Hitachi 4700, Hitachi Ltd., Tokyo, Japan) in which samples were coated with a thin conductive gold layer by a sputter coating unit (Polaron E5100, VG Microtech, London, UK). The images were taken at an accelerating voltage of 10.0 kV, and the used air pressure was 1.3–13 mPa during the analyses. The size of the nanotubes determined using ImageJ 1.51. (National Institute of Health, MD, USA).

The surface free energy of the functionalized TNTs was measured with a DataPhysicsOCA20 (DataPhysics Instruments GmbH, Filderstadt, Germany) optical contact angle tester applying sessile drop method. Polar and apolar test liquids (water and diiodomethane, respectively) were used and dropped onto the surface of 13-mm-diameter additive-free comprimates of the samples, which were prepared with a Specac hydraulic press (Specac Ltd., Orpington, UK) at a pressure of 3 tons. Disperse (γ_s^D) and polar (γ_s^p) components of the total surface free energy (γ_s) of the solid were calculated according to Wu Equations [17].

CHNS elemental analysis was applied for the rapid determination of carbon, hydrogen, nitrogen, and sulphur in organic materials. Samples were analyzed to detect the H, C, N, and S contents in a vario EL cube elemental analyzer (Elementar, Langenselbold, Germany). Sn-foils were filled with 50 to 100 mg samples (no flux added) which were ignited in oxygen–He gas atmosphere furnace at around 1150 °C. N, C, H, and S were analyzed by releasing the resulted gases in a set of chromatographic columns and analyzing those gases with a thermal conductivity detector. The sample measurement time was 9 mins and was repeated 3 times. All values were calibrated against the reference materials BAM-U110, JP-1, and CRPG BE-N.

Unfunctionalized nanotubes (Na-, H- and Mg-TNTs), and samples with the possible highest, and moderate hidrophobicity were selected form TCOS- and St-TNT series were selected for toxicity and permeability tests. Permeability and cytotoxicity experiments were tested on Caco-2 human adenocarcinoma cell line. Cells were maintained at 37°C in a 5% CO_2 atmosphere by regular passage in Dulbecco's modified Eagle's medium (Sigma–Aldrich), supplemented with 2 mM L-glutamine, 100 mg/l gentamycin and 10% heat inactivated foetal bovine serum (Sigma-Aldrich). The passage number of the cells was between 25 and 42. Dulbecco's modified Eagle's medium (Sigma–Aldrich) was used to keep the cells' regular passage in average of 25 to 42. Both experiments were performed 7 days after cell passaging when the monolayer was formed. The reagents were purchased from Sigma-Aldrich (Budapest, Hungary) and Caco-2 cell line was originated from the European Collection of Cell Cultures (UK). The cells

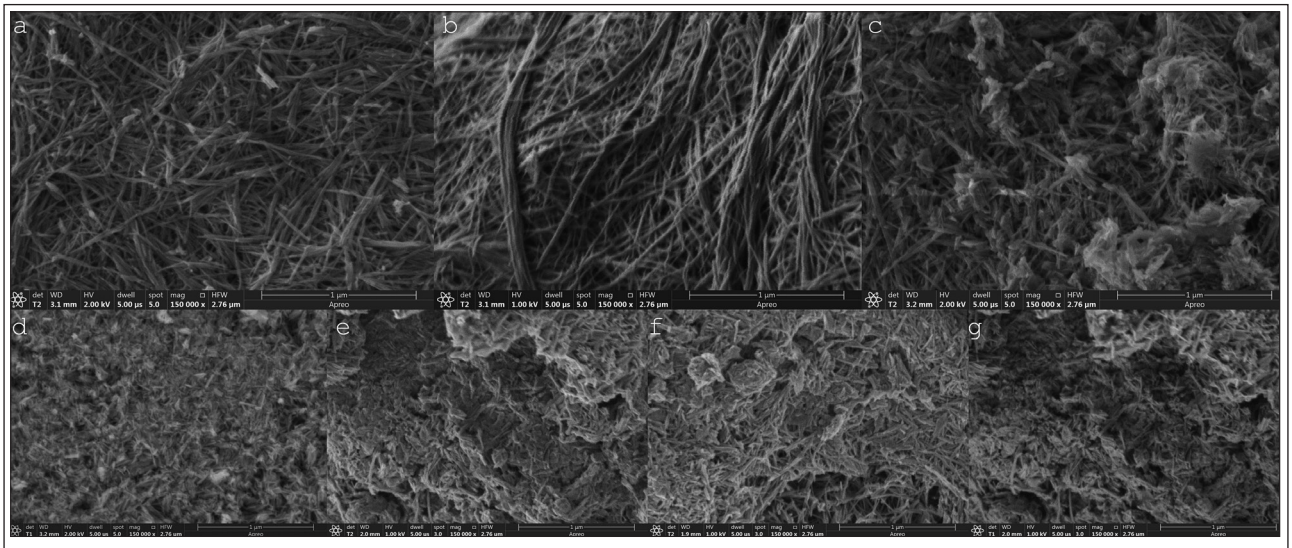

Figure 2 *Scanning electron micrographs of Na-TNT (a), H-TNT (b), Mg-TNT (c), TCOS-TNT 10 (d), TCOS-TNT 50 (e), St-TNT (0,05:1) (f) and St-TNT (0.1:1) (g) samples with 150.000x magnification*

had been monitored before and after the treatment via Olympos CKX41 Inverted Microscope by eye estimation. The monolayer did not show any alteration during the procedure.

Cytotoxicity was tested by the 3-(4,5-dimethylthiazol-2-yl)-2,5-diphenyltetrazolium bromide (Sigma catalog no. M2128)(MTT) assay in which Caco-2 cells were implanted in 96-well plates at a final density of 104 cells/well (VWR International, Radnor, Pennsylvania, United States) and exposed to increased concentrations of TNT in Hank's balanced salt solution (HBSS) at 37°C for 120 min.

The 5 mg/ml solution of MTT in PBS was filtered to sterilize and remove the remaining insoluble residue of MTT. The MTT solution (10 µl/100 µl medium) was added to all wells which were incubated at 37°C for 4 h followed by the addition of HCl-isopropanol which was mixed rigorously to dissolve the dark blue crystals. Within one hour, the plates were read on a Dynatech MR580 Microelisa reader using a test wavelength of 570 nm, a reference wavelength of 690 nm and a calibration setting of 1.99 (or 1.00 if the samples were strongly colored). Extreme high concentrations were applied to evaluate MTT test sensitivity in these measurements. To exclude any interferences between the absorbance of living cells performed formazan crystals and the test solutions, a phosphate buffer (PBS) washing method had been deployed after the TNTs sample incubation. Cell viability was represented as a percentage of the untreated control.

To test permeability, Caco-2 cells were seeded on ThinCert™ (Greiner Bio-One, Hungary) inserts at a final density of $8x10^4$ cells/insert, and monolayers were incubated apically with 1 mg/ml TNT for 120 min after removing cell culture medium. The donor and acceptor phases were then completely removed. The concentration of Ti in the two phases were measured with an energy dispersive X-ray fluorescent analyzer (Philips MiniPal PW 4025, Philips Analytical, the Netherlands), using standard sample holder, with a 3.6 µm thick polyesterpetp X-ray film. The internal diameter of the sample holders was narrowed to 8 mm to ensure approx. 1 cm layer thickness, with 500 µL sample volume. 30 s measurement time was applied with 100 µA current and 8 kV acceleration voltage, using Kapton filter. Six parallel measurements were performed with each sample.

Results and discussion

Physical properties of the functionalized TNTs

Pristine Na-TNTs (Figure 2a) have considerably elongated structure with 8-12 nm outer diameter, and highly variable length (100-1000 nm). H-TNTs (Figure 2b) exert identical physical dimensions but have increased aggregation tendency due the decreasing electrostatic repulsion resulted by the removal of Na^+ ions. Mg-TNTs (Figure. 2c) have the same 8-12 nm outer diameter but the mechanical agitation during the ion-exchange procedure resulted considerable fragmentation, so the length of the nanotubes varies mostly in the 100-300 nm range. Similar fragmentation of the longer nanotubes was observed in case of the functionalized

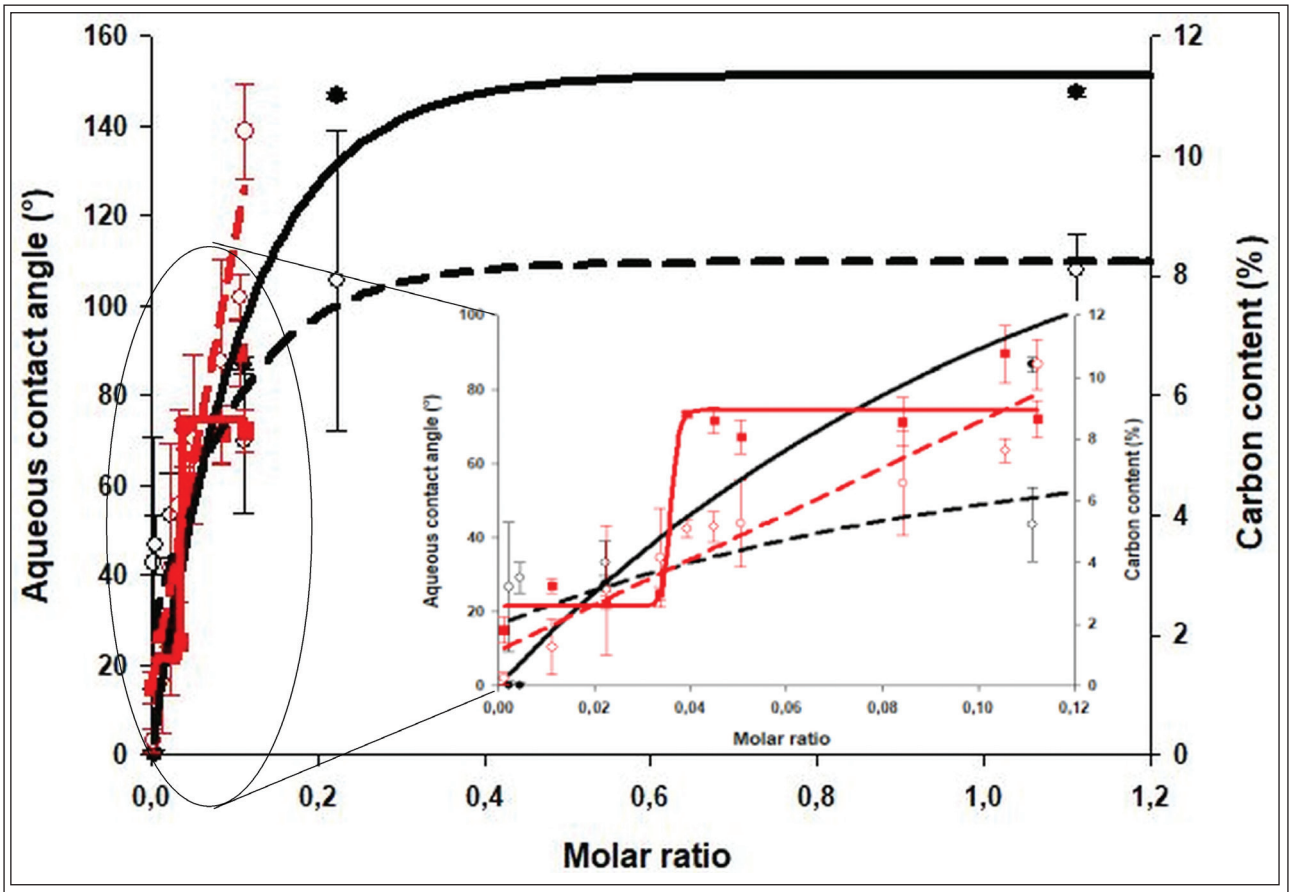

Figure 3 *The aqueous contact angles (CA) and carbon percentage (C%) of TCOS-TNTs and St-TNTs at different reagent concentrations (CA of TCOS-TNT (black line); C% of TCOS-TNT (black dashed line), CA of St-TNT (red line), C% of St-TNT (red dashed line)*

samples (Figure. 2d-g) along with a slight increment of the outer diameter which depends on the amount and orientation of the functionalizing agent on the TNTs surface. Nevertheless, all samples have strongly elongated tubular structure with an aspect ratio >10.

The OCA measurement showed a gradual increment in the aqueous contact angle with the increasing volume of TCOS up to 100 μL volume. Those results were supported by the CHNS elemental analysis that displayed a continuous augmentation in carbon percentage with the increasing amount of functionalizing TCOS (Figure.3).

In contrast, the OCA measurement revealed that low concentrations of St could just slightly increase the aqueous contact angle of the Mg-TNTs, but after the exceeding of a certain threshold around 0.035:1 ratio and despite the linear increment of the carbon content, the surface turned from hydrophilic to hydrophobic (Figure. 3). A possible explanation that above this threshold the St molecules are oriented differently on the surface of TNTs, prohibiting the access of water to the sample. After that only a slight increment could be detected until it stabilizes between 80-90°, but it should be noted, that the maximum aqueous contact angle is considerably smaller as in the case of TOCS-TNTs.

Toxicity and permeability of the functionalized TNTs

In a previous study no detectable cytotoxicity of Na-TNTs was observed up to 5 mg/ml concentration (27), but in the current study a considerable decrease in cell viability was observed if Mg-TNTs were applied in this concentration (Figure 4). This may indicate that the replacement of Na^+ to Mg^{2+} ions on the surface of TNTs also has negative influence on the cell interactions but based on the MTT cytotoxicity test it still be considered as non-cytotoxic in the 0,01-2 mg/ml concentration range. In addition, considerable differences were observed in the toxicity of various functionalized TNTs especially at higher concentrations. In case of St functionalized samples, the cell viability decrease was only observed at 5 mg/ml, which

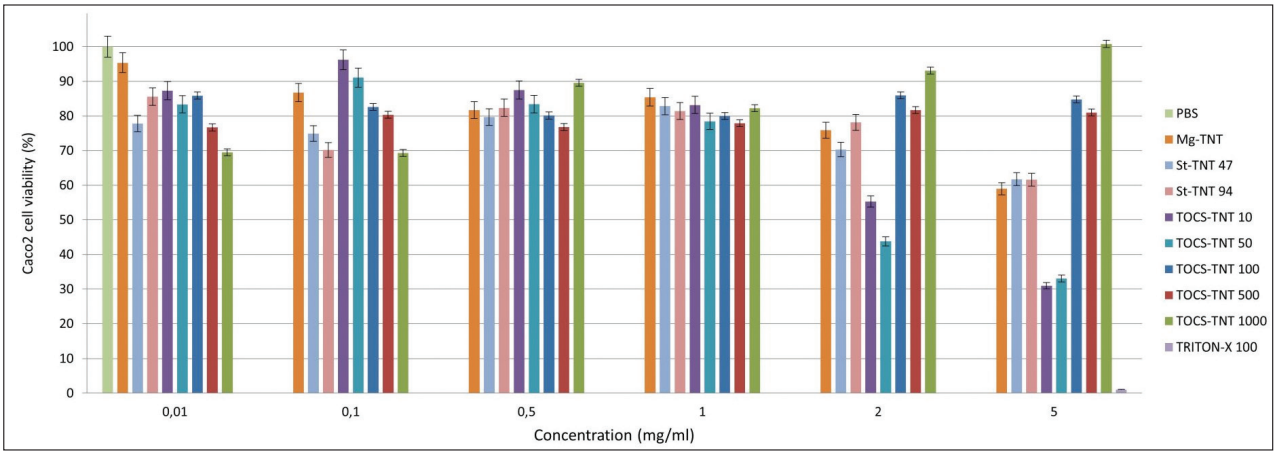

Figure 4 *The viability assays of Caco-2 cells after being exposed to functionalized TNTs*

showed no difference from the values observed at Mg-TNTs.

Permeability results:

During permeability test the highest safe concentration (1 mg/ml) was applied, to enable the achievement of higher maximum drug-dose during further utilization. The transepithelial electrical resistance (TEER) of the cells before TNTs exposure was 602±116 Ω/cm^2. For Caco-2 cells this value may vary in a very high range (200-2400 Ω/cm^2) (36), the obtained results indicate an intact cell layer. Nevertheless, a considerable relative decrease (22.1±16.7%, 12.4±11.1%, 37.1±8.4% and 23.6±17.4% for TCOS-TNT 10, TCOS-TNT 50, St-TNT (0.05:1), and St-TNT (0.1:1) samples, respectively) of the TEER values was observed after TNTs exposure, indicating the perturbation of the integrity of cell-membrane or tight-junctions. However, microscopic investigation showed no change in the cell morphology or layer-integrity, before and after the test, which may indicate a periodic distortion of the membrane integrity by the penetrating nanotubes. Nevertheless, the relative change of various samples showed partial correlation with the results of permeability tests (Table 1), which revealed that the aqueous contact angle (CA) values should be between 60-90° to achieve appropriate absorption, while the cell integrity was exhibited the smallest distortion for samples between 80-90°CA. Below 40° the surface is too hydrophilic to achieve passive transportation through the cell membrane, while in the 40-60° range the samples may absorbed considerably slower as the ones with 60-90° CA, and causes higher distortions in cell integrity, possibly due to the higher hydrophilicity.

According to OCA and CHNS measurements for TCOS-TNTs, it is well visible that the increasing amount of the reagent highly increased the surface hydrophobicity and complete surface coverage was achieved by the application of 100 μL reagent volume (e.g. 0.2:1 molar ratio). However, the results were different in case of MgSt-TNTs where less St coverage resulted in getting a hydrophobic surface that may bear an advantage of keeping more binding sites for the drugs which may lead to a higher possible drug load in this system.

The toxicity results displayed a considerable decrease in the cell viability in case of TCOS-TNT 10- and 50- samples, possibly due the use of H-TNT as starting material, which would be in accordance of the previously discussed findings (28, 29). However, no similar effect was shown by the

Table 1 Results of the permeability tests

Material	Apical amount (%)	Basal amount (%)
TCOS-TNT 10	40,94±10,49	8,47±0,30
TCOS-TNT 50	27,94±14,83	8,39±0,24
TCOS-TNT 100	n.m	n.m
St-TNT 47	26,98±6,66	8,75±0,78
St-TNT 94	27,16±11,13	11,49±0,67

n.m = not measurable

100- 500- and 1000 µL samples. A possible explanation, that these samples were too hydrophobic for appropriate dispersion/dissolution in the aqueous media, and therefore were not taken up by the cells. On the other hand, the lower toxicity presented by MgSt-TNTs which was like Mg-TNTs indicates that the effect may be connected to the presence of Mg^{2+} ions and not to the St molecules.

In this study, the best permeability rate was observed for samples with 90° CA, while in case of sample TCOS-TNT 100 where the CA was around 140° no detectable amount was measured both in apical and basal compartment. A possible explanation that due to the inappropriate wetting and dispersion, the TNTs were sedimented and adhered to the cell layer without visible absorption through the membranes or were completely accumulated in the cells, which would bear a potential risk of toxicity. Nevertheless, in both cases the sample is inappropriate for the planned application.

Conclusions

In the present study, two various approaches of TNTs functionalization were compared to obtain increased hydrophobicity and enhance their absorption from GIT. TCOS, TCOdS and St were used for this purpose in different concentrations to optimize the functionalization method and determine the optimal functionalization percentage.

The results revealed a linear relation between the surface hydrophobicity and the concentration of the used TCOS and TCOdS. However, the different molecular size had no significant effect on the hydrophobicity of functionalized TNTs despite the increasing percentage of carbon that was displayed by CHNS elemental analysis. The maximum hydrophobicity was achieved by using 100 µL reagent which showed 140° aqueous CA.

In contrast, St functionalized TNTs exhibited 90° maximal aqueous CA, which depends nonlinearly on the carbon content. The change in the surface properties after a certain threshold may indicate the changing orientation of St molecules on TNTs surface. This result indicates that turning the surface properties with St is more complicated and can be done in narrower range, but the optimal surface hydrophobicity could still be achieved. Furthermore, the fact that Mg-TNTs exhibit lower degree of cytotoxicity as H-TNTs, and the functionalization is done in aqueous medium instead of organic solvents supports the superiority of the St method for the proposed approach since the preparation was cheaper, faster, easier to be upscaled and less toxic.

Conflict of interest

The authors declare no conflict of interest.

References:

1. Hong F, Yu X, Wu N, Zhang YQ. Progress of in vivo studies on the systemic toxicities induced by titanium dioxide nanoparticles. Toxicol. Res. 2017;6:115-133. https://doi.org/10.1039/c6tx00338a
2. Allen R. The cytotoxic and genotoxic potential of titanium dioxide (TiO2) nanoparticles on human SH-SY5Y neuronal cells in vitro. 2016. http://hdl.handle.net/10026.1/14126
3. Samat MH, Ali AM, Taib MF, Hassan OH, Yahya MZ. Hubbard U calculations on optical properties of 3d transition metal oxide TiO2. Results Phys. 2016;6:891-896. https://doi.org/10.1016/j.rinp.2016.11.006
4. Weir A, Westerhoff P, Fabricius L, Hristovski K, Von Goetz N. Titanium dioxide nanoparticles in food and personal care products. Environ. Sci. Technol. 2012;46:2242-2250. https://doi.org/10.1021/es204168d
5. Vance ME, Kuiken T, Vejerano EP, McGinnis SP, Hochella Jr MF, Rejeski D, Hull MS. Nanotechnology in the real world: Redeveloping the nanomaterial consumer products inventory. Beilstein J. Nanotechnol. 2015;6:1769-1780. https://doi.org/10.3762/bjnano.6.181
6. Chen Z, Wang Y, Zhuo L, Chen S, Zhao L, Luan X, Wang H, Jia G. Effect of titanium dioxide nanoparticles on the cardiovascular system after oral administration. Toxicol. Lett. 2015;239:123-130. https://doi.org/10.1016/j.toxlet.2015.09.013
7. EFSA Panel on Food Additives and Nutrient Sources added to Food (ANS). Re-evaluation of titanium dioxide (E 171) as a food additive. Efsa Journal. 2016;14:e04545. https://doi.org/10.2903/j.efsa.2016.4545
8. IARC Working Group on the Evaluation of Carcinogenic Risks to Humans. Carbon black, titanium dioxide, and talc. IARC monographs on the evaluation of carcinogenic risks to humans. 2010;93:1.
9. Acar MS, Bulut ZB, Ateş A, Nami B, Koçak N, Yıldız B. Titanium dioxide nanoparticles induce cytotoxicity and reduce mitotic index in human amniotic fluid-derived cells. Hum Exp Toxicol. 2015;34:74-82. https://doi.org/10.1177/0960327114530742
10. Jugan ML, Barillet S, Simon-Deckers A, Herlin-Boime N, Sauvaigo S, Douki T, Carriere M. Titanium dioxide nanoparticles exhibit genotoxicity and impair DNA repair activity in A549 cells. Nanotoxicology. 2012;6:501-513. https://doi.org/10.3109/17435390.2011.587903
11. Bahadar H, Maqbool F, Niaz K, Abdollahi M. Toxicity of nanoparticles and an overview of current experimental models. Iran. Biomed. J. 2016;20:21. https://doi.org/10.7508/ibj.2016.01.001
12. Wang J, Zhou G, Chen C, Yu H, Wang T, Ma Y, Jia G, Gao Y, Li B, Sun J, Li Y. Acute toxicity and biodistribution of different sized titanium dioxide particles in mice after oral administration. Toxicol. Lett. 2007;168:176-185. https://doi.org/10.1016/j.toxlet.2006.12.001
13. Mano SS, Kanehira K, Sonezaki S, Taniguchi A. Effect

of polyethylene glycol modification of TiO2 nanoparticles on cytotoxicity and gene expressions in human cell lines. Int. J. Mol. Sci. 2012;13:3703-3717. https://doi.org/10.3390/ijms13033703
14. Tedja R, Soeriyadi AH, Whittaker MR, Lim M, Marquis C, Boyer C, Davis TP, Amal R. Effect of TiO 2 nanoparticle surface functionalization on protein adsorption, cellular uptake and cytotoxicity: the attachment of PEG comb polymers using catalytic chain transfer and thiol–ene chemistry. Polym. Chem. 2012;3:2743-2751. https://doi.org/10.1039/C2PY20450A
15. Warheit DB, Donner EM. Risk assessment strategies for nanoscale and fine-sized titanium dioxide particles: Recognizing hazard and exposure issues. Food Chem. Toxicol. 2015;85:138-147. https://doi.org/10.1016/j.fct.2015.07.001
16. Jones K, Morton J, Smith I, Jurkschat K, Harding AH, Evans G. Human in vivo and in vitro studies on gastrointestinal absorption of titanium dioxide nanoparticles. Toxicol. Lett. 2015;233:95-101. https://doi.org/10.1016/j.toxlet.2014.12.005
17. Catalan-Figueroa J, Palma-Florez S, Alvarez G, Fritz HF, Jara MO, Morales JO. Nanomedicine and nanotoxicology: the pros and cons for neurodegeneration and brain cancer. Nanomedicine. 2016;11:171-187. https://doi.org/10.2217/nnm.15.189
18. Krawczyńska A, Dziendzikowska K, Gromadzka-Ostrowska J, Lankoff A, Herman AP, Oczkowski M, Królikowski T, Wilczak J, Wojewódzka M, Kruszewski M. Silver and titanium dioxide nanoparticles alter oxidative/inflammatory response and renin–angiotensin system in brain. Food Chem Toxicol. 2015;85:96-105. https://doi.org/10.1016/j.fct.2015.08.005
19. Geraets L, Oomen AG, Krystek P, Jacobsen NR, Wallin H, Laurentie M, Verharen HW, Brandon EF, de Jong WH. Tissue distribution and elimination after oral and intravenous administration of different titanium dioxide nanoparticles in rats. Part *Fibre* Toxicol. 2014;11:1-21. https://doi.org/10.1186/1743-8977-11-30
20. Landsiedel R, Fabian E, Ma-Hock L, Wohlleben W, Wiench K, Oesch F, van Ravenzwaay B. Toxico-/biokinetics of nanomaterials. Arch. Toxicol. 2012;86:1021-1060. https://doi.org/10.1007/s00204-012-0858-7
21. Kamal N, Zaki AH, El-Shahawy AA, Sayed OM, El-Dek SI. Changing the morphology of one-dimensional titanate nanostructures affects its tissue distribution and toxicity. Toxicol. Ind. Health. 2020;36:272-286. https://doi.org/10.1177/0748233720921693
22. Kamal N, Zaki AH, El-Shahawy AA, Sayed OM, El-Dek SI. Changing the morphology of one-dimensional titanate nanostructures affects its tissue distribution and toxicity. Toxicol Ind *Health.* 2020;36:272-286. https://doi.org/10.1016/j.toxlet.2012.08.019
23. van Ravenzwaay B, Landsiedel R, Fabian E, Burkhardt S, Strauss V, Ma-Hock L. Comparing fate and effects of three particles of different surface properties: nano-TiO2, pigmentary TiO2 and quartz. Toxicol. Lett. 2009;186:152-159. https://doi.org/10.1016/j.toxlet.2008.11.020
24. Kong R, Sun Q, Cheng S, Fu J, Liu W, Letcher RJ, Liu C. Uptake, excretion and toxicity of titanate nanotubes in three stains of free-living ciliates of the genus Tetrahymena. Aquat. Toxicol. 2021;233:105790. https://doi.org/10.1016/j.aquatox.2021.105790
25. Ranjous Y, Regdon Jr G, Pintye-Hódi K, Sovány T. Standpoint on the priority of TNTs and CNTs as targeted drug delivery systems. Drug Discov. Today. 2019;24:1704-1709. https://doi.org/10.1016/j.drudis.2019.05.019
26. Wadhwa S, Rea C, O'Hare P, Mathur A, Roy SS, Dunlop PS, Byrne JA, Burke G, Meenan B, McLaughlin JA. Comparative in vitro cytotoxicity study of carbon nanotubes and titania nanostructures on human lung epithelial cells. J. Hazard. Mater. 2011;191:56-61. https://doi.org/10.1016/j.jhazmat.2011.04.035
27. Fenyvesi F, Kónya Z, Rázga Z, Vecsernyés M, Kása P, Pintye-Hódi K, Bácskay I. Investigation of the cytotoxic effects of titanate nanotubes on Caco-2 cells. AAPS PharmSciTech. 2014;15:858-861. https://doi.org/10.1208/s12249-014-0115-x
28. Maurizi L, Papa AL, Boudon J, Sudhakaran S, Pruvot B, Vandroux D, Chluba J, Lizard G, Millot N. Toxicological risk assessment of emerging nanomaterials: cytotoxicity, cellular uptake, effects on biogenesis and cell organelle activity, acute toxicity and biodistribution of oxide nanoparticles. Unraveling the Safety Profile of Nanoscale Particles and Materials-From Biomedical to Environmental Applications. 2018:17-36. http://dx.doi.org/10.5772/intechopen.71833
29. Magrez A, Horváth L, Smajda R, Salicio V, Pasquier N, Forro L, Schwaller B. Cellular toxicity of TiO2-based nanofilaments. Acs Nano. 2009;3:2274-2280. https://doi.org/10.1021/nn9002067
30. Pan R, Liu Y, Chen W, Dawson G, Wang X, Li Y, Dong B, Zhu Y. The toxicity evaluation of nano-trititanate with bactericidal properties in vitro. Nanotoxicology. 2012;6:327-337. https://doi.org/10.3109/17435390.2011.579629
31. Entezari M, Ghanbary F. Toxicity of Manganese Titanate on Rat Vital Organ Mitochondria. Iran J Pharm Res: IJPR. 2019;18:713. https://dx.doi.org/10.22037/ijpr.2019.1100639
32. Abdelgied M, El-Gazzar AM, Alexander DB, Alexander WT, Numano T, Iigou M, Naiki-Ito A, Takase H, Abdou KA, Hirose A, Taquahashi Y. Pulmonary and pleural toxicity of potassium octatitanate fibers, rutile titanium dioxide nanoparticles, and MWCNT-7 in male Fischer 344 rats. Arch. Toxicol. 2019;93:909-920. https://doi.org/10.1007/s00204-019-02410-z
33. Papa AL, Maurizi L, Vandroux D, Walker P, Millot N. Synthesis of titanate nanotubes directly coated with USPIO in hydrothermal conditions: a new detectable nanocarrier. J. Phys. Chem. C. 2011;115:19012-19017. https://doi.org/10.1021/jp2056893
34. Papa AL, Boudon J, Bellat V, Loiseau A, Bisht H, Sallem F, Chassagnon R, Bérard V, Millot N. Dispersion of titanate nanotubes for nanomedicine: comparison of PEI and PEG nanohybrids. Dalton Trans. 2015;44:739-746. https://doi.org/10.1039/C4DT02552K
35. Sipos B, Pintye-Hódi K, Kónya Z, Kelemen A, Regdon Jr G, Sovány T. Physicochemical characterisation and investigation of the bonding mechanisms of API-titanate nanotube composites as new drug carrier systems. Int. J. Pharm. 2017;518:119-129. https://doi.org/10.1016/j.ijpharm.2016.12.053
36. Srinivasan B, Kolli AR, Esch MB, Abaci HE, Shuler ML, Hickman JJ. TEER measurement techniques for in vitro barrier model systems. J. Lab. Autom. 2015;20:107-126. https://doi.org/10.1177/2211068214561025